An electron microscopic method to identify peptidergic neurons in connectomes

Dissertation

der Mathematisch-Naturwissenschaftlichen Fakultät

der Eberhard Karls Universität Tübingen

zur Erlangung des Grades eines

Doktors der Naturwissenschaften

(Dr. rer nat)

vorgelegt von

Réza Shahidi

aus Teheran, Iran

Tübingen

2016

Gedruckt mit Genehmigung der Mathematisch-Naturwissenschaftlichen Fakultät der Eberhard Karls Universität Tübingen.

Tag der mündlichen Qualifikation:	12. 09. 2016
Dekan:	Prof. Dr. Wolfgang Rosenstiel
1. Berichterstatter:	Dr. Gáspár Jékely
2. Berichterstatter:	Prof. Dr. Oliver Betz

ACKNOWLEDGEMENTS

"When you make the finding yourself - even if you're the last person on Earth to see the light - you'll never forget it." Carl Sagan

I am truly grateful and honored for the opportunity I received to complete this ambitious and inspiring project. I am forever thankful to my supervisor Gáspár Jékely for his continual support and his scientific guidance throughout my dissertation. His research laboratory was an extraordinary place of excellence and growth.

I am thankful to all my lab-mates with whom I shared and developed many wonderful ideas, especially those who helped with the project (Markus Conzelmann, Nadine Randel, Aurora Panzera, Luis Bezares, Albina Asadulina, Csaba Verasztó, Sanja Jasek, Steffen Schmidt), with special thanks to Elizabeth A. Williams for her sustained encouragement and support over the years, and to Philipp Bauknecht for his assistance with German translations.

I cordially thank Prof. Dr. Oliver Betz for his time and supervision for the completion of my thesis.

I would like to thank all the members of the Electron Microscopy Facility at the MPI for their scientific suggestions and much help during my project, with special thanks to Heinz Schwarz and Matthias Flötenmeyer for their patience and guidance. Thanks also to my first year biology professor who has undoubtedly proven that a passionate teacher could make all the difference in a student's academic journey.

Last but not least, my heartfelt thanks to my parents and my brother for being the ever source of illumination on my path to success.

Table of Contents

ZUSAMMENFASSUNG

Nervensysteme von Tieren sind komplexe Verbindungsnetzwerke zwischen verschiedenen Arten von Neuronen und Effektorgeweben. Die Kartierung der Verbindungen von molekular identifizierten Neuronentypen auf synaptischer Ebene würde unser Verständnis der Struktur und Funktion des Nervensystems erheblich verbessern. Studien auf synaptischer Ebene benötigen hochauflösende Analysetechniken, und die Technik mit dem stärksten Auflösungsvermögen bisher ist die Elektronenmikroskopie (EM) [1].

In meiner Dissertation habe ich einen großen seriellen EM-Datensatz für die neuronale Netzwerkanalyse, die Rekonstruktion der Schaltkreise und Studien zur Stereotypie im Nervensystem der Larven des meeresbewohnenden Ringelwurms *Platynereis dumerilii* erstellt. Ich entwickelte auch eine innovative Methode, um peptidergen Neuronen direkt im EM-Datensatz molekulare Identitäten zuzuweisen.

Ich benutzte serielle Dünnschnitt-Transmissionselektronenmikroskopie (ssTEM) in Kombination mit serieller Multiplex-Immunogoldfärbung (siGOLD) um mehrere peptiderge Neurone verschiedenen Typs zu identifizieren. siGOLD ist eine Antikörperfärbung von Gruppen von Dünnschnitten, die die molekularen Identitäten von einzelnen Neuronen offenbart. Unter Ausnutzung der hohen Immunogenität von Neuropeptiden und ihrer großen Verbreitung entlang der Axone, verwendete ich Antikörper gegen Neuropeptide, um die siGOLD-Methode zu etablieren. Ich zeige die Wirksamkeit von siGOLD unter Verwendung von 11 Neuropeptid-Antikörpern in einem Ganzkörper-ssTEM-Datensatz einer *Platynereis*-Larve. Die siGOLD-Markierung erlaubt es mir, mehrere verschiedene Arten von peptidergen Neuronen im ganzen Larvenkörper spezifisch zu anzufärben. siGOLD wurde auch angewendet, um einen peptidergen neuralen Schaltkreis zu rekonstruieren, der die sensorischen Nuchalorgane umfasst, die das circadiane Neuropeptid pigment dispersing factor (PDF) exprimieren. Dieser Ansatz ermöglicht die direkte Überlagerung von chemisch-neuromodulatorischen Informationen auf synaptische Konnektom-Karten bei der Erforschung von Nervensystemen. Der Ganzkörper-EM-Datensatz von *Platynereis* lieferte Beweise für die Stereotypie der Anatomie und Funktion der neuronalen Schaltungen zwischen Individuen der gleichen Spezies. Er stellt außerdem eine Datenbank dar, aus der in naher Zukunft ein Ganzkörper-Konnektom rekonstruiert werden kann.

SUMMARY

Animal nervous systems are complex networks of connections between diverse types of neurons and effector tissues. Mapping the connections of molecularly identified neuron types at the synaptic level would greatly enhance our understanding of the structure and function of the nervous system. Synapse-level studies require high-resolution analysis, and the technique that delivers the strongest resolving power to date is electron microscopy (EM) [1].

In this thesis, I created a large serial EM dataset for neuronal network analysis, circuit reconstruction and stereotypy studies in the nervous system of the larvae of the marine annelid *Platynereis dumerilii.* I also developed an innovative method to assign molecular identities to peptidergic neurons directly in the EM dataset.

I used serial-section transmission electron microscopy (ssTEM) combined with serial multiplex immunogold labeling (siGOLD) to molecularly identify multiple different neuron types. siGOLD is the labeling of subsets of sections with various antibodies to reveal the molecular identities of specific neurons. Taking advantage of the high immunogenicity of neuropeptides and their broad distribution throughout the axons, I used neuropeptide antibodies to establish the siGOLD method. I demonstrate the effectiveness of siGOLD by using 11 neuropeptide antibodies on a full-body larval ssTEM dataset of a *Platynereis* larva. siGOLD labeling allowed me to specifically label several distinct types of peptidergic neurons throughout the larval body. siGOLD was also applied in the reconstruction of a peptidergic circuit comprising the sensory nuchal organs that express the circadian neuropeptide pigment-dispersing factor (PDF). This approach enables the direct overlaying of chemical neuromodulatory maps onto synaptic connectomic maps in the study of nervous systems. The full-body *Platynereis* EM dataset provided evidence for stereotypy between neuronal circuit anatomy and function in individuals of the same species. It also provided a database that can be reconstructed into a full-body connectome in the near future.

PUBLICATIONS INCORPORATED IN THE THESIS

N Randel *, R Shahidi *, C Verasztó, LA Bezares-Calderón, S Schmidt, G Jékely:

Inter-individual stereotypy of the *Platynereis* larval visual connectome.
Elife. 2015; **4**:e08069

<div align="right">* Contributed equally</div>

R Shahidi, EA Williams, M Conzelmann, A Asadulina, C Verasztó, S Jasek, LA Bezares-Calderón, G Jékely:

A serial multiplex immunogold labeling method for identifying peptidergic neurons in connectomes.
Elife. 2015; **4**.

LIST OF ABBREVIATIONS

5

Catmaid	Collaborative annotation toolkit for massive amounts of image data
CLEM	Correlative light and electron microscopy
DCV	Dense core vesicle
dpf	Days post-fertilization
DTI	Diffusion tensor imaging
EM	Electron microscopy
FS	Freeze substitution
HPF	High-pressure freezing
IF	Immunofluorescence
IN	Interneuron
MN	Motorneuron
MRI	Magnetic resonance imaging
PDF	Pigment dispersing factor
PRC	Photoreceptor cell
siGOLD	Serial multiplex immuno-gold
smGFP	Soluble-modified green fluorescent protein
ssTEM	Serial section transmission electron microscopy
TEM	Transmission electron microscopy
VNC	Ventral nerve cord

INTRODUCTION

Connectomics: Mapping the neuronal connections

Nervous systems can be intricate, with hundreds of different cell types, and billions of different connections between them [2]. Understanding the structure of neuronal circuits, including the complex branching and connection patterns of neurons is essential to understanding how the nervous system functions. Ever since the work of Santiago Ramón y Cajal, who showed the interconnected polarized organization of nerve cells [3,4], it has been acknowledged that function and neural connectivity are interrelated [5]. Large-scale and low-resolution mapping of connectivity in the brain is now possible via several approaches, including magnetic resonance imaging (MRI), diffusion tensor imaging (DTI), or the Brainbow technique [6–9].

However, low-resolution imaging is not sufficient, since neurons interact by electrical and chemical means through synapses [10], and the definitive goal of connectomics is to map the precise nature of neuronal projections and synaptic connections in large blocks of neural tissue at the synapse level [11,12]. Such dense synapse-level connectomics is very challenging, because synapses and fine neuronal processes are very small (in the nanometer range) and not always resolvable by light microscopy. Synapse-level circuit mapping therefore requires the use of electron microscopy (EM).

Utility of ssTEM in synapse-level connectivity and circuit analysis

Reconstruction of dense neural circuits and interpreting convolutions of morphologically fine, long, thin, densely packed arbors with synapses along their length requires high resolution [13–16](Figure 2C). To date, the highest achievable resolution with detailed ultra-structural context is through the use of an electron microscope [5]. No other instrument has come close to matching the resolving power of EM. Transmission electron microscopy (TEM) has proven valuable to cellular biologists and continues to produce the most detailed image results at ultrastructural levels [17]. TEM sections can be easily examined, where with only a couple of heavy metal stains, such as uranyl acetate and lead citrate, almost all cellular membranes and intracellular organelles are contrasted and made visible [18]. At high-

resolution, distinct membranes and synapses are readily observable (Figure 2C). TEM sections allow direct access to subcellular structures for protein immunolocalization studies (Figure 2B), they allow for examination of a relatively large specimen area of homogeneous thickness, and the sections are storable for later screening.

The most challenging part of a TEM study is specimen preparation [19]. Samples must be fixed and embedded for serial sectioning. The samples are very thinly sliced [20] and for the examination of large blocks of neural tissue, it is imperative that no sections are lost. Recent advances in EM, however, have improved resolution, decreased section loss while allowing for thinner slices, and made automated data collection possible [5]. Ultramicrotome, the instrument that allows for thin slicing of specimens, has also greatly improved and new protocols for better serial and 'ribbon' sectioning have been implemented [18,21].
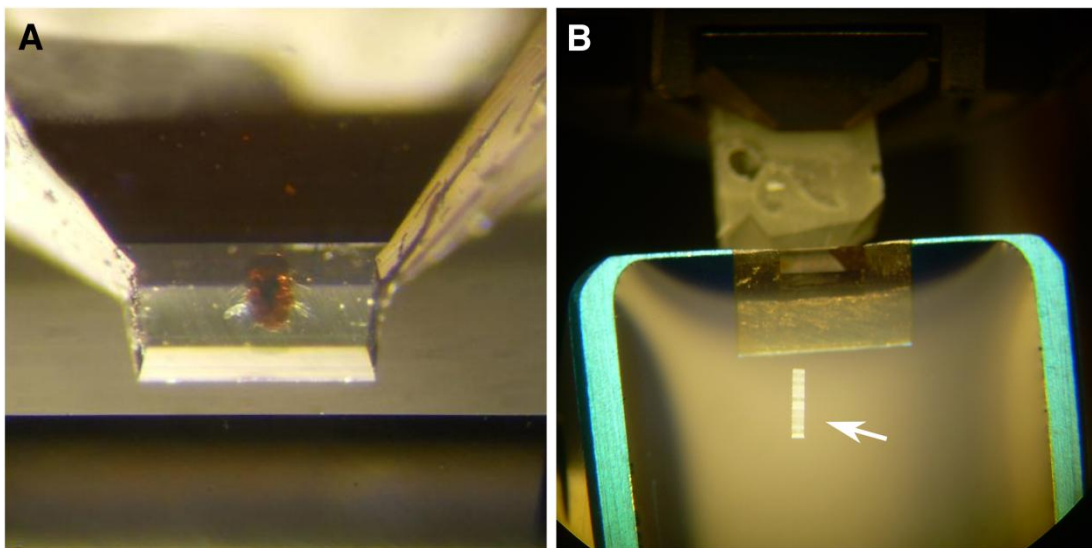
Figure 1: Ultramicrotomy and serial 'ribbon' sectioning.

(**A**) Trimmed Epon-resin block with a 3 dpf *Platynereis* larvae embedded inside, ready for sectioning. (**B**) A serial ribbon of 17 sections for collection, on the water surface in the boat of the diamond knife (arrow).

There is an elaborate workflow in obtaining TEM datasets for connectomic studies. The mode of fixation and processing of the tissue specimen is crucial for the success of the ensuing sectioning, imaging, and analysis. For example, high-pressure freezing (HPF) followed by freeze substitution (FS), as opposed to chemical fixation, was shown to provide the best tissue

preservation for connectomics [22–25]. For serial studies, the processed tissue blocks are sequentially sectioned with a diamond knife (Figure 1A & 1B) on an ultra-microtome and mounted on EM grids. Sections on grids can then be stored, pending relevant treatments and contrasting protocols before imaging.

A TEM with a digital camera and image acquisition software, such as SerialEM [26], is used for imaging. Once they are all collected, serial images are digitally montaged and aligned into a traceable serial stack. Tracing software such as Catmaid [27] is then used for neuronal circuit reconstruction and building of connectomes. (Figure 2A)
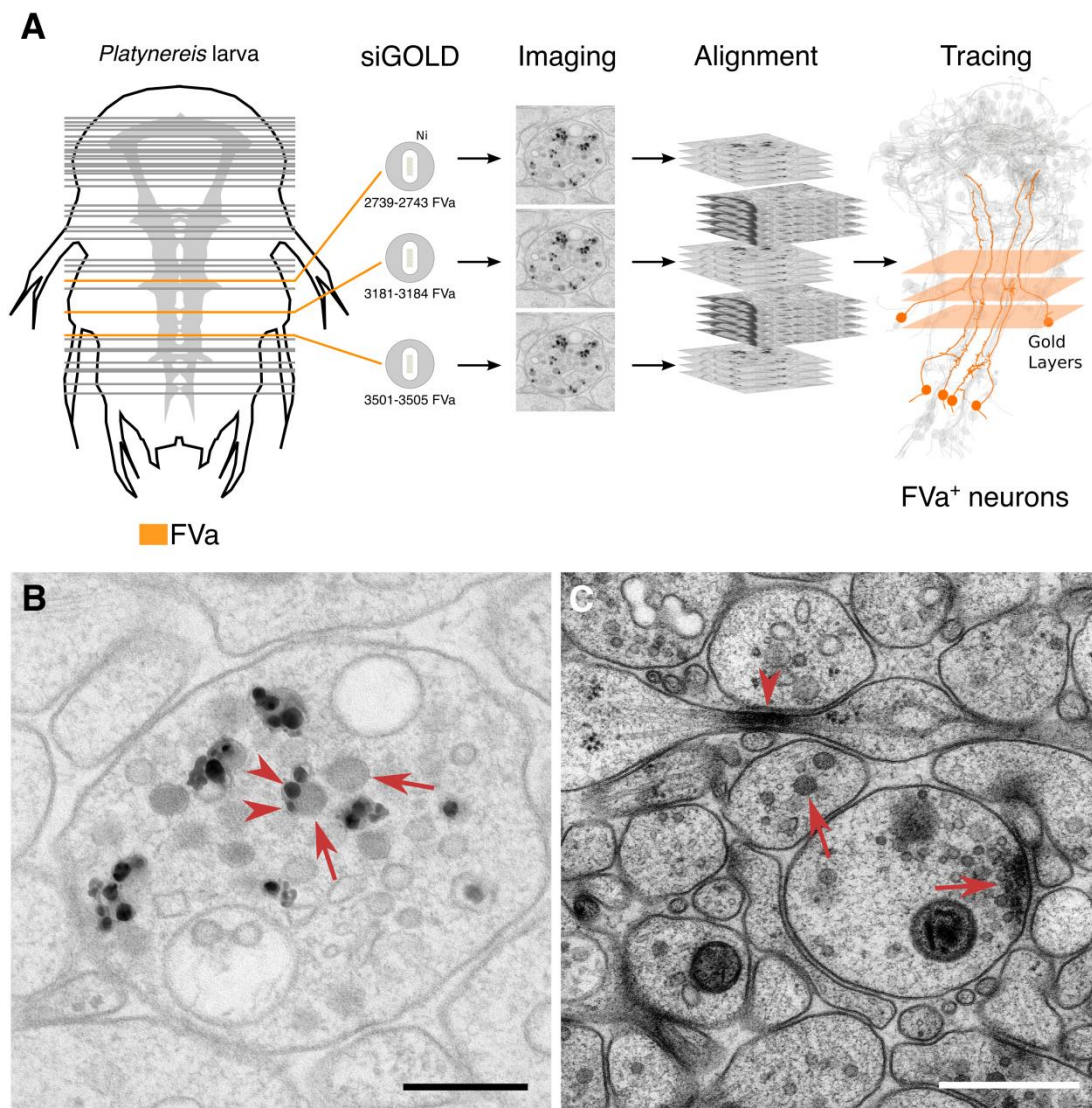

Figure 2: ssTEM and ImmunoEM on *Platynereis* larva

(**A**) A schematic workflow of siGOLD using FVa neuropeptide antibody on 3 dpf *Platynereis* larvae, from serial sectioning to neuronal reconstruction. Serial sections collected from three different areas of the ventral nerve cord (VNC) are immunogold labeled, imaged, serially aligned, and reconstructed. (**B**) A high-resolution TEM micrograph of a FVa labeled axon cross-section, showing silver-enhanced gold particles (arrowheads) inside the dense-core vesicles (DCVs) (arrows). (**C**) A counter-stained TEM micrograph showing ultrastructure of neurons in the *Platynereis* ventral nerve cord. Neuron profiles contain many types of vesicles, vesicle densities and/or synapses (arrows). Neurons could become very narrow and thin along their length, collapsed around the microfilaments (arrowhead). Scale bar in B: 0.2µm; C: 0.5µm

Methods that combine ssTEM and molecular identification of neurons

EM images provide a rich source of information about neuronal ultrastructure. However, micrographs alone do not reveal the molecular nature of neurons and their synapses to complement the connectome. To fully understand nervous system function, we need to know the neurotransmitters, receptors, channels, neuromodulators and other types of molecules that are expressed in each neuron that is represented in a connectome map.

Several methods have been developed to assign molecular identities to neurons in EM images. For example, genetically encoded protein tags [28,29], virus injection [30], fluorescent protein tags by correlative light and electron microscopy (CLEM) [31–37], array tomography [11,38], or even direct immunogold labeling of transgenically expressed reporters (e.g., smGFPs) [39]. However, many of these techniques rely on transgenic markers, or proteins that need to be expressed in specific neurons [40]. Other techniques, such as array tomography or CLEM, require registration and alignment of immunofluorescent (IF) images with EM images [11,38]. Many of the available methods compromise ultrastructural preservation and membrane contrast of EM sections [11], and often lack the synapse-level resolution for reliable circuit reconstruction. Therefore, a more direct identification method at high resolution is required in order to assign molecular identities to neurons in connectome datasets.

Immunogold labeling for electron microscopy has been in use for more than half a century and allows for the direct visualization of labeled proteins [41]. Antibodies conjugated to gold particles used for labeling will appear as electron dense dots on EM sections (Figure 2B). However, it has been difficult to combine immunoEM with connectomics, because large-scale ssTEM projects usually rely on embedding the tissue in epoxy resins (e.g.,

Epon). Such resins provide better stability during sectioning and show optimal ultrastructural preservation while imaging [42–47]. Unfortunately the Epon-embedding procedure, namely osmium-fixation and resin polymerization, compromises the viability and in particular, the immunogenicity, of many endogenous targets [48–50].

A class of molecules that show good immunopreservation after EM processing are neuropeptides [51–54]. Neuropeptides are short amino acid sequences that act as signaling molecules in neuronal circuits and shape circuit activity [55]. They are initially synthesized as inactive propeptides that are cleaved and chemically altered in the Golgi complex to yield smaller biologically active peptides [56–58].

Neuropeptides are packaged inside dense core vesicles (DCV) at the Golgi apparatus and the DCVs are transported by microtubules to their release sites [59–62]. Some neurons express multiple neuropeptides, which can be packaged in the same DCVs [63,64]. Chemical modifications, such as C-terminal amidation [65], can make short peptides more stable and immunogenic [65–67]. Moreover, neuropeptides show neuron-type specific expression and are distributed throughout the axons, which makes them useful identifiers [61,68]. Mapping specific neuropeptides to their corresponding neurons at synaptic level would greatly improve connectomics and thus enhance our understanding of circuit function. In *Drosophila melanogaster*, for example, the circadian clock is controlled by endogenous pacemaker neurons [69], and the neuropeptide pigment-dispersing factor (PDF) is an important output signal from these neurons [70]. A recent study, using postembedding immunoEM, has described the subcellular morphology of these PDF-positive neurons and reconstructed their neural circuits in *Drosophila melanogaster* [54].

In this thesis, I characterize the utility of a postembedding serial multiplex immunolabeling technique with several neuropeptide antibodies on a whole-body ssTEM dataset and describe peptidergic circuits based on the tracing and reconstruction of serially labeled neurons (Figure 3 & 2A).
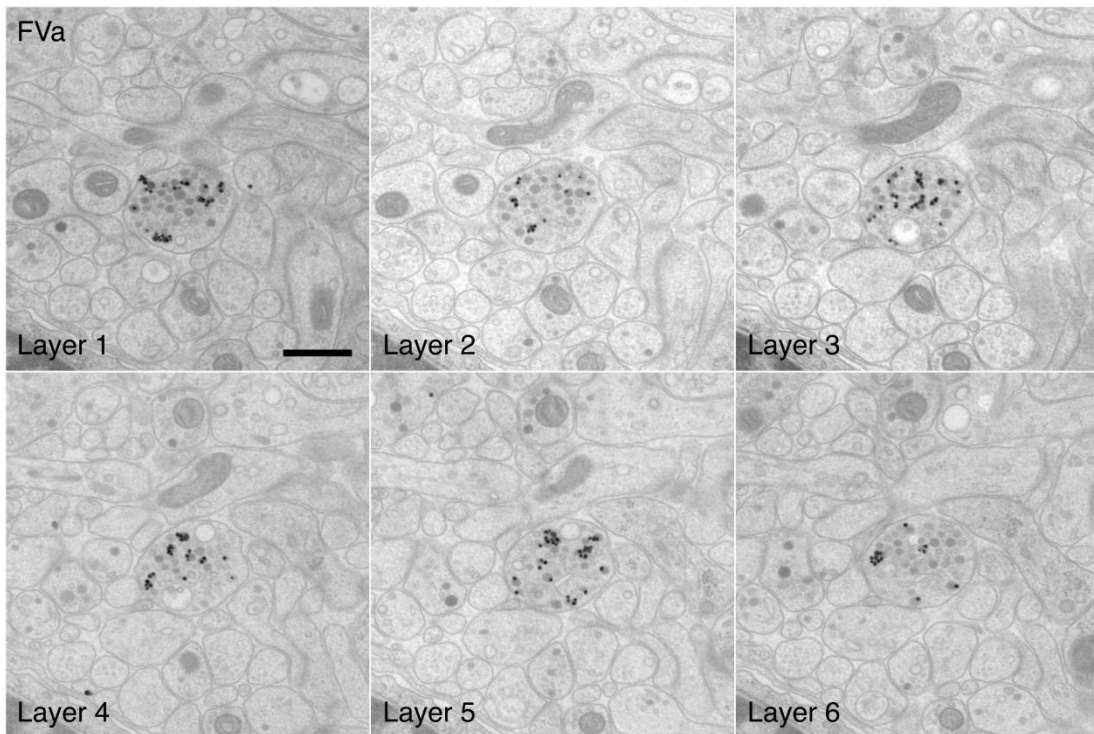
Figure 3: Immunolabeling on serial Epon sections.

Representative micrographs of serial immunogold labeled FVa-positive peptidergic axon cross-sections; six adjacent sections are shown (FVa Layer 1–6). Scale bar: 0.5μm.

Circuit neuroscience, stereotypy, and whole-body connectomics

The main goal of circuit neuroscience is to decipher the computational logic of circuits and how structure relates to function [71–73]. A potential criticism of the connectomics approach is that circuits will be shaped by activity and experience, therefore mapping them in precise detail in one individual will circumvent generalizations. It is therefore of interest to find the extent to which neuronal circuits are hard-wired or variable between individuals. To answer this question would require comparison of connectomic maps of the same circuit from different individuals of the same species.

In our stereotypy study of the eye circuit connectomes, we compare the two *Platynereis* larvae at synaptic and circuit levels. This analysis was possible by the creation of the second ssTEM dataset and it confirms the benefit of extra serial EM datasets for connectome projects

Platynereis dumerilii, an emerging lab-model for circuit neuroscience

In terms of the complete animal nervous system atlas and large serial section electron microscopy studies, *C. elegans* has long been the only animal with a

fully mapped connectome [47,74,75]. The revolution in EM and computer technology has sparked new interest in connectomics and currently several large-scale projects are underway. Animal models where we already have or will soon have large-scale connectome datasets include the *Drosophila* first instar larva [76–78], and the mouse [79,80].

However, reconstructing the complete neuronal circuitry of an entire animal is still very challenging and labor intensive [5,72,81]. Therefore, the choice of specimen is crucial [72,81,82], since imaging resolution and data volume are key factors that must be considered.

For my thesis, I used the nectochaete larval stage of the marine annelid *Platynereis dumerilii*. At ~ 250 µm length, this specimen is only one quarter of the size of *C. elegans*, has approximately 95% less neurons than the *Drosophila* brain, and is about 12,000 times smaller, in volume, than the mouse brain [72]. *Platynereis* has recently emerged as a powerful model for circuit neuroscience, genetics, and whole-body connectomics [83–87]. The relatively small size of a *Platynereis* larva allows for its full ssTEM reconstruction in a comparatively short time. Despite its small size, this larvae exhibits several distinct complex behaviors [88–91]. It also harbours molecularly identified neurons with signaling molecules and regulatory hormones, such as neuropeptides and hundreds of neuropeptide complements, that are conserved across many phyla [89,92–94]. Also, the *Platynereis* larval brain contains simple sensory-motor cells, visual eyes, and several other sensory organs, including a chemosensory apical organ, a pair of nuchal organs, ciliary bands, and a complex musculature for locomotion[89,90,95]. These larvae have also been extensively used to study zooplankton behavior [90]. The larval visual circuit, as it relates to phototactic behavior, and its visual connectome stereotypy to another *Platynereis* individual are the traits I will discuss in my thesis [85]. Hence, *Platynereis* is a promising organism for connectomics and behavioral studies.

AIM OF THE THESIS

The comprehensive study of nervous systems requires knowledge of the precise connectivity of neurons. The biggest challenge in mapping neuronal networks is to resolve neural connectivity at synapse-level, in an approach called cellular connectomics [5,96].

For my thesis, I worked on establishing resources and technologies for cellular connectomics in the marine annelid *Platynereis dumerilii*. The first aim was to generate a whole-body EM dataset of the larval stage of this animal to be used for reconstruction of neuronal circuits. The second aim was to identify neurons by direct molecular labeling in the generated serial EM dataset. I worked on establishing an immunological labeling technique to tag neuropeptides directly on EM sections, allowing the identification and reconstruction of diverse peptidergic neurons and their circuits at high resolution. I propose that the methods I have established in my thesis can be adapted to create similar protocols in nervous system of other organisms.

RESULTS

Summary of Publication 1

N Randel *, R Shahidi *, C Verasztó, LA Bezares-Calderón, S Schmidt, G Jékely:

Inter-individual stereotypy of the *Platynereis* larval visual connectome.

Elife. 2015; **4**:e08069

* Contributed equally

Similarity in behaviours between animals of the same species [97–100] is likely due to similarities in the structure and function of their neuronal circuits, established during the stereotypical process of neural development. Little is known, however, about stereotypical development at single neuron and synaptic levels [101]. Since examination of neuronal connections at the synapse level requires high resolution and ultra-structural detail, I carried out an electron microscopic (EM) study to explore the stereotypy of neural connectivity in depth.

The first larva that we used for ssTEM reconstruction of the visual eye circuit neuronal connectome, a nectochaete of the bilaterian marine annelid *Platynereis dumerilii*, encompassed the entire head and part of the first trunk segment. It consisted of 1,690 thin serial sections (40-50 nm) from an Epon-embedded 3 day post fertilization (dpf) larva imaged at 3.72 nm/pixel resolution. The eye circuit of this larva contained 71 neurons, with photoreceptors cells connecting via three layers of interneurons to motorneurons, which innervated the trunk muscles [85]. However, we could not establish the precise morphology of all innervations due to sectioning discontinuity in the trunk.

In this paper, I further expand our earlier eye circuit study by creating a full-body serial section EM dataset. Using classical and current knowledge in ultramicrotomy, I sectioned an entire 3 days-old *Platynereis dumerilii* larva into 5056 serial sections to create a whole-body EM data set. I used an ultramicrotome fitted with a diamond knife to cut sections of 40 nm thickness. I set a subset of 246 sections aside throughout the serial dataset for immunological experiments, but contrasted and carbon-coated all other

sections for imaging. I imaged all contrasted sections using an FEI TECNAI Spirit transmission electron microscope equipped with an UltraScan 4000 4X4k digital camera and image acquisition software Digital Micrograph (Gatan Software Team Inc., Pleasanton) and SerialEM [26]. The resolution of scanned images was 5.71 nm/pixel. Once the serial imaging was completed, I montaged and aligned the images into a digital stack, using TrakEM2 software [102]. Neurons, cellular structures and organelles of interest were traced, segmented, and 3D reconstructed using TrakEM2 and Catmaid software [27,102]. We identified and reconstructed 106 eye circuit neurons and their synaptic partners through the larval head and the body of *Platynereis*. From image reconstruction, synaptic connectivity between partner neurons was analyzed and circuit maps were established. Evidence is presented for similarities between individuals of the same species by comparing neuronal circuit anatomy and function.

Principally, cross-section detail revealed the disk-like nature of the larva's plexus, the symmetrical shape of the ventral nerve cord system, the overall length and shape of the nerve cells, and the morphology of many synapses. In this dataset, we traced the neuronal circuitry downstream of the visual eyes and of the larval eyespots. The visual eye circuit of the second larva consists of 106 neurons, plus several ciliated and muscle effector cells, compared to 71 neurons of the first larval eye circuit [85]. The full-body dataset allowed us to trace the projections of the ventral motorneurons (MN) in the trunk of the larva, a region that was not sectioned in the previous larva. This further tracing revealed the presence of more MN synapses to the trunk muscles.

Even though many of the neurons and circuits are still developing in the trunk of the young larvae, the new dataset provides all ciliated locomotor cells. This includes 23 prototroch cells, organized into an anterior ring and a posterior ring, formed by 11 cell pairs and one unpaired cell. Our analysis of the ciliary rings-MN connection revealed only the posterior band was innervated by the MN cells. These results confirm the cellular-level stereotypy of neuronal circuitry in *Platynereis* larvae and place the visual eye circuitry in a full-body context.

To test the stereotypy at synaptic level, we used several measures to compare patterns of connectivity between the two larval connectomes.

Results

Initially, we defined a grouped connectivity matrix and then correlated the two grouped matrices. We found a strong correlation between the two groups (Spearman's r=0.62, p=0.0001). Next, we calculated the geometric mean of the two connectivity matrices and generated a combined matrix with all major connections and reciprocal connections for more detailed comparison. We found the same strong correlation in both individuals.

Scoring the correlation of the synaptic maturation of the photoreceptor cells (PRC) with photoreceptor-cell rhabdom volume and axon length also revealed similar relationships in both larvae. To further test stereotypy, we examined correlation at single and group neuron level and at projection pattern of pre- and postsynaptic sites for each level between the two larvae. We found significant correlations between both pre- and postsynaptic submatrices for most neuron types and similar projection patterns and spatial distribution of pre- and postsynaptic sites between all neuron groups in both individuals.

We analyzed certain circuit elements in detail and found that the strongest connection for all eyes was from PRCs to the cross-wise primary interneuron (IN1). The analysis of the pre- and postsynaptic partners of the MN cells showed that synaptic stereotypy can be found at the single neuron level, and also applies to left-right asymmetric motifs in the network.

Our analysis shows that the visual eye connectome in *Platynereis* larvae has strong stereotypy both globally and at the single neuron level. We could demonstrate this for patterns of neural projections, synapse distribution along neurites, identity of synaptic partners, number of connections, and left-right asymmetries in connectivity.

We also fully reconstructed the neuronal circuitry of the larval eyespots in the new larva. The larval eyespots develop in early trochophore larval stages and mediate positive phototaxis in early larval stages by innervating adjacent ciliary band cells [90]. In trochophore larvae (1-2 dpf) each larval eyespot consists of one pigment cell and one photoreceptor cell, the latter of which expresses a rhabdomeric opsin. A preliminary ssTEM analysis in the first larva identified a second photoreceptor cell with an axon projecting towards the brain neuropil, indicating changes in eyespot structure during development.

Here, we have fully reconstructed the neuronal circuitry downstream of both eyespot photoreceptor cells. The two eyespot PRCs connect to very distinct downstream circuitries, suggesting functional specialization.

The connectome of the eyespots suggests that both PRCs share the same effectors with the visual eyes, yet connect to these effectors by distinct circuitry. The eyespots are not able to mediate phototaxis at 3 dpf [85], but their continued connection to the visual eye circuit suggests that they may play a role in modulating phototaxis or mediating a distinct sensory-motor response.

Results

Summary of Publication 2

R Shahidi, EA Williams, M Conzelmann, A Asadulina, C Verasztó, S Jasek,
LA Bezares-Calderón, G Jékely:

A serial multiplex immunogold labeling method for identifying peptidergic neurons in connectomes.

Elife. 2015; **4**.

Neurons pass molecular information to one another by connecting through synapses. A complete view of how the nervous system functions requires precise understanding of the neuronal connectivity and all the specific molecular expressions of each neuron. Exactly what molecular information is exchanged between neurons to elicit certain behaviors in an organism is largely unknown [10,103]. The challenge of connectomics is to map the synapse-level connectivity of entire neural circuits [13]. However, wiring diagrams alone cannot provide a complete picture of the nervous system, since they do not indicate the molecular nature of neurons.

Neuromodulators, including neuropeptides, actively modify the expression of neuronal circuits at synapse level with respect to their output [104–107]. To reveal the neuropeptidergic complement of different neurons, I began to investigate the morphology and molecular nature of neurons in the nervous system of the larvae of *Platynereis*.

I used the same sectioned full-body ssTEM dataset of a 3 dpf *Platynereis* larva, derived from the same larval batch as previously used [85], and imaged 5056 sections with conventional transmission electron microscopy (TEM), as described in more detail in the first summary. It has been demonstrated that neuropeptides are useful markers for neuron-type identification, since they show specific expression and are sparsely distributed along axons [61,68]. It is also known that colloidal gold particles conjugated to secondary antibodies make useful tags for visualization with EM [41]. I reasoned that ImmunoEM performed on only a few selected layers from a large series of EM sections could identify individual neuron profiles that contain specific neuropeptide antigens.

For my thesis work, in order to identify peptidergic neurons, I developed a method to immunogold label a selected number of sections throughout the

serial EM data set. By doing so, only a random sample of neuron population was necessary for testing against a particular antibody. I named this method 'siGOLD' or serial-multiplex immunogold. siGOLD is 'multiplex' in that, one can simultaneously identify multiple peptidergic neurons within the same serial data set (Figure 3). Unlike other labeling techniques, this method allows for the direct labeling of antigens on the surface of EM serial sections. No further alignment at high resolution is necessary to match the labeled antigen to the target cell or membrane, as in CLEM or IF. The only alignment necessary is to replace the siGOLD labeled layers back in the serial EM stack.

Short amidated neuropeptides survive the EM process inside DCVs

Epoxy resins are known for their durability during sectioning and for the better image contrast they provide in EM [42–47]. Unfortunately, embedding, osmication, and curing procedures restrict and sometimes completely destroy the immunogenicity of many antigenic targets [48–50]. The quest in ImmunoEM has always been to strike a balance between improved antigen detection sensitivity and optimal ultra-structural tissue preservation [24,108]. Current techniques are thus not conducive to optimal immunolabeling. However, some antigens, neurotransmitters, and neuropeptides highly concentrated inside secretory vesicles do survive the harsh EM processing treatment [109]. One such example is short amidated neuropeptide antigens in dense core vesicles (DCV) that show good immunopreservation when embedded in epoxy resins [51–54]. These amidated neuropeptides are potential antigenic candidates for finding specific peptidergic neurons with EM and therefore combining ImmunoEM and connectomics.

I established an ImmunoEM procedure to label ultrathin sections with neuronal-type specific antibodies. I devised this method with a class of neuropeptide antibodies that were successfully tested on whole-mount *Platynereis* larvae at light microscope level. I also developed a safe procedure for parallel multiple EM grid handling during the immunolabeling and contrasting protocol. To optimize immunolabeling, I used secondary antibodies coupled to ultra small gold particles combined with a silver-enhancement protocol [110].

Results

In preliminary siGOLD tests, I found strong and localized labeling in a small subset of neurites using 11 different polyclonal antibodies generated against short amidated neuropeptides of *Platynereis*. To test the specificity and reproducibility of this method, I labeled two grids separated by a serial distance of approximately 50 sections with each of the 11 neuropeptide-antibodies. I found that the same specific antibody labeled the same set of neurites, regardless of the serial distance. Also, in consecutive sections, the same neurite was often strongly labeled with the same antibody. Many of the gold-labeled neurite sections had dense core vesicles (DCVs) in their cytoplasm, as evidenced by their peptidergic nature. At high-resolution I could observe gold labeling associated with DCVs, suggesting that siGOLD labeled mature neuropeptides packed inside these vesicles.

Specificity of gold labeling in immunoEM is quantifiable [111–113]. I scored the distribution of gold particles in the ventral nerve cord (VNC) series for each antibody. The quantifications revealed a high neurite-specificity of immunogold labeling for all 11 neuropeptide antibodies. Also, I could identify a small number of neurites that consistently showed strong labeling across different sections for each antibody. The labeling pattern of the neurites in the VNC showed the labeling of specific peptidergic neuron populations on both the left and the right sides of the body, supporting bilateral symmetry of this larva.

Gene knockdowns are often used as a method to reduce the cellular expression of certain proteins [88,114,115]. To test the specificity of neuropeptide antibodies used in immunolocalization, morpholino-mediated knockdown experiments of proneuropeptide expression were used followed by immunofluorescent staining on whole-mount 3 dpf larval samples. 80% of the knockdowns showed reduction in IF signal, which confirmed the specificity of the neuropeptide antibody labeling.

I also analyzed the labeling of all 11 antibodies on whole-mount *Platynereis* 3 dpf larval samples, to determine whether the spatial arrangement of peptidergic neurites were consistent between siGOLD and IF labeling of whole specimens. All antibodies labeled distinct subsets of longitudinal neuronal tracks spanning the VNC and occurred in various mediolateral positions. Overall, the arrangement of peptidergic axons in the VNC reconstructed by siGOLD was similar to that in the VNC reconstructed by IF.

Results

The specificity and the reproducibility of ImmunoEM labeling across the serial dataset, and the spatial correspondence between siGOLD and whole-mount IF labeling corroborates the accuracy of peptidergic neuron identification in a serial EM dataset.

To test the scalability of siGOLD, I applied this method to the whole-body EM series encompassing the entire 3 dpf *Platynereis* larva. In a whole-body context, immunogold labeling allows for identification and reconstruction of complete neurons or circuits. To this end, I identified and traced several neurons with different peptidergic identities.

As in the test larva, I mapped the distribution of peptidergic axons using the 11 antibodies across the first trunk segment of the whole-body larva and compared it to the distributions in the preliminary test and the IF samples. Again, I found similar patterns across both siGOLD-labeled larvae and the IF samples. For selected neurons, I quantified the number of gold particles in every immunolabeled section. These counts demonstrated that the same neurons could be repeatedly labeled in different sections, often spaced several hundred sections apart. siGOLD also allowed the detection of neuropeptide coexpression in several neurites. Neuropeptides have previously been shown to co-localize in neuroscecretory granules [116].

The reconstruction of several neurons in the whole-body serial EM dataset allowed the further test of the specificity of the immunogold labels by comparing the morphology and position of reconstructed neurons to neurons that were identified by whole-body IF. I found comparable cellular morphologies and positions for six FVamide-positive, several PDF-positive, two RGWamide-positive, and four MIP-positive neurons between siGOLD and IF. These similarities further support the specificity of siGOLD in identification and reconstruction of peptidergic neurons from whole-body serial EM data.

To further illustrate this point, in my thesis work I fully reconstructed several peptidergic neurons identified by siGOLD in the *Platynereis* larva. In addition to the reconstruction of the larval eye circuits, which showed stereotypy between individual *Platynereis* 3 dpf larvae [46], the nuchal organs and their postsynaptic partners were identified by siGOLD and reconstructed. The nuchal organ is a paired putative chemosensory organ in the annelid head with sensory neurons projecting a sensory dendrite into an olfactory pit

[117,118]. They are varied amongst annelids and sometimes show great structural complexity [117–120]. I found several sensory neurons of the nuchal organs that were strongly labeled by the PDF antibody in three different PDF-labeled sections in the head. Mapping part of the circuit for the nuchal organs revealed a potential functional path linking them to the neuronal circuit for locomotion and the eye circuit [46].

Overall, this study demonstrates that siGOLD can be used in large serial EM datasets to assign molecular identities to multiple peptidergic neurons using different markers and to fully reconstruct and analyze the synaptic connectivity of these neurons at EM resolution. The mapping of neuro-chemical circuits together with synaptic connectivity circuits open up new avenues for the study of nervous systems in *Platynereis* and possibly in other marine invertebrates.

DISCUSSION AND CONCLUSION

EM based comparative connectomics

The development of the *Platynereis* larval nervous system is highly stereotypic [121]. By reconstructing the visual eye circuitry of a second *Platynereis* individual and comparing it to the first larva at the electron microscopic level, we found a high degree of inter-individual stereotypy in the two connectomes at every level of analysis.

Here, the stereotypy of neuronal projections and synaptic connectivity based on ssTEM reconstruction and anatomical comparisons was demonstrated. The two individuals are not identical; and not every neuron at single-cell level was compared. The observed differences may be due to developmental variation or technical variation. This study also demonstrates the benefit of a second dataset when employing an ssTEM approach. Inter-individual comparisons can increase the confidence in weak or asymmetric motifs. In *Platynereis*, the different sensory-motor circuits of the visual eye PRCs and eyespot PRCs show different levels of complexity. We identified examples for all degrees of sensory-motor contact, from direct sensory-motor innervation through sensory-MN to sensory-IN-MN. The fine gradations in the connectome of the *Platynereis* larval and visual eyes suggest that circuit evolution may have proceeded through the intercalation of new layers of neurons between sensors and effectors.

The overall gross anatomy and cell complement of the two larval eye circuits are very similar. All cell types and groups of cells that were described in the first larva, showed similar overall anatomical arrangement in the second larva. In addition, the gross anatomy and cell complement of some cell types, such as interneurons (IN) and some MNs, could be correlated at a single cell level in the two larvae.

Overall, this study shows that the visual eye connectome in *Platynereis* larvae has strong stereotypy both globally and at the single neuron level. We could demonstrate this for patterns of neural projections, synapse distribution along neurites, identity of synaptic partners, strength of connections, and left-right asymmetries in connectivity.

23

ImmunoEM identification of peptidergic neurons in an annelid's nervous system

Platynereis dumerilii is a marine annelid of the bilaterian superphylum lophotrochozoa with a pelagobenthic biphasic life cycle [122]. *Platynereis* larvae have a small yet relatively complex nervous system with several thousand neurons. To fully understand the nature of such a nervous system, a comprehensive map of its neuronal pathways, synaptic connections and function is requisite [11,12]. Nervous system function requires more than just neuronal connectivity; it also requires the expression of specific sets of molecules by each neuron type that confers unique neuronal identities. But current approaches fall short in simultaneously mapping both synaptic connectivity and the molecular identity of neurons.

In my thesis, I introduce a method that combines serial multiplex immunogold labeling (siGOLD) and serial-section transmission electron microscopy (ssTEM) to identify multiple peptidergic neurons in a connectome at high resolution. To do this, first I created a large EM serial dataset, which I placed into a traceable database. I then used antibodies against short amidated neuropeptide antigens to tag and identify peptidergic neurons. Neuropeptides have some useful characteristics with respect to ImmunoEM. They have a small size, occur in high abundance, are packed inside dense core vesicles (DCV), are distributed throughout the length of axons due to their active circulation [61], show good immunopreservation after EM processing [51–54], and are frequently amidated at their C-terminal, which increases their stability and immunogenicity as mature neuropeptides [65,67]. Through my thesis work, I also found that neuropeptide immunoreactivity lasts years after sectioning. Although I did not test other antibodies, several generic antibody markers, including antibodies against neurotransmitters, transporters, or enzymes [11], could in principle be suitable for neuron identification using siGOLD.

I established siGOLD on Epon-embedded samples that allowed robust sectioning of thousands of sections and provided high ultrastructural detail. Although Epon-embedding is known to compromise the immunogenicity of some antigens [48–50], labeling for such antigens could be carried out with

alternative embedding resins such as Lowicryl HM-20 that provide excellent ultra-structural contrast and are compatible with many antibodies [11].

siGOLD relies on the direct immunoEM labeling of sections, it takes full advantage of the resolving power of the electron microscope and no registration step is required. With siGOLD it is possible to use an arbitrarily large number of antibodies on different sections from a series that encompasses a large volume of tissue, allowing the multiplex identification of neuron types. siGOLD does not rely on the staining of every section with multiple markers, but rather the staining of sparsely distributed sections with one marker each. I was also able to identify individual DCVs that carried strong immunogold signal in the neurite profile of specific peptidergic neurons.

We reconstructed a candidate chemotactic circuit, the sensory neurons of the nuchal organs and their postsynaptic partners, in the *Platynereis* larval head. The presence of DCVs and lack of clusters of clear vesicles at presynaptic sites in these neurons suggest the presence of peptidergic transmission to the target interneurons. The molecular information obtained by siGOLD provides a rich base for the genetic investigation of this putative chemotactic circuit in *Platynereis*. In total, I identified 83 different peptidergic neurons out of approximately 2000 total neurons in the *Platynereis* whole-body dataset. I demonstrated that siGOLD can be used to molecularly identify neurons in large serial EM datasets. Further connectome tracing in these data will provide a rich source of information about specific peptidergic circuit motifs in this animal.

Utility of siGOLD method across species

Mapping of peptidergic neurons by siGOLD, together with the recent identification of several neuropeptide receptors in *Platynereis* [123], unlocks the possibility of a cellular-level analysis of peptidergic neurotransmission in diverse *Platynereis* neural circuits.

The siGOLD approach and the use of neuropeptide antibodies could also be adapted to enrich connectomic data with molecular information in other organisms. In *Platynereis*, as well as vertebrates, *C. elegans*, and *Drosophila*, the majority of mature neuropeptides are amidated [94,124], and several antibodies are available [125,126] or could readily be generated.

Some neuropeptide antibodies have already been shown to work with immunoEM. For example, PDF neuropeptide-containing neurons were identified in the *Drosophila* brain by immunoEM and their local synaptic inputs were reconstructed from a series of sections [54]. This and other antibodies could be used for siGOLD labeling in larger-scale connectome projects in *Drosophila*. Similar protocols and reagents could be established for other organisms. siGOLD could also be adapted to organisms where transgenic tools to deliver EM-compatible markers are not available. In such organisms, the use of cross-species antibodies [67,126] is a promising approach that would also allow the comparison of specific peptidergic neurons and their circuits across species. The bilateral projections of the nuchal organ sensory neurons in *Platynereis*, for example, are similar to that observed in *Drosophila* olfactory receptor neurons. In Drosophila, these receptor neurons form bilateral projections, and the lateralization of odor processing is achieved by an asymmetry in neurotransmitter release [127]. The *Platynereis* nuchal organ circuit may use a similar computational strategy, and this is likely different from the processing of visual information [46,85].

Conclusion

How do information relay, molecular expression, and patterns of activity in nervous systems induce the sensing of cues and corresponding behavioral responses [128]? Even after detailing a comprehensive connectomics map, much work is needed to decipher its 'real-time' function and translate it into behavioral decisions made by an animal [71,129].

In my thesis, I created a large serial EM dataset for ultrastructural studies of the nervous system in *Platynereis dumerilii.* I also established siGOLD as a method to assign molecular identities to multiple specific neurons based on immunogold labeling subsets of sections in large serial EM datasets and to allow full reconstruction and analysis of the identified neuronal circuits. The combined chemical neuromodulatory maps and synaptic connectivity maps of siGOLD open up a plethora of information about nervous systems and lay the groundwork for full body connectomics studies.

BIBLIOGRAPHY

1. Mikula S, Denk W: **High-resolution whole-brain staining for electron microscopic circuit reconstruction**. *Nat. Methods* 2015, **12**.

2. Masland RH: **Neuronal cell types.** *Curr. Biol.* 2004, **14**:R497–500.

3. De Carlos JA, Borrell J: **A historical reflection of the contributions of Cajal and Golgi to the foundations of neuroscience**. *Brain Res. Rev.* 2007, **55**:8–16.

4. Peters A: **Golgi, Cajal, and the fine structure of the nervous system.** *Brain Res. Rev.* 2007, **55**:256–63.

5. Lichtman JW, Denk W: **The big and the small: challenges of imaging the brain's circuits.** *Science* 2011, **334**:618–23.

6. Mori S, Oishi K, Faria A V: **White matter atlases based on diffusion tensor imaging.** *Curr. Opin. Neurol.* 2009, **22**:362–9.

7. van den Heuvel MP, Hulshoff Pol HE: **Exploring the brain network: A review on resting-state fMRI functional connectivity**. *Eur. Neuropsychopharmacol.* 2010, **20**:519–534.

8. Livet J, Weissman TA, Kang H, Draft RW, Lu J, Bennis RA, Sanes JR, Lichtman JW: **Transgenic strategies for combinatorial expression of fluorescent proteins in the nervous system.** *Nature* 2007, **450**:56–62.

9. Weissman TA, Pan YA: **Brainbow: new resources and emerging biological applications for multicolor genetic labeling and analysis.** *Genetics* 2015, **199**:293–306.

10. Pereda AE: **Electrical synapses and their functional interactions with chemical synapses**. *Nat Rev Neurosci* 2014, **15**:250–263.

11. Collman F, Buchanan J, Phend KD, Micheva KD, Weinberg RJ, Smith SJ: **Mapping synapses by conjugate light-electron array tomography.** *J. Neurosci.* 2015, **35**:5792–807.

12. Beyer J, Al-Awami A, Kasthuri N, Lichtman JW, Pfister H, Hadwiger M: **ConnectomeExplorer: query-guided visual analysis of large volumetric neuroscience data.** *IEEE Trans. Vis. Comput. Graph.* 2013, **19**:2868–77.

13. Morgan JL, Lichtman JW: **Why not connectomics?** *Nat. Methods* 2013, **10**:494–500.

14. Marblestone AH, Daugharthy ER, Kalhor R, Peikon ID, Kebschull JM, Shipman SL, Mishchenko Y, Lee JH, Dalrymple DA, Zamft BM, et al.: *Conneconomics: The Economics of Dense, Large-Scale, High-Resolution Neural Connectomics*. 2013.

15. Haehn D, Knowles-Barley S, Roberts M, Beyer J, Kasthuri N, Lichtman JW, Pfister H: **Design and Evaluation of Interactive Proofreading Tools for Connectomics**. *IEEE Trans. Vis. Comput. Graph.* 2014, **20**:2466–2475.

16. Helmstaedter M, Briggman KL, Denk W: **High-accuracy neurite**

reconstruction for high-throughput neuroanatomy. *Nat. Neurosci.* 2011, **14**:1081–8.

17. Winey M, Meehl JB, O'Toole ET, Giddings TH: **Conventional transmission electron microscopy.** *Mol. Biol. Cell* 2014, **25**:319–23.

18. Tapia JC, Kasthuri N, Hayworth KJ, Schalek R, Lichtman JW, Smith SJ, Buchanan J: **High-contrast en bloc staining of neuronal tissue for field emission scanning electron microscopy.** *Nat. Protoc.* 2012, **7**:193–206.

19. Oberti D, Kirschmann M a, Hahnloser RHR: **Projection neuron circuits resolved using correlative array tomography.** *Front. Neurosci.* 2011, **5**:50.

20. Albanese A, Chung K: **Whole-brain imaging reaches new heights (and lengths)**. *Elife* 2016, **5**.

21. Hoffpauir BK, Pope B a, Spirou G a: **Serial sectioning and electron microscopy of large tissue volumes for 3D analysis and reconstruction: a case study of the calyx of Held.** *Nat. Protoc.* 2007, **2**:9–22.

22. Studer D, Humbel BM, Chiquet M: **Electron microscopy of high pressure frozen samples: bridging the gap between cellular ultrastructure and atomic resolution.** *Histochem. Cell Biol.* 2008, **130**:877–89.

23. Studer D, Zhao S, Chai X, Jonas P, Graber W, Nestel S, Frotscher M: **Capture of activity-induced ultrastructural changes at synapses by high-pressure freezing of brain tissue.** *Nat. Protoc.* 2014, **9**:1480–95.

24. Rostaing P, Weimer RM, Jorgensen EM, Triller A, Bessereau J-L: **Preservation of Immunoreactivity and Fine Structure of Adult C. elegans Tissues Using High-pressure Freezing**. *J. Histochem. Cytochem.* 2004, **52**:1–12.

25. Moor H, Bellin G, Sandri C, Akert K: **The influence of high pressure freezing on mammalian nerve tissue.** *Cell Tissue Res.* 1980, **209**:201–16.

26. Mastronarde DN: **Automated electron microscope tomography using robust prediction of specimen movements.** *J. Struct. Biol.* 2005, **152**:36–51.

27. Saalfeld S, Cardona A, Hartenstein V, Tomancak P: **CATMAID: collaborative annotation toolkit for massive amounts of image data**. *Bioinformatics* 2009, **25**:1984–1986.

28. Martell JD, Deerinck TJ, Sancak Y, Poulos TL, Mootha VK, Sosinsky GE, Ellisman MH, Ting AY: **Engineered ascorbate peroxidase as a genetically encoded reporter for electron microscopy.** *Nat. Biotechnol.* 2012, **30**:1143–8.

29. Shu X, Lev-Ram V, Deerinck TJ, Qi Y, Ramko EB, Davidson MW, Jin Y, Ellisman MH, Tsien RY: **A genetically encoded tag for correlated light and electron microscopy of intact cells, tissues, and organisms.** *PLoS Biol.* 2011, **9**:e1001041.

30. Andrey P, Maurin Y: **Free-D: an integrated environment for three-dimensional reconstruction from serial sections.** *J. Neurosci. Methods* 2005, **145**:233–44.

31. de Boer P, Hoogenboom JP, Giepmans BNG: **Correlated light and electron**

microscopy: ultrastructure lights up! *Nat. Methods* 2015, **12**:503–513.

32. Padman BS, Bach M, Ramm G: **An improved procedure for subcellular spatial alignment during live-cell CLEM**. *PLoS One* 2014, **9**.

33. Vicidomini G, Gagliani MC, Cortese K, Krieger J, Buescher P, Bianchini P, Boccacci P, Tacchetti C, Diaspro A: **A novel approach for correlative light electron microscopy analysis.** *Microsc. Res. Tech.* 2010, **73**:215–24.

34. Colombelli J, Tängemo C, Haselman U, Antony C, Stelzer EHK, Pepperkok R, Reynaud EG: **A correlative light and electron microscopy method based on laser micropatterning and etching.** *Methods Mol. Biol.* 2008, **457**:203–13.

35. Maco B, Holtmaat A, Cantoni M, Kreshuk A, Straehle CN, Hamprecht FA, Knott GW: **Correlative in vivo 2 photon and focused ion beam scanning electron microscopy of cortical neurons.** *PLoS One* 2013, **8**:e57405.

36. Maco B, Cantoni M, Holtmaat A, Kreshuk A, Hamprecht F a, Knott GW: **Semiautomated correlative 3D electron microscopy of in vivo-imaged axons and dendrites.** *Nat. Protoc.* 2014, **9**:1354–66.

37. Urwyler O, Izadifar A, Dascenco D, Petrovic M, He H, Ayaz D, Kremer A, Lippens S, Baatsen P, Guérin CJ, et al.: **Investigating CNS synaptogenesis at single-synapse resolution by combining reverse genetics with correlative light and electron microscopy.** *Development* 2015, **142**:394–405.

38. Micheva KD, Smith SJ: **Array tomography: a new tool for imaging the molecular architecture and ultrastructure of neural circuits.** *Neuron* 2007, **55**:25–36.

39. Viswanathan S, Williams ME, Bloss EB, Stasevich TJ, Speer CM, Nern A, Pfeiffer BD, Hooks BM, Li W-P, English BP, et al.: **High-performance probes for light and electron microscopy**. *Nat. Methods* 2015, **12**.

40. Lin T-Y, Luo J, Shinomiya K, Ting C-Y, Lu Z, Meinertzhagen IA, Lee C-H: **Mapping chromatic pathways in the Drosophila visual system.** *J. Comp. Neurol.* 2016, **524**:213–27.

41. Amiry-Moghaddam M, Ottersen OP: **Immunogold cytochemistry in neuroscience.** *Nat. Neurosci.* 2013, **16**:798–804.

42. Bock DD, Lee W-CA, Kerlin AM, Andermann ML, Hood G, Wetzel AW, Yurgenson S, Soucy ER, Kim HS, Reid RC: **Network anatomy and in vivo physiology of visual cortical neurons.** *Nature* 2011, **471**:177–82.

43. Briggman KL, Helmstaedter M, Denk W: **Wiring specificity in the direction-selectivity circuit of the retina.** *Nature* 2011, **471**:183–8.

44. Bumbarger DJ, Riebesell M, Rödelsperger C, Sommer RJ: **System-wide Rewiring Underlies Behavioral Differences in Predatory and Bacterial-Feeding Nematodes**. *Cell* 2013, **152**:109–119.

45. Ohyama T, Schneider-Mizell CM, Fetter RD, Aleman JV, Franconville R, Rivera-Alba M, Mensh BD, Branson KM, Simpson JH, Truman JW, et al.: **A multilevel multimodal circuit enhances action selection in Drosophila**. *Nature* 2015, **520**:633–9.

46. Randel N, Jékely G: **Phototaxis and the origin of visual eyes Main Text**. 2015, [no volume].

47. White JG, Southgate E, Thomson JN, Brenner S: **The Structure of the Nervous System of the Nematode Caenorhabditis elegans**. *Philos. Trans. R. Soc. B Biol. Sci.* 1986, **314**:1–340.

48. Brorson SH: **Comparison of the immunogold labeling of single light chains and whole immunoglobulins with anti-kappa on LR-white and epoxy sections.** *Micron* 1998, **29**:439–43.

49. Brorson SH, Reinholt FP: **The intensity of immunogold labeling of deplasticized acrylic sections compared to deplasticized epoxy sections-Theoretical deductions and experimental data.** *Micron* 2008, **39**:144–50.

50. De Paul AL De, Mukdsi JH, Petiti JP, Gutiérrez S, Quintar A a, Maldonado C a, Torres AI: **Immunoelectron Microscopy: A Reliable Tool for the Analysis of Cellular Processes**. *Appl. Immunocytochem.* 2012, [no volume].

51. Hamanaka Y, Park D, Yin P, Annangudi SP, Edwards TN, Sweedler J, Meinertzhagen I a., Taghert PH: **Transcriptional Orchestration of the Regulated Secretory Pathway in Neurons by the bHLH protein DIMM**. *Curr. Biol.* 2010, **20**:9–18.

52. Koizumi O, Wilson JD, Grimmelikhuijzen CJ, Westfall JA: **Ultrastructural localization of RFamide-like peptides in neuronal dense-cored vesicles in the peduncle of Hydra**. *J. Exp. Zool.* 1989, **249**:17–22.

53. Merighi A, Cruz F, Coimbra A: **Immunocytochemical staining of neuropeptides in terminal arborization of primary afferent fibers anterogradely labeled and identified at light and electron microscopic levels.** *J. Neurosci. Methods* 1992, **42**:105–13.

54. Yasuyama K, Meinertzhagen IA: **Synaptic connections of PDF-immunoreactive lateral neurons projecting to the dorsal protocerebrum of Drosophila melanogaster**. *J. Comp. Neurol.* 2010, **518**:292–304.

55. Li C: **Neuropeptides**. *WormBook* 2008, doi:10.1895/wormbook.1.142.1.

56. Pierce SB: **Regulation of DAF-2 receptor signaling by human insulin and ins-1, a member of the unusually large and diverse C. elegans insulin gene family**. *Genes Dev.* 2001, **15**:672–686.

57. Li W: **daf-28 encodes a C. elegans insulin superfamily member that is regulated by environmental cues and acts in the DAF-2 signaling pathway**. *Genes Dev.* 2003, **17**:844–858.

58. Nathoo AN, Moeller RA, Westlund BA, Hart AC: **Identification of neuropeptide-like protein gene families in Caenorhabditis elegans and other species**. *Proc. Natl. Acad. Sci.* 2001, **98**:14000–14005.

59. de Wit J, Toonen RF, Verhage M: **Matrix-Dependent Local Retention of Secretory Vesicle Cargo in Cortical Neurons**. *J. Neurosci.* 2009, **29**:23–37.

60. Ludwig M, Leng G: **Dendritic peptide release and peptide-dependent behaviours**. *Nat. Rev. Neurosci.* 2006, **7**:126–136.

61. Wong MY, Zhou C, Shakiryanova D, Lloyd TE, Deitcher DL, Levitan ES:

Neuropeptide delivery to synapses by long-range vesicle circulation and sporadic capture. *Cell* 2012, **148**:1029–38.

62. Goldstein LSB, Yang Z: **Microtubule-Based Transport Systems in Neurons: The Roles of Kinesins and Dyneins**. *Annu. Rev. Neurosci.* 2000, **23**:39–71.

63. Gulbenkian S, Merighi A, Wharton J, Varndell IM, Polak JM: **Ultrastructural evidence for the coexistence of calcitonin gene-related peptide and substance P in secretory vesicles of peripheral nerves in the guinea pig**. *J. Neurocytol.* 1986, **15**:535–542.

64. Merighi A, Polak JM, Gibson SJ, Gulbenkian S, Valentino KL, Peirone SM: **Ultrastructural studies on calcitonin gene-related peptide-, tachykinins- and somatostatin-immunoreactive neurones in rat dorsal root ganglia: evidence for the colocalization of different peptides in single secretory granules.** *Cell Tissue Res.* 1988, **254**:101–9.

65. Eipper BA, Stoffers DA, Mains RE: **The biosynthesis of neuropeptides: peptide alpha-amidation.** *Annu. Rev. Neurosci.* 1992, **15**:57–85.

66. Edison a S, Espinoza E, Zachariah C: **Conformational ensembles: the role of neuropeptide structures in receptor binding.** *J. Neurosci.* 1999, **19**:6318–26.

67. Conzelmann M, Jékely G: **Antibodies against conserved amidated neuropeptide epitopes enrich the comparative neurobiology toolbox.** *Evodevo* 2012, **3**:23.

68. Zupanc GKH: **Peptidergic transmission: From morphological correlates to functional implications**. *Micron* 1996, **27**:35–91.

69. Kaneko M, Hall JC: **Neuroanatomy of cells expressing clock genes in Drosophila: transgenic manipulation of the period and timeless genes to mark the perikarya of circadian pacemaker neurons and their projections.** *J. Comp. Neurol.* 2000, **422**:66–94.

70. Helfrich-Förster C, Homberg U: **Pigment-dispersing hormone-immunoreactive neurons in the nervous system of wild-type Drosophila melanogaster and of several mutants with altered circadian rhythmicity.** *J. Comp. Neurol.* 1993, **337**:177–90.

71. Yuste R: **Circuit neuroscience: the road ahead.** *Front. Neurosci.* 2008, **2**:6–9.

72. Alivisatos AP, Chun M, Church GM, Greenspan RJ, Roukes ML, Yuste R: **The brain activity map project and the challenge of functional connectomics.** *Neuron* 2012, **74**:970–4.

73. Nern A, Pfeiffer BD, Rubin GM: **Optimized tools for multicolor stochastic labeling reveal diverse stereotyped cell arrangements in the fly visual system.** *Proc. Natl. Acad. Sci. U. S. A.* 2015, **112**:E2967–E2976.

74. Pan RK, Chatterjee N, Sinha S: **Mesoscopic organization reveals the constraints governing Caenorhabditis elegans nervous system.** *PLoS One* 2010, **5**:e9240.

75. Towlson EK, Vértes PE, Ahnert SE, Schafer WR, Bullmore ET: **The rich club

of the C. elegans neuronal connectome. *J. Neurosci.* 2013, **33**:6380–7.

76. Cardona A, Saalfeld S, Preibisch S, Schmid B, Cheng A, Pulokas J, Tomancak P, Hartenstein V: **An integrated micro- and macroarchitectural analysis of the Drosophila brain by computer-assisted serial section electron microscopy.** *PLoS Biol.* 2010, **8**.

77. Lin C-W, Lin H-W, Chiu M-T, Shih Y-H, Wang T-Y, Chang H-M, Chiang A-S: **Automated in situ brain imaging for mapping the Drosophila connectome.** *J. Neurogenet.* 2015, **29**:157–68.

78. Takemura SY: **Connectome of the fly visual circuitry**. *Microscopy* 2015, **64**:37–44.

79. Oh SW, Harris JA, Ng L, Winslow B, Cain N, Mihalas S, Wang Q, Lau C, Kuan L, Henry AM, et al.: **A mesoscale connectome of the mouse brain.** *Nature* 2014, **508**:207–14.

80. Bota M, Dong H-W, Swanson LW: **Combining collation and annotation efforts toward completion of the rat and mouse connectomes in BAMS.** *Front. Neuroinform.* 2012, **6**:2.

81. DeFelipe J: **The anatomical problem posed by brain complexity and size: a potential solution.** *Front. Neuroanat.* 2015, **9**:104.

82. Peddie CJ, Collinson LM: **Exploring the third dimension: volume electron microscopy comes of age.** *Micron* 2014, **61**:9–19.

83. Backfisch B, Veedin Rajan VB, Fischer RM, Lohs C, Arboleda E, Tessmar-Raible K, Raible F: **Stable transgenesis in the marine annelid *Platynereis dumerilii* sheds new light on photoreceptor evolution**. *Proc. Natl. Acad. Sci.* 2013, **110**:193–198.

84. Bannister S, Antonova O, Polo A, Lohs C, Hallay N, Valinciute A, Raible F, Tessmar-Raible K: **TALENs Mediate Efficient and Heritable Mutation of Endogenous Genes in the Marine Annelid *Platynereis dumerilii*. *Genetics* 2014, **197**:77–89.

85. Randel N, Asadulina A, Bezares-Calderón LA, Verasztó C, Williams EA, Conzelmann M, Shahidi R, Jékely G: **Neuronal connectome of a sensory-motor circuit for visual navigation.** *Elife* 2014, **3**.

86. Veedin-Rajan VB, Fischer RM, Raible F, Tessmar-Raible K: **Conditional and Specific Cell Ablation in the Marine Annelid *Platynereis dumerilii*. *PLoS One* 2013, **8**:e75811.

87. Zantke J, Bannister S, Rajan VB V., Raible F, Tessmar-Raible K: **Genetic and Genomic Tools for the Marine Annelid *Platynereis dumerilii*. *Genetics* 2014, **197**:19–31.

88. Williams EA, Conzelmann M, Jékely G: **Myoinhibitory peptide regulates feeding in the marine annelid *Platynereis*. *Front. Zool.* 2015, **12**:1.

89. Conzelmann M, Williams E a, Tunaru S, Randel N, Shahidi R, Asadulina A, Berger J, Offermanns S, Jékely G: **Conserved MIP receptor-ligand pair regulates *Platynereis* larval settlement.** *Proc. Natl. Acad. Sci. U. S. A.* 2013, **110**:8224–9.

90. Jékely G, Colombelli J, Hausen H, Guy K, Stelzer E, Nédélec F, Arendt D:

Mechanism of phototaxis in marine zooplankton. *Nature* 2008, **456**:395–399.

91. Zantke J, Ishikawa-Fujiwara T, Arboleda E, Lohs C, Schipany K, Hallay N, Straw AD, Todo T, Tessmar-Raible K: **Circadian and circalunar clock interactions in a marine annelid.** *Cell Rep.* 2013, **5**:99–113.

92. Conzelmann M, Williams E a, Krug K, Franz-Wachtel M, Macek B, Jékely G: **The neuropeptide complement of the marine annelid *Platynereis dumerilii.*** *BMC Genomics* 2013, **14**:906.

93. Nässel DR: **Neuropeptides in the nervous system of Drosophila and other insects: multiple roles as neuromodulators and neurohormones.** *Prog. Neurobiol.* 2002, **68**:1–84.

94. Jékely G: **Global view of the evolution and diversity of metazoan neuropeptide signaling.** *Proc. Natl. Acad. Sci. U. S. A.* 2013, **110**:8702–7.

95. Conzelmann M, Offenburger S-L, Asadulina A, Keller T, Münch T a, Jékely G: **Neuropeptides regulate swimming depth of *Platynereis* larvae.** *Proc. Natl. Acad. Sci. U. S. A.* 2011, **108**:E1174–83.

96. Helmstaedter M: **Cellular-resolution connectomics: challenges of dense neural circuit reconstruction.** *Nat. Methods* 2013, **10**:501–7.

97. Jarrell TA, Wang Y, Bloniarz AE, Brittin CA, Xu M, Thomson JN, Albertson DG, Hall DH, Emmons SW: **The Connectome of a Decision-Making Neural Network**. *Science (80-.).* 2012, **337**:437–444.

98. Kabra M, Robie A a, Rivera-Alba M, Branson S, Branson K: **JAABA: interactive machine learning for automatic annotation of animal behavior.** *Nat. Methods* 2013, **10**:64–7.

99. Berman GJ, Choi DM, Bialek W, Shaevitz JW: **Mapping the stereotyped behaviour of freely moving fruit flies**. *J. R. Soc. Interface* 2014, **11**:20140672–20140672.

100. Vogelstein JT, Park Y, Ohyama T, Kerr R a, Truman JW, Priebe CE, Zlatic M: **Discovery of Brainwide Neural-Behavioral Maps via Multiscale Unsupervised Structure Learning**. *Science (80-.).* 2014, **344**:386–392.

101. Portugues R, Feierstein CE, Engert F, Orger MB: **Whole-Brain Activity Maps Reveal Stereotyped, Distributed Networks for Visuomotor Behavior**. *Neuron* 2014, **81**:1328–1343.

102. Cardona A, Saalfeld S, Schindelin J, Arganda-Carreras I, Preibisch S, Longair M, Tomancak P, Hartenstein V, Douglas RJ: **TrakEM2 software for neural circuit reconstruction.** *PLoS One* 2012, **7**:e38011.

103. Friedrich RW, Genoud C, Wanner A a: **Analyzing the structure and function of neuronal circuits in zebrafish.** *Front. Neural Circuits* 2013, **7**:71.

104. Bargmann CI: **Beyond the connectome: how neuromodulators shape neural circuits.** *Bioessays* 2012, **34**:458–65.

105. Bargmann CI, Marder E: **From the connectome to brain function**. *Nat. Methods* 2013, **10**:483–490.

106. Bucher D, Marder E: **SnapShot: Neuromodulation**. *Cell* 2013, **155**:482–482.e1.

107. Marder E: **Neuromodulation of Neuronal Circuits: Back to the Future**. *Neuron* 2012, **76**:1–11.

108. Dupuis-Williams P, Fleury-Aubusson A, de Loubresse NG, Geoffroy H, Vayssié L, Galvani A, Espigat A, Rossier J: **Functional role of ɛ-tubulin in the assembly of the centriolar microtubule scaffold**. *J. Cell Biol.* 2002, **158**:1183–1193.

109. Skepper JN: **Immunocytochemical strategies for electron microscopy: choice or compromise.** *J. Microsc.* 2000, **199**:1–36.

110. Baschong W, Stierhof YD: **Preparation, use, and enlargement of ultrasmall gold particles in immunoelectron microscopy.** *Microsc. Res. Tech.* 1998, **42**:66–79.

111. Lucocq JM, Gawden-Bone C: **Quantitative assessment of specificity in immunoelectron microscopy.** *J. Histochem. Cytochem.* 2010, **58**:917–27.

112. Gundersen V, Chaudhry FA, Bjaalie JG, Fonnum F, Ottersen OP, Storm-Mathisen J: **Synaptic vesicular localization and exocytosis of L-aspartate in excitatory nerve terminals: a quantitative immunogold analysis in rat hippocampus.** *J. Neurosci.* 1998, **18**:6059–70.

113. Larsson LI: **Immunogold labelling of neuroendocrine peptides with special reference to antibody specificity and multiple staining techniques**. *Histochem. Cell Biol.* 1996, **106**:93–103.

114. Heasman J, Kofron M, Wylie C: **βCatenin Signaling Activity Dissected in the Early Xenopus Embryo: A Novel Antisense Approach**. *Dev. Biol.* 2000, **222**:124–134.

115. Summerton J: **Morpholino antisense oligomers: the case for an RNase H-independent structural type**. *Biochim. Biophys. Acta - Gene Struct. Expr.* 1999, **1489**:141–158.

116. Landry M, Vila-Porcile E, Calas A: **Immunogold detection of co-localized neuropeptides: methodological aspects.** *J. Histochem. Cytochem.* 2004, **52**:617–627.

117. Schlötzer-Schrehardt U: **Ultrastructural investigation of the nuchal organs ofPygospio elegans (Polychaeta). I. Larval nuchal organs**. *Helgoländer Meeresuntersuchungen* 1986, **40**:397–417.

118. Purschke G: **Ultrastructure of Nuchal Organs in Polychaetes (Annelida) - New Results and Review**. *Acta Zool.* 1997, **78**:123–143.

119. Purschke G: **Sense organs in polychaetes (Annelida)**. *Hydrobiologia* 2005, **535-536**:53–78.

120. Purschke G, Wolfrath F, Westheide W: **Ultrastructure of the nuchal organ and cerebral organ in Onchnesoma squamatum (Sipuncula, Phascolionidae)**. *Zoomorphology* 1997, **117**:23–31.

121. Fischer AHL, Arendt D: **Mesoteloblast-Like Mesodermal Stem Cells in the Polychaete Annelid *Platynereis dumerilii* (Nereididae)**. *J. Exp. Zool. Part B Mol. Dev. Evol.* 2013, **320**:94–104.

122. Rieger RM: **The Biphasic Life Cycle—A Central Theme of Metazoan Evolution**. *Am. Zool.* 1994, **34**:484–491.

123. Bauknecht P, Jékely G: **Large-Scale Combinatorial Deorphanization of *Platynereis* Neuropeptide GPCRs**. *Cell Rep.* 2015, **12**:684–693.

124. Mirabeau O, Joly J-S: **Molecular evolution of peptidergic signaling systems in bilaterians**. *Proc. Natl. Acad. Sci.* 2013, **110**:E2028–E2037.

125. Johard HAD, Enell LE, Gustafsson E, Trifilieff P, Veenstra JA, Nässel DR: **Intrinsic neurons of Drosophila mushroom bodies express short neuropeptide F: Relations to extrinsic neurons expressing different neurotransmitters**. *J. Comp. Neurol.* 2008, **507**:1479–1496.

126. Nässel DR: **Insect myotropic peptides: differential distribution of locustatachykinin- and leucokinin-like immunoreactive neurons in the locust brain.** *Cell Tissue Res.* 1993, **274**:27–40.

127. Gaudry Q, Hong EJ, Kain J, de Bivort BL, Wilson RI: **Asymmetric neurotransmitter release enables rapid odour lateralization in Drosophila**. *Nature* 2012, **493**:424–428.

128. Clark DA, Freifeld L, Clandinin TR: **Mapping and cracking sensorimotor circuits in genetic model organisms.** *Neuron* 2013, **78**:583–95.

129. Anderson JR, Jones BW, Yang J-H, Shaw M V, Watt CB, Koshevoy P, Spaltenstein J, Jurrus E, U V K, Whitaker RT, et al.: **A computational framework for ultrastructural mapping of neural circuitry.** *PLoS Biol.* 2009, **7**:e1000074.

OWN CONTRIBUTION TO THE PUBLICATIONS

N Randel *, R Shahidi *, C Verasztó, LA Bezares-Calderón, S Schmidt, G Jékely: **Inter-individual stereotypy of the *Platynereis* larval visual connectome.**

<div align="right">* Contributed equally</div>

I performed all the serial ultra-microtomy, grid preparation, contrasting, carbon coating, and imaging on the specimen provided by NR. I montaged and aligned the image dataset equally with AA and LABC.

The figure and movie preparation, drafting of the manuscript, and the study design was shared equally with GJ and NR.

R Shahidi, EA Williams, M Conzelmann, A Asadulina, C Verasztó, S Jasek, LA Bezares-Calderón, G Jékely: **A serial multiplex immunogold labeling method for identifying peptidergic neurons in connectomes.**

I performed all the serial ultra-microtomy, contrasting, carbon coating, and imaging on the processed specimen, using self-prepared grids. I montaged and aligned 50% of the dataset, but was helped by AA and LABC. I equally shared the tracing of the peptidergic neurons with GJ, SJ, and CV. I reviewed >90% of the neurons. The nuchal organ tracing was done by GJ, but I equally helped with review of the tracing. I created >60% of the figures in the manuscript, the rest were created equally between EAW and GJ. Manuscript writing and design of the study was shared with GJ.

APPENDIX: PUBLICATIONS

Publication 1: **Inter-individual stereotypy of the *Platynereis* larval visual connectome.** *Elife* (2015)

Randel*, Shahidi* *et al.*

* Contributed equally

Inter-individual stereotypy of the *Platynereis* larval visual connectome

Nadine Randel[†], Réza Shahidi[†], Csaba Verasztó, Luis A Bezares-Calderón, Steffen Schmidt, Gáspár Jékely*

Max Planck Institute for Developmental Biology, Tübingen, Germany

Abstract Developmental programs have the fidelity to form neural circuits with the same structure and function among individuals of the same species. It is less well understood, however, to what extent entire neural circuits of different individuals are similar. Previously, we reported the neuronal connectome of the visual eye circuit from the head of a *Platynereis dumerilii* larva (*Randel et al., 2014*). We now report a full-body serial section transmission electron microscopy (ssTEM) dataset of another larva of the same age, for which we describe the connectome of the visual eyes and the larval eyespots. Anatomical comparisons and quantitative analyses of the two circuits reveal a high inter-individual stereotypy of the cell complement, neuronal projections, and synaptic connectivity, including the left-right asymmetry in the connectivity of some neurons. Our work shows the extent to which the eye circuitry in *Platynereis* larvae is hard-wired.

DOI: 10.7554/eLife.08069.001

Introduction

Innate stereotypical behaviors commonly observed in animals (*Jarrell et al., 2012*; *Kabra et al., 2013*; *Berman et al., 2014*; *Vogelstein et al., 2014*; *Zhang et al., 2014*) rely on the precise wiring of neuronal circuits during development. However, the stereotypy of neuronal circuits between individuals of the same species at the level of synaptic connectivity is not well known. Previously, several studies have addressed nervous system stereotypy at the level of single neurons, neuronal projection patterns, or neuronal activity. For example, in the zebrafish larval brain, neuronal spatiotemporal activity is highly stereotypical between individuals (*Portugues et al., 2014*). The fruit fly *Drosophila melanogaster* has stereotypical neuron types, axonal projection patterns, neuronal activity patterns and patterns of synaptic connectivity (*Yu et al., 2010*; *Mosca and Luo, 2014*; *Zhang et al., 2014*). A recent connectomic study found that the connectivity of interneurons mediating rolling behavior in *Drosophila* larvae were reproducible between two individuals (*Ohyama et al., 2015*). Nematodes also have a nervous system that is considered highly stereotypical (*White et al., 1986*).

Other studies that quantitatively addressed the stereotypy in connectivity patterns have found considerable variation among individuals. In the fly, inter-individual comparisons of local interneurons in the antennal lobe (*Chou et al., 2010*), as well as comparisons of segmentally repeated motor neurons (MNs) in the same individual (*Couton et al., 2015*) revealed considerable variation in finer-scale connectivity. Likewise, in mice, there is significant structural variation in connectivity patterns of MNs innervating the interscutularis muscles between the left and right sides of the same animal (*Lu et al., 2009*).

Here, we use serial-section transmission electron microscopy (ssTEM) to quantify the synaptic level inter-individual stereotypy of an entire sensory-motor circuit, the visual eye circuit of larvae of the marine annelid *Platynereis dumerilii* (*Randel et al., 2014*). Previously, we reported the neuronal connectome of this circuit, reconstructed from a 72 hr post fertilization (hpf) larva. *Platynereis* larvae develop following a strict cell lineage (*Fischer and Arendt, 2013*) and different individuals of the

*For correspondence: gaspar. jekely@tuebingen.mpg.de

[†]These authors contributed equally to this work

same developmental stage have a stereotypical complement of neurons (*Tomer et al., 2010*). However, whether synapse-level connectomes are reproducible among different *Platynereis* individuals is unclear. To test the stereotypy of the neuronal projection patterns and synaptic connectivity of individual neurons, we have reconstructed the visual eye circuitry of a second individual from the same batch, allowing the detailed comparison of two larval connectomes in *Platynereis*.

Results

Reconstruction of the visual eye circuit from a full-body ssTEM dataset of a *Platynereis* larva

We acquired a full-body ssTEM dataset of a 72 hr post fertilization (hpf) *Platynereis* larva (HT9-4) (*Figure 1A*), derived from the same batch as the previously described larva (HT9-3) (*Randel et al., 2014*). We imaged 5056 sections (40 nm/section) using conventional TEM. In this dataset, we traced the neuronal circuitry downstream of the visual eyes. The visual eye circuit of the second larva consists of 106 neurons, plus several ciliated and muscle effector cells (*Video 1*, *Source code 1*, and *Figure 1—source data 1*).

Inter-individual stereotypy of the connectomes

The gross anatomy and cell complement of the HT9-4 eye circuit is very similar to that of HT9-3 (*Figure 1C*). We identified all cell types and groups of cells that we described for HT9-3. All cell types showed similar overall anatomical arrangement in the two individuals. For some cell types, including IN^1 interneurons and six ventral MNs (MN^{l1-3} and MN^{r1-3}), we could correlate the two individuals at a single-cell level.

To test the stereotypy of synaptic connections, we compared patterns of connectivity between the two individuals (*Figure 1B,C*, *Figure 2B*, *Figure 1—figure supplement 1*, *Figure 2—source data 1*). We used several measures to compare the two connectomes. First, we defined a grouped connectivity matrix for HT9-4, similar to that of HT9-3 (*Randel et al., 2014*) (*Figure 2—source data 1*). We then correlated the two grouped matrices and found a strong correlation (Spearman's r = 0.62, p = 0.0001). For a more detailed comparison, we calculated the geometric mean of the two connectivity matrices and generated a combined matrix (*Figure 2A*). In this matrix, only connections are shown that are present in both animals. The combined matrix is similar to the individual matrices and we could find all major connections.

We also identified all reciprocal connections for HT9-4 and found the same strong reciprocal IN^1 motif as that of HT9-3 (*Figure 2—figure supplement 2*, *Figure 2—source data 1*). Additionally, we scored the correlation of the synaptic maturation of the HT9-4 photoreceptor cells (PRCs) with photoreceptor-cell rhabdom volume and axon length and found similar relationships as in HT9-3 (*Figure 3—figure supplement 1*, *Figure 3—figure supplement 1—source data 1*). All these measures indicate that the *Platynereis* eye circuit is strongly stereotypical at the global level of its synaptic connectivity.

Next, we focused on the stereotypy of single neuron types. First, we analyzed the correlation of connectivity between corresponding neuron types of HT9-3 and HT9-4.

We found significant correlations between both pre- and post-synaptic submatrices for most neuron types (*Figure 2C*). The neurons that did not show significant correlations between the two individuals were those with weak connections to the eye network, with only a few synapses in one or both individuals (e.g., IN^{dcr} IN^{vcl}) or those that were truncated in HT9-3 (MN^{r3}, MN^{l3}).

To further test stereotypy at the single neuron level, we looked at the projection pattern and the distribution of pre- and post-synaptic sites in corresponding neurons between the two individuals. All neuron groups had similar projection patterns and spatial distribution of pre- and post-synaptic sites (*Figure 2—figure supplement 1*).

We also analyzed certain circuit elements in more detail. We first compared the connectivity of the visual eye PRCs (*Figure 3A*) and IN^1 cells. The visual eye PRCs showed very similar connectivity with the IN^1 interneurons in both animals. The strongest connection for all eyes was from PRCs to the cross-wise IN^1. However, we also identified a weak innervation of the ipsilateral IN^1 by the posterior eye PRCs that was consistent between the two animals (*Figure 3A*).

Next, we analyzed the pre- and post-synaptic partners of the MN cells. All MN cells, with the exception of MN^{r3}, are strongly innervated by 2–3 ipsilateral, plus 2–3 contralateral, IN^{sn} cells in both
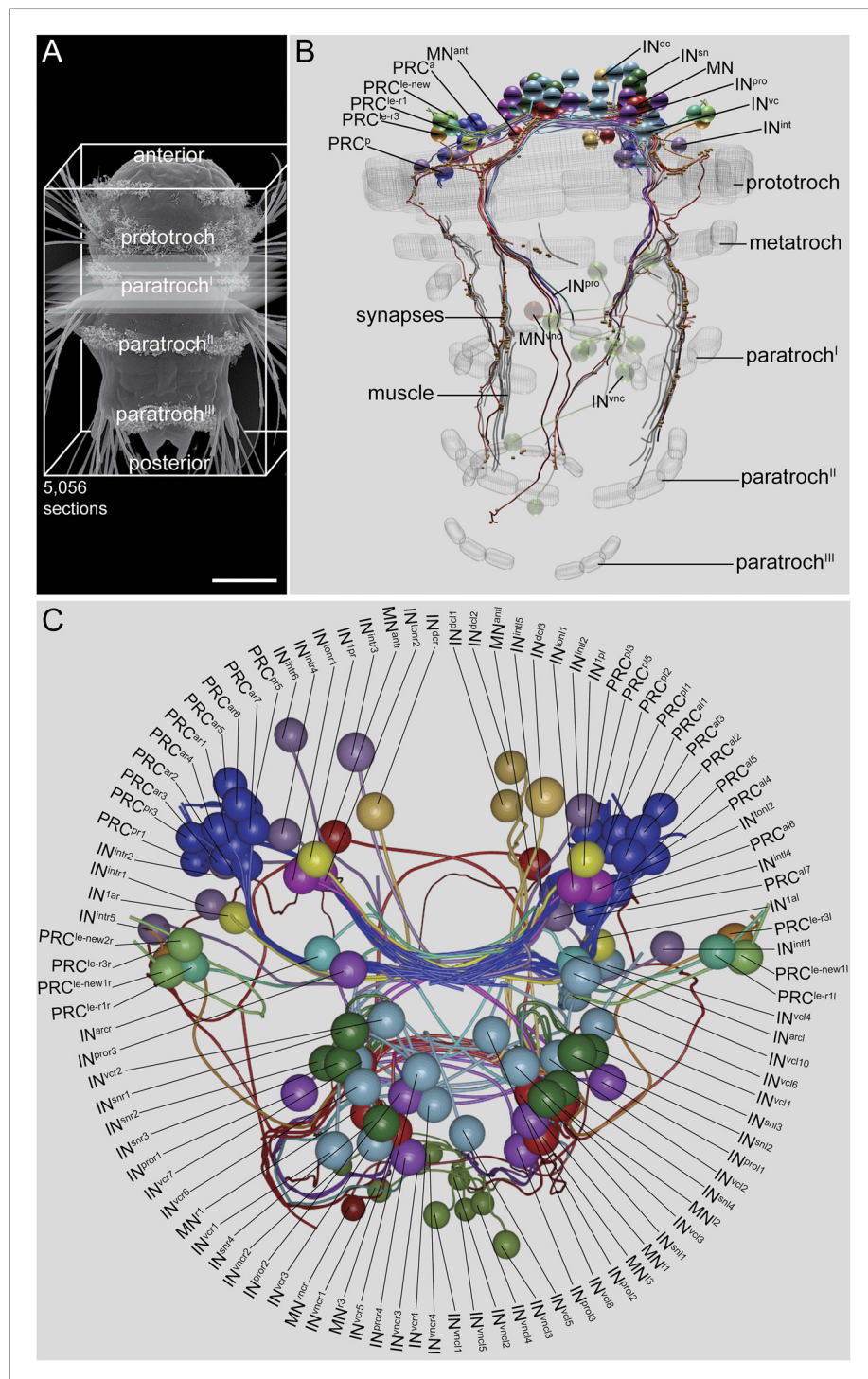
Figure 1. Visual eye and larval eyespot circuit reconstructed from a full-body dataset (HT9-4). (**A**) Scanning electron micrograph of a 72 hpf larva, dorsal view. (**B**, **C**) Blender visualization of the cell complement in ventral (**B**) and anterior (**C**) views. IN[1], primary interneuron; IN[arc], arc interneuron; IN[dc], dorsal interneuron; IN[int], intrinsic interneuron; *Figure 1. continued on next page*

Figure 1. Continued

INˢⁿ, Schnörkel-interneuron; INᵗᵒⁿ, trans-optic neuropil interneuron; INᵖʳᵒ, projection interneuron; INᵛᶜ, ventral interneuron; INᵛⁿᶜ, ventral nerve cord interneuron; MN, ventral motor neuron; MNᵃⁿᵗ, anterior motor neuron; MNᵛⁿᶜ, ventral nerve cord motor neuron; PRC, photoreceptor cell of the visual eye; PRCˡᵉ⁻ʳ¹ᐟ³, photoreceptor cell of the larval eye, expressing *r-opsin3* or *r-opsin1*; a, anterior; p, posterior; l, left; r, right. Scale bar in (**A**) 50 μm.

animals (*Figure 3B*). MNʳ³ is also unique in another aspect of its connectivity. This neuron in both animals consistently displayed a highly left-right asymmetric connectivity pattern. MNʳ³ is anatomically similar to MNˡ¹. Both cells are ciliomotor and muscle MNs, with strong connections to contralateral prototroch cells, to the longitudinal muscles and the paratrochs. However, MNʳ³'s connectivity is unique in forming several synapses on contralateral MN cells (*Figure 3C*), being thus the only MN to potentially influence both contralateral and ipsilateral effectors. We could detect this asymmetric connectivity pattern for MNʳ³ in both individuals. These results show that synaptic stereotypy can be found at the single neuron level and also applies to left-right asymmetric motifs in the network.

Our analysis shows that the visual eye connectome in *Platynereis* larvae has strong stereotypy both globally and at the single-neuron level. We could demonstrate this for patterns of neural projections, synapse distribution along neurites, identity of synaptic partners, strength of connections, and left-right asymmetries in connectivity. These results place the visual eye circuitry in a full-body context and establish the cellular-level stereotypy of neuronal circuitry in *Platynereis* larvae.

Differences between the two datasets

The full-body dataset of HT9-4 allowed us to trace the projections of the ventral MNs in the trunk of the larva, a region that was not sectioned in HT9-3. This extended tracing revealed the presence of many more MN synapses to the trunk longitudinal muscles (maximum 68 synapses/MN) than were detected in HT9-3 (maximum 13 synapses/MN).
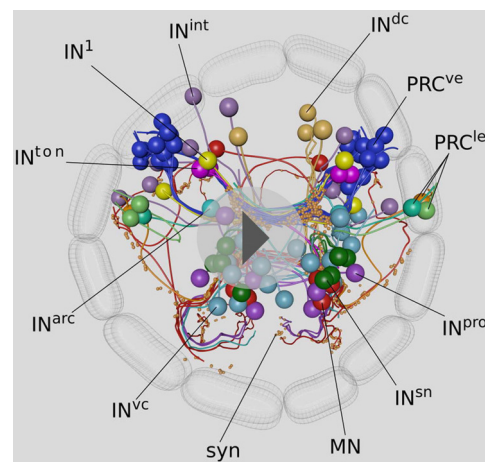
Video 1. 3D visualization of the cell complement of the *Platynereis* larval visual and larval eye circuit.
DOI: 10.7554/eLife.08069.005

In HT9-4, we also identified a new interneuron type, which we named projection interneuron (INᵖʳᵒ). Like the MNs, INᵖʳᵒ cells receive input from INˢⁿ cells and project to the trunk at a more medial position. In the trunk, INᵖʳᵒ cells form weak connections to a group of ventral nerve cord interneurons (INᵛⁿᶜ). The INᵖʳᵒ and INᵛⁿᶜ neurons are only weakly connected and likely represent a developing trunk circuitry. Based on new information from HT9-4, some of the cells previously described as MNs in HT9-3 have been reclassified as INᵖʳᵒ. INᵖʳᵒ cells have somas near the MN somas and also project to the larval trunk, as revealed by the full-body dataset of HT9-4. In HT9-3, we classified 11 cells as MNs based on incoming synapses, soma positions, and projection patterns, but five of these cells did not form synapses on effector cells. Initially, we assumed these missing connections likely occurred in trunk sections posterior to the first segment in HT9-3. However, based on the data from HT9-4 (*Figure 1B*), these neurons more
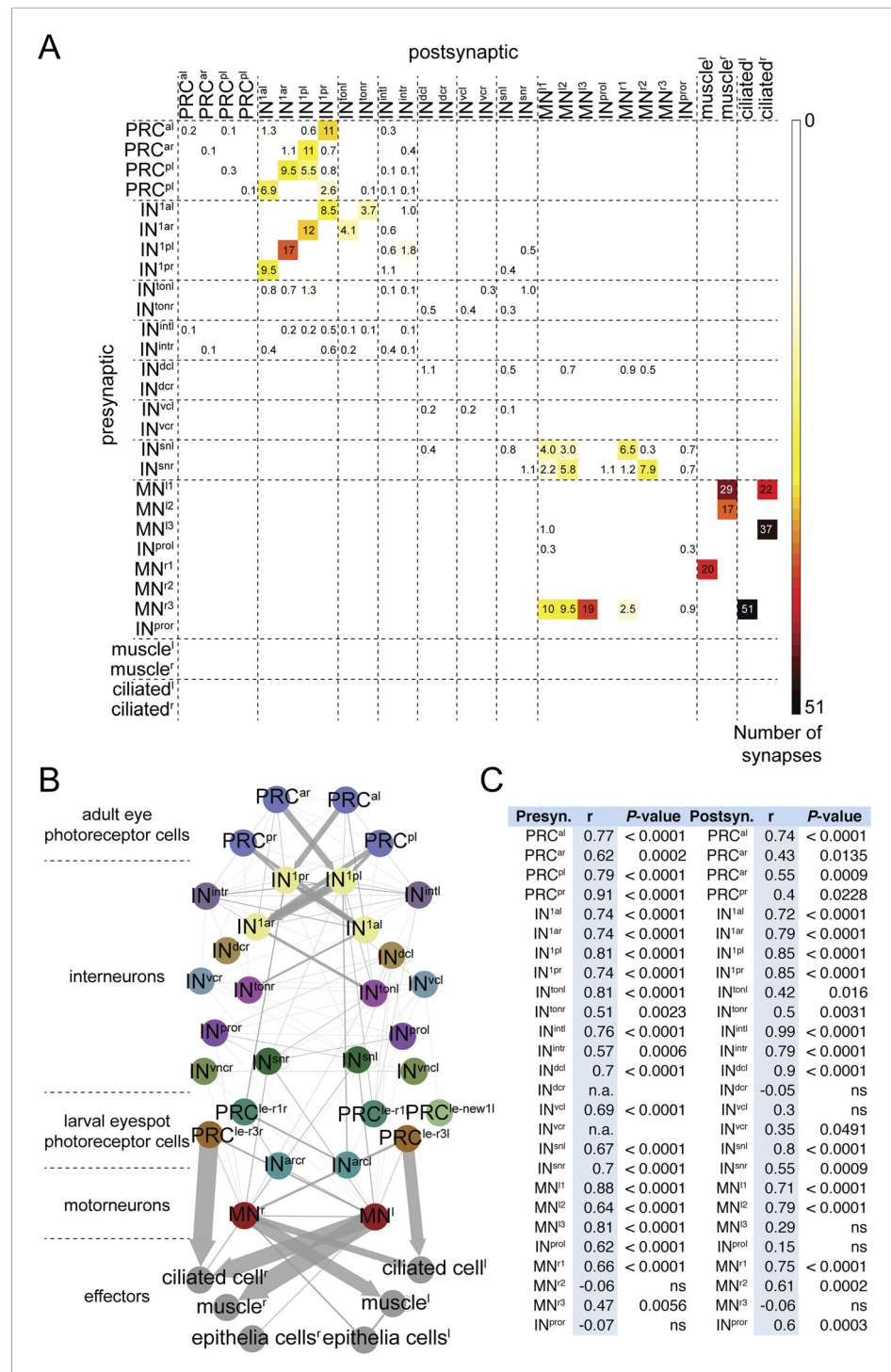
Figure 2. Comparative analysis of HT9-3 and HT9-4 visual eye circuits. (**A**) Geometric mean of the neuron types between both individuals, using the averaged synapse number of neuronal groups and the total synapse number on effectors. (**B**) Connectivity graph of the visual and larval eye circuit. Edges are weighted by averaged synapse
Figure 2. continued on next page

likely represent incompletely reconstructed IN^{pro} cells.

The new dataset also provides full coverage of all ciliated locomotor cells. The larva has 23 prototroch cells, organized into an anterior and a posterior tier, formed by 11 cell pairs and one unpaired cell (at position 11 o'clock). There are 8 ventral metatroch cells, and three bands of paratrochs^{I-III}, one in each segment. The paratrochs have 8^I, 14^{II}, and 12^{III} ciliated cells (*Figure 1B*, *Figure 3E*). We analyzed the innervation of the ciliary bands by MNs in more detail. We found that only the posterior tier of the prototroch receives synapses by MN cells. We also found that several MNs projected to and formed synapses on the paratrochs both on the dorsal and the ventral side (*Figure 3D*, *Source code 1*).

Larval eyespot connectome reveals sensory-motor circuits of varying complexities

We also fully reconstructed the neuronal circuitry of the larval eyespots or ocelli (structures located ventrally in the head) in HT9-4 (*Figure 4*). The larval eyespots develop in early trochophore larval stages and mediate positive phototaxis in early larval stages by innervating adjacent ciliary band cells (*Jékely et al., 2008*). In trochophore larvae (24–48 hpf), each larval eyespot consists of one pigment cell and one PRC^{r3}, the latter of which expresses a rhabdomeric opsin, *r-opsin3*. A preliminary ssTEM analysis in HT9-3 (72 hpf) identified a second PRC^{r1} with an axon projecting towards the brain neuropil (a cerebral PRC), indicating changes in eyespot structure during development. The second PRC expresses another opsin, *r-opsin1* (*Randel et al., 2013*).

Here, we have fully reconstructed the neuronal circuitry downstream of both eyespot PRCs in the 72 hpf larva. The two eyespot PRCs connect to very distinct downstream circuitries, suggesting functional specialization. PRC^{r3} forms *en passant* synapses on ipsilateral ciliary band cells, as previously described for both trochophore and nectochaete stages (*Jékely et al., 2008*; *Randel et al., 2013*). The distal part of the PRC^{r3} axon then turns and meets the secondary optic neuropil, forming synapses on the ipsil- and contralateral MNs. PRC^{r3} is therefore both a direct sensory-MN and a sensory neuron that connects to MNs.

The other eyespot photoreceptor, PRC^{r1}, projects into the primary optic neuropil and forms a circuitry distinct from that of PRC^{r3}. PRC^{r1} differentiates shortly before 72 hpf, as demonstrated by the late onset of *r-opsin1* expression in this cell (*Randel et al., 2013*). PRC^{r1} is only weakly connected to its target neurons, suggesting that this circuit is not yet fully developed at 72 hpf. However, we identified three cells postsynaptic to PRC^{r1}, including the IN^1 and IN^{int} interneurons of the visual eye circuit and another interneuron, that we named arc interneuron (IN^{arc}). IN^{arc} cells synapse on ventral MNs of the visual eye circuitry and two newly identified anterior MNs (MN^{ant}), which project to ciliary band cells. We also found 1 or 2 further PRC cells in both eyespots (PRC^{new}). These cells had small rhabdoms and short axons with no synapses, indicating that they are still developing.

The connectome of the eyespots suggest that both PRCs share the same effectors with the visual eyes, yet connect to these effectors by distinct circuitry. The eyespots are not able to mediate phototaxis at 72 hpf (*Randel et al., 2014*), but their continued connection to the visual eye circuit suggests that they may play a role in modulating phototaxis or mediating a distinct sensory-motor response.
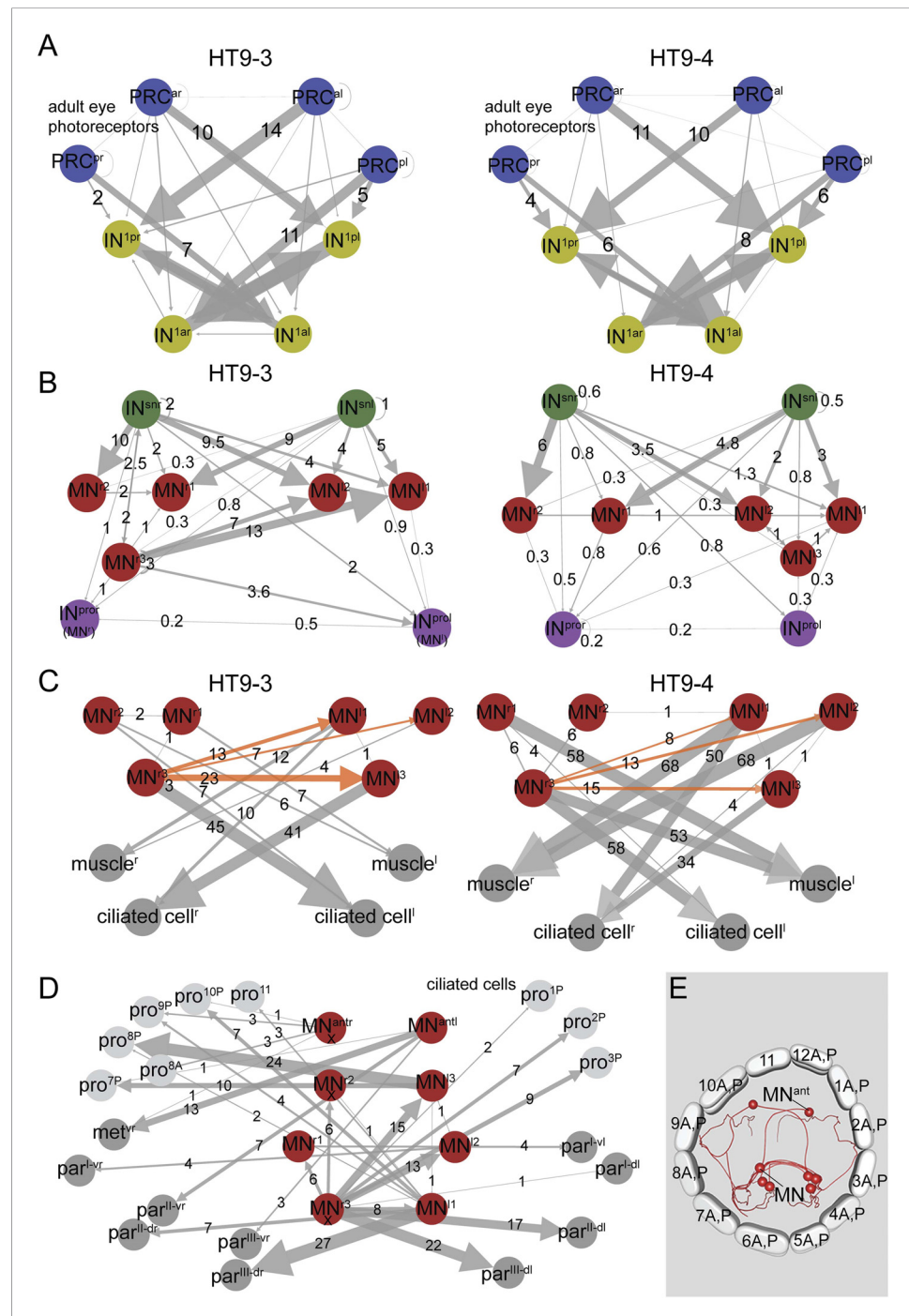
Figure 3. Subcircuits of the visual eye connectome of both individuals and the innervation of all ciliary bands in the fully reconstructed second larva (HT9-4). (**A–D**) Connectivity graphs show the connectivity between selected neuron groups and effectors. Edges are weighted by the number of synapses. The number of synapses is also shown for each edge. Nodes are colored using the color scheme of the neuron types. In **A–C**, HT9-3 is left and HT9-4 right.
(**A**) Connectivity graph of the grouped PRCs of the visual eyes with IN^1 cells. The synapses of the PRCs from each eye are averaged. (**B**) Connectivity graph of IN^{sn} cells with MNs and IN^{pro} cells. The previous nomenclature of the IN^{pro} cells
Figure 3. continued on next page

Figure 3. Continued

in HT9-3 identified as MNs is shown in brackets. (**C**) Connectivity graph of MNs and their effectors. The synapse numbers shown for ciliated cells and muscles represent the total number of synapses on groups of effector cells. (**D**) Connectivity graph of the MNs of the visual and larval eye circuit of HT9-4 with all ciliary bands. The synapse number of the metatroch and paratrochs are summed. Incompletely traced MNs are labeled with 'X'. (**E**) Blender visualization of the MNs and prototroch cells, apical view. The prototroch cells are numbered in a clockwise fashion. The numbering of the MNs of the left and the right body side within a single larva is not consistent with anatomical pairs, to stick to the nomenclature introduced for HT9-3. Note that the prototroch cell in position 11 is unpaired. met, metatroch; par, paratroch; pro, prototroch; A, anterior; P, posterior. Additional abbreviations are shown in *Figure 1*.
DOI: 10.7554/eLife.08069.010

The following figure supplement is available for figure 3:

Figure supplement 1. Maturation of photoreceptor connections in HT9-4.
DOI: 10.7554/eLife.08069.011

The following source data is available for figure 3s1:

Figure supplement 1—source data 1. Development of photoreceptor connectivity in HT9-4.
DOI: 10.7554/eLife.08069.012

Discussion

We have reconstructed the entire larval visual eye circuitry from a second *Platynereis* individual and compared inter-individual connectome stereotypy at the electron microscopic level. We found a high degree of inter-individual stereotypy in the two connectomes at every level of analysis. *Platynereis* larvae develop via a highly stereotypic cell lineage (*Fischer and Arendt, 2013*) and the systematic comparison of gene expression patterns across individuals has revealed the stereotypical position of
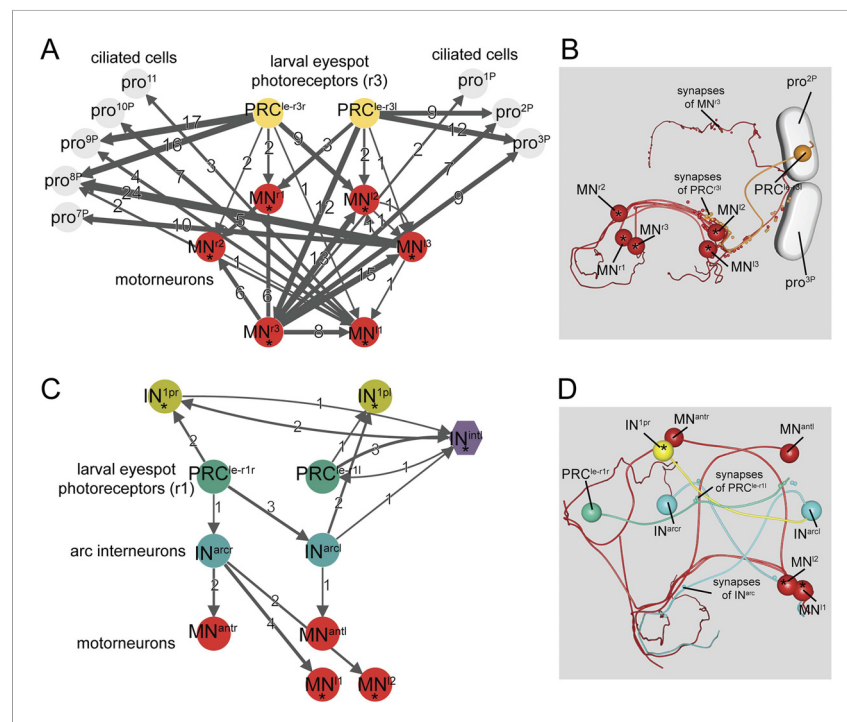
Figure 4. Minimal eye circuit of the larval eye. Neurons that are also part of the visual eye circuit are marked by an 'asterisk'. Connectivity graph of the *r-opsin3*-expressing PRC^r3 (**A**) and *r-opsin1*-expressing PRC^r1 (**C**). Connectivity graph edges are weighted by the number of synapses and synapse numbers are shown. Blender visualization of the left PRC^r3l cell (**B**) and PRC^r1r circuitry (**D**). Abbreviations are shown in *Figure 1*.
DOI: 10.7554/eLife.08069.013

neuronal cell bodies in the 48 hpf trochophore and 72 hpf nectochaete larval stages (*Tomer et al., 2010*; *Asadulina et al., 2012*). Here, we have demonstrated the stereotypy of neuronal projections and synaptic wiring based on ssTEM reconstruction and anatomical comparisons.

The two connectomes are not identical and we could not compare every neuron at a single-cell level. Despite this, clearly identifiable groups of the same cell types could be analyzed. The differences we observed may be due to developmental variation or technical variation. ssTEM datasets are inherently noisy and both datasets contained several neurite fragments that we could not assign to a neuron. However, the fact that our reconstructions resulted in the same overall circuitry indicates that the reconstructions are robust against noise. Our study also demonstrates the benefit of a second dataset when employing an ssTEM approach. Inter-individual comparisons can increase the confidence in weak or asymmetric motifs.

In *Platynereis*, the different sensory-motor circuits of the visual eye PRCs and eyespot PRCs show different levels of complexity. We identified examples for all degrees of sensory-motor contact, from direct sensory-motor innervation through sensory-MN to sensory-IN-MN. The fine gradations in the connectome of the *Platynereis* larval and visual eyes suggest that circuit evolution may have proceeded through the intercalation of new layers of neurons between sensors and effectors.

Conclusion

Our results indicate that the connectome of the larval visual system in *Platynereis* is highly stereotypical between individuals. These results support our previous findings on stereotypy through the intra-individual analysis of connectivity between neurons on the left and right body sides (*Randel et al., 2014*). Reconstructions from more than one individual can greatly benefit connectome projects.

Materials and methods

ssTEM

A 72 hpf *Platynereis* larva (HT9-4) was prepared for serial sectioning and imaging as previously described (*Conzelmann et al., 2013*; *Randel et al., 2014*). Sato's lead citrate was used for contrasting (*Hanaichi et al., 1986*). Images were obtained with SerialEM v3.2.2 (Gatan, Pleasanton, CA) imaging software in conjunction with Digital Micrograph (Gatan). We generated a full-body dataset consisting of 5056 sections, with a thickness of 40 nm per section (*Figure 1—source data 1*). Imaging was performed with a resolution of (5.7 nm/pixel). We lost 1.9% of the sections (98 layers) and the three biggest gaps encompassed five sections. 113 layers distributed across the series were not imaged. We could trace across these gaps using a combination of local and global cues. Additionally, to help the tracing in the neuropil, we re-imaged some of the sections (1229 layers) at high resolution (2.22 nm/pixel) (*Figure 1—source data 1*). Stitching and alignment of the images was carried out using TrakEM2 (*Cardona et al., 2010*). Reconstruction of the cells and connectivity was carried out using Catmaid (*Saalfeld et al., 2009*) (4845 layers). Neurons were traced and reviewed primarily by NR and GJ, with contributions from LABC, CV, and RS.

Catmaid was installed on a Linux container (LXC; linuxcontainers.org) utilizing 8 CPUs (Intel Xeon 2.67 GHz, Intel, Santa Clara, CA) and 8 GB RAM. The server was setup using PostgreSQL (postgresql.org) and nginx/gunicorn (nginx.org; gunicorn.org). The image stacks (1 TB) were served from the same site.

Neuronal classification, visualization and network analyses

In order to quantify the stereotypy of synaptic connectivity between individuals, we reconstructed the circuitry of the four visual eyes. We traced neurons in synaptic paths downstream of the eye photoreceptors. Cells presynaptic to the eye circuit and weakly connected sensory neurons were not considered. 164 fragments could not be traced (100 fragments < 4 µm, 46 fragments 4–40 µm, and 18 fragments > 40 µm). Fragments are defined as neurons for which a soma could not be found.

We were able to identify the same interneuron and MN types that we reported previously based on the HT9-3 dataset. The stereotypy analysis is mainly based on neuronal groups. For grouped neurons, we used the average synapse number for the calculations. For the effectors, we used the sum of incoming synapses from a group of MNs. Connections were calculated separately for groups of cells with their soma on the left or right side of the body.

Only the primary interneurons and MNs could be compared on a single-cell basis. Anatomical features and neuronal connectivity data were imported into Blender 2.71. Neurons were smoothed such that short branches (<2 μm) were not shown. Network analysis and visualization were performed using Catmaid v0.24, Gephi 0.8.2., prism 5.0, and Blender 2.71.

Acknowledgements

Additional information

Author contributions

NR, GJ, Conception and design, Analysis and interpretation of data, Drafting or revising the article; RS, Acquisition of data, Analysis and interpretation of data, Drafting or revising the article; CV, LAB-C, Analysis and interpretation of data, Drafting or revising the article; SS, Setting up and administering the Catmaid server, Analysis and interpretation of data, Drafting or revising the article

Author ORCIDs

Gáspár Jékely, http://orcid.org/0000-0001-8496-9836

Additional files

Supplementary file

• Source code 1. Blender file containing the visual eye and larval eyespot connectome reconstructed from HT9-4. The file contains the complete anatomical model and connectivity information of the reconstructed visual eye and eyespot circuit from the whole-body dataset of HT9-4. Blender can be downloaded from [http://www.blender.org/]. Display settings can be changed and the connectivity can be analyzed as described in (*Asadulina et al., 2015*).
DOI: 10.7554/eLife.08069.014

References

Asadulina A, Conzelmann M, Williams EA, Panzera A, Jékely G. 2015. Object-based representation and analysis of light and electron microscopic volume data using Blender. *BMC Bioinformatics.* (in press).

Asadulina A, Panzera A, Verasztó C, Liebig C, Jékely G. 2012. Whole-body gene expression pattern registration in *Platynereis* larvae. *EvoDevo* **3**:27. doi: 10.1186/2041-9139-3-27.

Berman GJ, Choi DM, Bialek W, Shaevitz JW. 2014. Mapping the stereotyped behaviour of freely moving fruit flies. *Journal of the Royal Society, Interface / the Royal Society* **11**:20140672. doi: 10.1098/rsif.2014.0672.

Cardona A, Saalfeld S, Preibisch S, Schmid B, Cheng A, Pulokas J, Tomancak P, Hartenstein V. 2010. An integrated micro- and macroarchitectural analysis of the *Drosophila* brain by computer-assisted serial sectionelectron microscopy. *PLOS Biology* **8**:e1000502. doi: 10.1371/journal.pbio.1000502.

Chou YH, Spletter ML, Yaksi E, Leong JC, Wilson RI, Luo L. 2010. Diversity and wiring variability of olfactory local interneurons in the *Drosophila* antennal lobe. *Nature Neuroscience* **13**:439–449. doi: 10.1038/nn.2489.

Conzelmann M, Williams EA, Tunaru S, Randel N, Shahidi R, Asadulina A, Berger J, Offermanns S, Jékely G. 2013. Conserved MIP receptor-ligand pair regulates *Platynereis* larval settlement. *Proceedings of the National Academy of Sciences of USA* **110**:8224–8229. doi: 10.1073/pnas.1220285110.

Couton L, Mauss AS, Yunusov T, Diegelmann S, Evers JF, Landgraf M. 2015. Development of connectivity in a motoneuronal network in *Drosophila* larvae. *Current Biology* **25**:568–576. doi: 10.1016/j.cub.2014.12.056.

Fischer AH, Arendt D. 2013. Mesoteloblast-like mesodermal stem cells in the polychaete annelid *Platynereis dumerilii* (Nereididae). *Journal of Experimental Zoology. Part B, Molecular and Developmental Evolution* **320**: 94–104. doi: 10.1002/jez.b.22486.

Hanaichi T, Sato T, Iwamoto T, Malavasi-Yamashiro J, Hoshino M, Mizuno N. 1986. A stable lead by modification of Sato's method. *Journal of Electron Microscopy* **35**:304–306.

Jarrell TA, Wang Y, Bloniarz AE, Brittin CA, Xu M, Thomson JN, Albertson DG, Hall DH, Emmons SW. 2012. The connectome of a decision-making neural network. *Science* **337**:437–444. doi: 10.1126/science.1221762.

Jékely G, Colombelli J, Hausen H, Guy K, Stelzer E, Nédélec F, Arendt D. 2008. Mechanism of phototaxis in marine zooplankton. *Nature* **456**:395–399. doi: 10.1038/nature07590.

Kabra M, Robie AA, Rivera-Alba M, Branson S, Branson K. 2013. JAABA: interactive machine learning for automatic annotation of animal behavior. *Nature Methods* **10**:64–67. doi: 10.1038/nmeth.2281.

Lu J, Tapia JC, White OL, Lichtman JW. 2009. The interscutularis muscle connectome. *PLOS Biology* **7**:e32. doi: 10.1371/journal.pbio.1000032.

Mosca TJ, Luo L. 2014. Synaptic organization of the Drosophila antennal lobe and its regulation by the Teneurins. *eLife* **3**:e03726. doi: 10.7554/eLife.03726.

Ohyama T, Schneider-Mizell CM, Fetter RD, Aleman JV, Franconville R, Rivera-Alba M, Mensh BD, Branson KM, Simpson JH, Truman JW, Cardona A, Zlatic M. 2015. A multilevel multimodal circuit enhances action selection in Drosophila. *Nature* **520**:633–639. doi: 10.1038/nature14297.

Portugues R, Feierstein CE, Engert F, Orger MB. 2014. Whole-brain activity maps reveal stereotyped, distributed networks for visuomotor behavior. *Neuron* **81**:1328–1343. doi: 10.1016/j.neuron.2014.01.019.

Randel N, Asadulina A, Bezares-Calderón LA, Verasztó C, Williams EA, Conzelmann M, Shahidi R, Jékely G. 2014. Neuronal connectome of a sensory-motor circuit for visual navigation. *eLife* **3**:e02730. doi: 10.7554/eLife.02730.

Randel N, Bezares-Calderón LA, Gühmann M, Shahidi R, Jékely G. 2013. Expression dynamics and protein localization of rhabdomeric opsins in *Platynereis* larvae. *Integrative and Comparative Biology* **53**:7–16. doi: 10.1093/icb/ict046.

Saalfeld S, Cardona A, Hartenstein V, Tomancak P. 2009. CATMAID: collaborative annotation toolkit for massive amounts of image data. *Bioinformatics* **25**:1984–1986. doi: 10.1093/bioinformatics/btp266.

Tomer R, Denes AS, Tessmar-Raible K, Arendt D. 2010. Profiling by image registration reveals common origin of annelid mushroom bodies and vertebrate pallium. *Cell* **142**:800–809. doi: 10.1016/j.cell.2010.07.043.

Vogelstein JT, Park Y, Ohyama T, Kerr RA, Truman JW, Priebe CE, Zlatic M. 2014. Discovery of brainwide neural-behavioral maps via multiscale unsupervised structure learning. *Science* **344**:386–392. doi: 10.1126/science.1250298.

White JG, Southgate E, Thomson JN, Brenner S. 1986. The structure of the nervous system of the nematode *Caenorhabditis elegans*. *Philosophical Transactions of the Royal Society of London. Series B, Biological Sciences* **314**:1–340. doi: 10.1098/rstb.1986.0056.

Yu JY, Kanai MI, Demir E, Jefferis GS, Dickson BJ. 2010. Cellular organization of the neural circuit that drives Drosophila courtship behavior. *Current Biology* **20**:1602–1614. doi: 10.1016/j.cub.2010.08.025.

Zhang W, Yan Z, Li B, Jan LY, Jan YN. 2014. Identification of motor neurons and a mechanosensitive sensory neuron in the defecation circuitry of Drosophila larvae. *eLife* **3**:e03293. doi: 10.7554/eLife.03293.
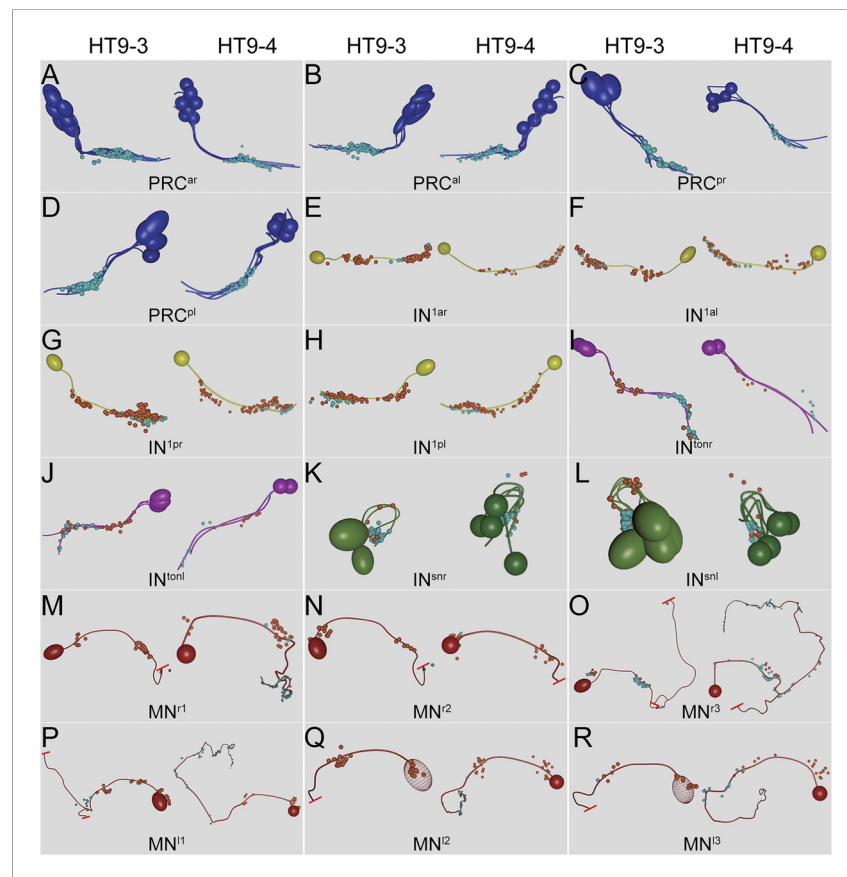
figure supplements

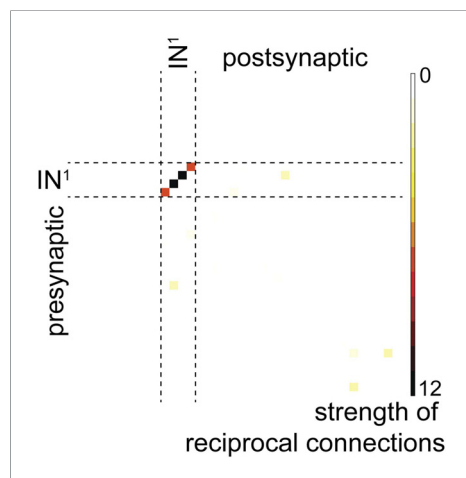Inter-individual stereotypy of the *Platynereis* larval visual connectome
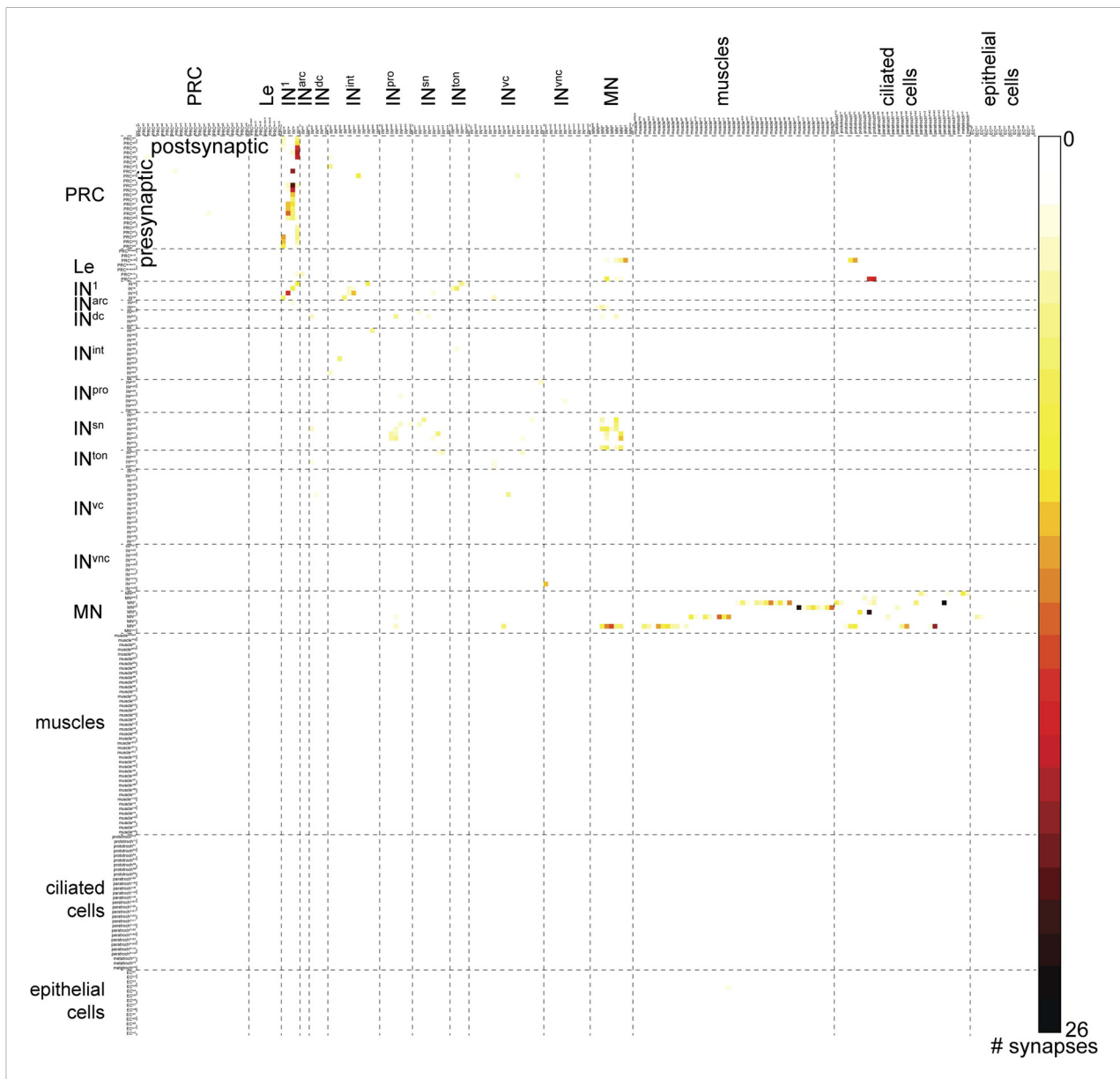
Figure 1—figure supplement 1. Full connectivity matrix of the visual and larval eye circuit of the fully reconstructed larva HT9-4.
DOI: 10.7554/eLife.08069.004

Figure 2—figure supplement 1. Comparison of the neuronal projections and synapse positions of both individuals. Neuronal projections and synapse positions of (**A**) PRC^{ar}, (**B**) PRC^{al}, (**C**) PRC^{pr}, (**D**) PRC^{pl}, (**E**) IN^{1ar}, (**F**) IN^{1al}, (**G**) IN^{1pr}, (**H**) In^{1pl}, (**I**) IN^{tonr}, (**J**) IN^{tonl}, (**K**) IN^{snr}, (**L**) IN^{snl}, (**M**) MN^{r1}, (**N**) MN^{r2}, (**O**) MN^{r3}, (**P**) MN^{l1}, (**Q**) MN^{l2}, and (**R**) MN^{l3} cells in HT9-3 and HT9-4.
DOI: 10.7554/eLife.08069.008

Figure 2—figure supplement 2. Reciprocal connection strength between all neuron pairs in the complete visual circuit (HT9-4). Strength is defined as the geometric mean of the number of synapses of a given neuron 'A' on another neuron 'B' and the number of synapses of neuron 'B' on neuron 'A'. Single neuron identifiers are not shown for simplicity.
DOI: 10.7554/eLife.08069.009
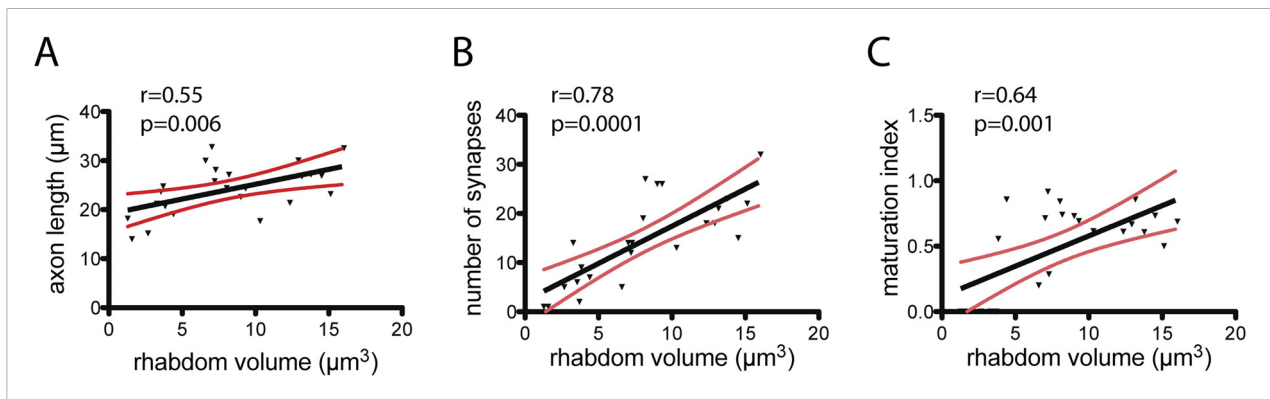
Figure 3—figure supplement 1. Maturation of photoreceptor connections in HT9-4. (**A**) Relationship of rhabdom volume to photoreceptor axon length. (**B**) Relationship of rhabdom volume to photoreceptor synapse number. (**C**) Relationship of photoreceptor connectivity-maturation index to rhabdom volume. In **A**–**C** the black line shows linear regression with 95% confidence interval (red lines). Pearson r and p-value are shown.
DOI: 10.7554/eLife.08069.011

Publication 2: **A serial multiplex immunogold labeling method for identifying peptidergic neurons in connectomes.** *Elife*. (2015)

Shahidi *et al.*

A serial multiplex immunogold labeling method for identifying peptidergic neurons in connectomes

Réza Shahidi, Elizabeth A Williams, Markus Conzelmann, Albina Asadulina, Csaba Verasztó, Sanja Jasek, Luis A Bezares-Calderón, Gáspár Jékely*

Max-Planck-Institute for Developmental Biology, Tübingen, Germany

Abstract Electron microscopy-based connectomics aims to comprehensively map synaptic connections in neural tissue. However, current approaches are limited in their capacity to directly assign molecular identities to neurons. Here, we use serial multiplex immunogold labeling (siGOLD) and serial-section transmission electron microscopy (ssTEM) to identify multiple peptidergic neurons in a connectome. The high immunogenicity of neuropeptides and their broad distribution along axons, allowed us to identify distinct neurons by immunolabeling small subsets of sections within larger series. We demonstrate the scalability of siGOLD by using 11 neuropeptide antibodies on a full-body larval ssTEM dataset of the annelid *Platynereis*. We also reconstruct a peptidergic circuitry comprising the sensory nuchal organs, found by siGOLD to express pigment-dispersing factor, a circadian neuropeptide. Our approach enables the direct overlaying of chemical neuromodulatory maps onto synaptic connectomic maps in the study of nervous systems.
DOI: 10.7554/eLife.11147.001

Introduction

A comprehensive understanding of nervous system function requires knowledge of not only precise neuronal connectivity but also the unique combinations of molecules expressed by each neuron. Connectomics using serial-sectioning electron microscopy (EM) aims to map the synapse-level connectivity of entire neural circuits (*Morgan and Lichtman, 2013*). However, wiring diagrams provide an incomplete picture of the nervous system, since they lack information about the molecular nature of neurons.

One important class of molecules are neuromodulators, including monoamines and neuropeptides, that actively shape the output of circuits by modifying synaptic function and neuron excitability (*Bargmann, 2012*; *Bargmann and Marder, 2013*; *Bucher and Marder, 2013*; *Marder, 2012*). The direct mapping of specific neuromodulators to their source cells in synapse-level anatomical maps would help to integrate connectomic and neuromodulatory perspectives, thereby enriching our understanding of circuit function.

Several approaches have been developed to assign molecular identities to neurons on EM sections. Genetically encoded tags with enzymatic activity, such as miniSOG and APEX probes, allow the resolution of cells or subcellular structures by EM following incubation with a substrate that is converted to electron-dense deposits (*Martell et al., 2012*; *Shu et al., 2011*). Fixation-resistant protein tags compatible with EM procedures and observable by correlative light and electron microscopy (CLEM) or directly by immunogold labeling (immunoEM), such as the smGFPs (*Viswanathan et al., 2015*), have also been developed. In CLEM, fluorescently labeled neurons or organelles can be imaged live prior to fixation, sectioning, and EM imaging of the specimen. Fiducial markers allow the correlation of cellular structures in the immunofluorescence (IF) and EM images (*Colombelli et al., 2008*; *Maco et al., 2013*; *Maco et al., 2014*; *Urwyler et al., 2015*). However,

*For correspondence: gaspar.jekely@tuebingen.mpg.de

eLife digest In the nervous system, cells called neurons connect to each other to form large "neural" networks. The most powerful method that is currently available for tracing neurons and mapping the connections between them is called electron microscopy. This requires slicing brain tissue into ultrathin sections, which are then imaged one by one. However, while electron microscopy provides highly detailed information about the structure of the connections between neurons, it does not reveal which molecules the neurons use to communicate with each other.

To address this question, Shahidi et al. have developed a new approach called 'siGOLD'. Unlike previous approaches, siGOLD allows signal molecules inside cells to be labeled with protein tags called antibodies without compromising the ability to examine the tissue with electron microscopy. The technique was developed using the larvae of a marine worm called *Platynereis*. A single larva was sliced into 5000 sections thin enough to view under an electron microscope, and 150 of these were selected to represent the entire body. Because neurons are typically long and thin, individual neurons usually spanned multiple slices.

To identify the neurons, Shahidi et al. then applied an antibody that recognizes a specific signal molecule to a subset of the slices. The antibodies were labeled with gold particles, which show up as black dots under the electron microscope. Because the molecules recognized by the antibodies are present all along the neuron, and because individual neurons extend over multiple slices, it was possible to trace single neurons by labeling only a small number of slices. Repeating this process in different subsets of slices with antibodies that bind to different signal molecules allowed entire neural circuits to be mapped.

In the future, Shahidi et al.'s approach could be adapted to study neural networks in other organisms such as flies, fish and mice.

DOI: 10.7554/eLife.11147.002

---

the neuron-specific probes employed by these technologies must be expressed using transgenesis, limiting their use to one or a few markers, such as in the 'two-tag' labeling approach (*Lin et al., 2015*).

An alternative approach to assigning molecular identities to neurons is the use of endogenous targets in fixed specimen, as in array tomography, a method employing sequential IF with several different antibodies on large series of sections (*Collman et al., 2015*; *Micheva and Smith, 2007*). IF imaging can be combined with scanning EM imaging of selected sections to resolve ultrastructural detail. The sequentially acquired IF and EM images can be registered, allowing for correlative analysis of images of different modalities (*Collman et al., 2015*). However, the sequential IF procedure compromises the membrane contrast in EM, preventing the reliable tracing of fine processes across series of sections (*Collman et al., 2015*). Array tomography also relies on embedding the specimen in porous, hydrophilic acrylic resins to allow optimal immunolabeling. For large-scale serial sectioning projects, epoxy resins, such as Epon, are favored due to their higher stability during sectioning and imaging and the optimal ultrastructural preservation they provide (*Bock et al., 2011*; *Briggman et al., 2011*; *Bumbarger et al., 2013*; *Ohyama et al., 2015*; *Randel et al., 2015*; *White et al., 1986*). Unfortunately, the Epon-embedding procedure, including osmium-fixation and resin polymerization at 60°C, compromises the immunogenicity of many endogenous targets (*Brorson, 1998*; *Brorson and Reinholt, 2008*; *De Paul et al., 2012*). Current immunolabeling approaches therefore sacrifice the mechanical stability and ultrastructural contrast of the sample for optimal immunolabeling.

One exception is short amidated neuropeptide antigens that show good immunopreservation in epoxy-embedded samples (*Hamanaka et al., 2010*; *Koizumi et al., 1989*; *Merighi et al., 1992*; *Yasuyama and Meinertzhagen, 2010*). Such antigens represent promising targets in an attempt to combine connectomics on Epon-embedded samples and immunogold labeling for specific neuromodulators. Neuropeptides are often chemically modified, including C-terminal amidation (*Eipper et al., 1992*), which confers stability and high immunogenicity to even very short peptides (*Conzelmann and Jékely, 2012*). Furthermore, neuropeptides show neuron-type specific expression

and are distributed throughout the axon of peptidergic neurons (*Wong et al., 2012*; *Zupanc, 1996*), representing useful markers for neuron-type identification.

Here, we introduce serial-multiplex immunogold (siGOLD), a method for immunolabeling connectomes. siGOLD involves immunogold labeling of small subsets of sections from large series with different neuron-type-specific neuropeptide antibodies. The molecularly identified neurons and their synaptic partners are then reconstructed from the entire aligned series using standard EM-based connectomics.

We established siGOLD using larval stages of *Platynereis dumerilii*, a marine annelid that has recently emerged as a powerful model for circuit neuroscience, genetics, and whole-body connectomics (*Backfisch et al., 2013*; *Bannister et al., 2014*; *Gühmann et al., 2015*; *Randel et al., 2014*; *Randel et al., 2015*; *Tosches et al., 2014*; *Veedin-Rajan et al., 2013*; *Zantke et al., 2014*). We identified several amidated neuropeptide epitopes that showed long-term immunopreservation in Epon-embedded samples, allowing us to simultaneously obtain high ultrastructural detail and specific immunogold signal. Using siGOLD with 11 distinct antibodies on the same specimen, we identified several neuropeptide-containing neuron profiles in a whole-body *Platynereis* larval serial EM dataset (*Randel et al., 2015*). Furthermore, taking advantage of the whole-body series, we fully reconstructed several peptidergic neurons identified by siGOLD in the *Platynereis* larva. We also identified and reconstructed the postsynaptic partners of selected peptidergic neurons, focusing on the nuchal organs, paired, putatively chemosensory organs with high structural complexity and variability among the annelids (*Purschke, 1997*; *Purschke, 2005*; *Purschke et al., 1997*; *Schlötzer-Schrehardt, 1987*). Our work demonstrates that siGOLD can be used in large serial EM datasets to assign molecular identities to multiple neurons using different markers and to fully reconstruct and analyze the synaptic connectivity of these neurons at EM resolution.

Results

Multiplex neuron identification with siGOLD on serial sections

In order to selectively label individual neurons in large-scale serial EM datasets, we established an immunoEM procedure to label ultrathin sections with neuronal cell-type specific antibodies. We reasoned that immunoEM performed on only a few layers from a large series of sections could identify neuron profiles that contain the antigen (*Figure 1A*). We first performed immunoEM on 40-nm serial sections from the ventral nerve cord (VNC) of a 72 hr post-fertilization (hpf) *Platynereis* larva (specimen HT9-5, *Figure 1B,C*). For specimen preparation, we used a conventional serial TEM protocol including high-pressure freezing, fixation with a freeze substitution medium containing 2% osmium tetroxide and 0.5% uranyl acetate, and embedding in Epon. We also developed a procedure for the safe handling of several grids in parallel during the immunostaining and contrasting procedure. We optimized the immunolabeling protocol to achieve high specificity for immunoEM and high ultrastructural detail. In our protocol, we use secondary antibodies coupled to ultra small gold particles and a silver-enhancement procedure. We also fine-tuned the contrast-staining protocol to optimize contrast for both gold labeling and ultrastructural detail.

In preliminary tests, we found strong and localized labeling in neurites using 11 different polyclonal antibodies generated against short amidated neuropeptides of *Platynereis* (*Table 1*).

To test the specificity and reproducibility of immunoEM with the 11 neuropeptide-antibodies, we collected two sets of transverse serial sections from the first trunk segment of the HT9-5 specimen. Four to 18 consecutive serial sections were collected on each EM grid for immunoEM. For each antibody, we stained two grids separated by a serial distance of approximately 50 sections (*Figure 1C*). We imaged the VNC region in each section at a resolution of 2.22 nm/pixel followed by stitching and alignment of the images. We found strong and localized labeling in only a small subset of neurites for each antibody (*Figure 2A*, *Shahidi, et al., 2015*). In consecutive sections, the same neurite was often strongly labeled with the same antibody (*Figure 2A*, FVa, layers 1–5). In sections collected on different grids that were labeled with different antibodies, we found distinct patterns of neurite-specific labeling (*Figure 2B,C*). In many sections, we could observe dense core vesicles (DCVs) in the cytoplasm of the gold-labeled neurites, indicative of the peptidergic nature of these cells (*Figure 2A–F*, *Shahidi, et al., 2015*). In high-resolution (0.22 nm/pixel) images, we could observe gold labeling associated with DCVs (*Figure 2D–F*), suggesting that our immunoEM procedure
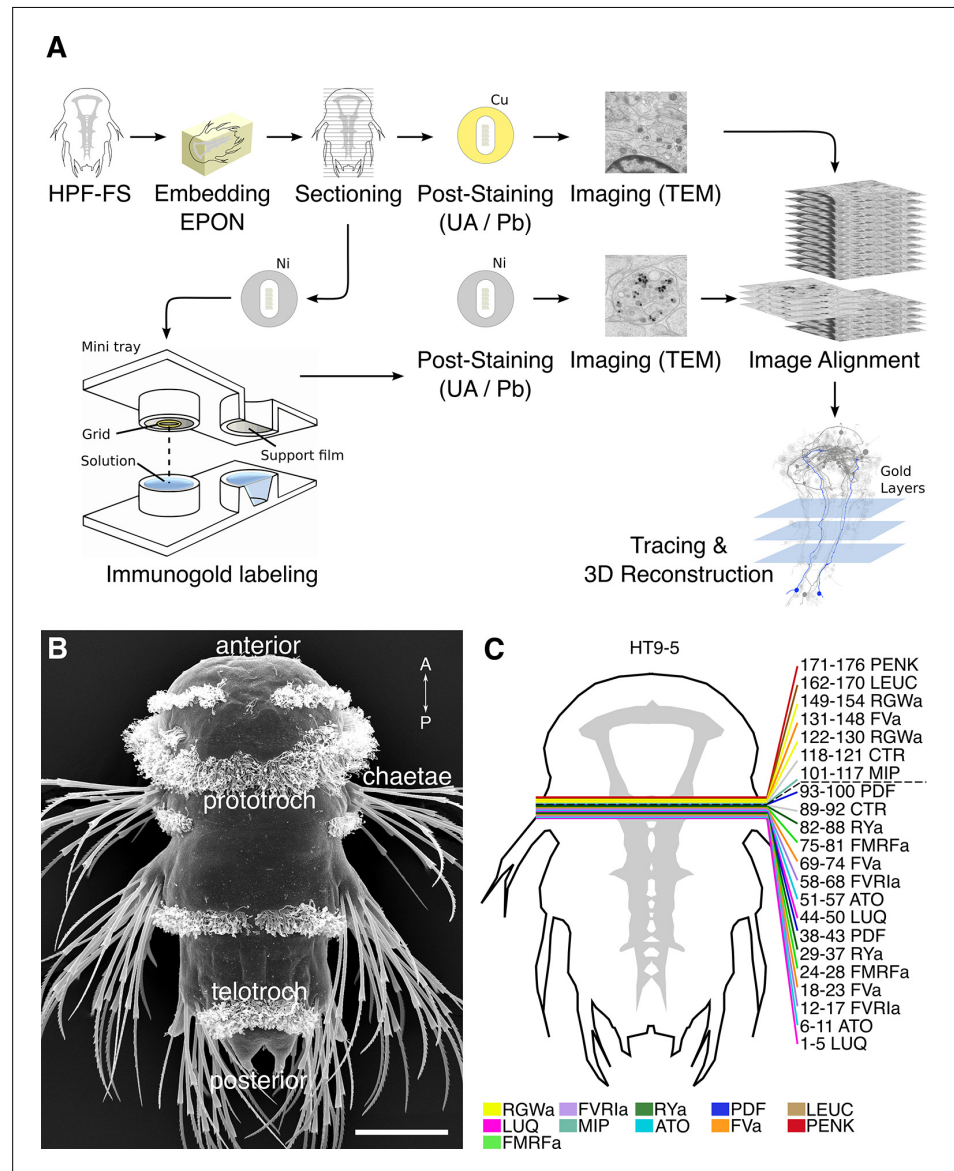
Figure 1. Development of the siGOLD method. (**A**) Schematic flowchart of the siGOLD labeling approach from high-pressure freezing and freeze substitution (HPF-FS) to tracing and 3D reconstruction. Ni, nickel grid, Cu, copper grid. (**B**) SEM micrograph of a 72 hpf *Platynereis* larva. (**C**) Schematic of the HT9-5 sample showing the position of the ventral nerve cord (VNC), ventral view. Colored lines indicate where cross-sections through the VNC were taken, near the base of the circumesophageal connectives at the level of the first commissure. Layer number(s) followed by neuropeptide ID are indicated for each colored line. Dashed line indicates the gap (approximately 10 missing sections) between the first and second series of sections. Scale bar: (**B**) 50 μm.
DOI: 10.7554/eLife.11147.003

labeled mature neuropeptides residing inside these vesicles. Several ultra-small gold particles were not enlarged during the silver-enhancement procedure but were also associated with DCVs (*Figure 2D*–F).

Next, we comprehensively scored the distribution of gold particles in the VNC series (*Figure 3*). We selected all neurites that were labeled with two or more gold particles in any of the immunoEM

Table 1. List of antibodies used

NP precursor name	Abbreviation	Antigen
FMRFamide	FMRFa	(C)FMRFa
RYamide	RYa	(C)VFRYa
Myoinhibitory peptide/Allatostatin B	MIP	(C)AWNKNSMRVWa or (C)VWa
RGWamide	RGWa	(C)RGWa or (C)GWa
Proenkephalin	PENK	(C)YGDLSFSNSNYa
Luqin	LUQ	(C)WRPQGRFa
Allatotropin	ATO	(C)GFRTGAYDRFSHGFa
Pigment dispersing factor	PDF	(C)NPGTLDAVLDMPDLMSLa
Leucokinin	LEUC	(C)KFTPWAa
FVamide	FVa	(C)AHRFVa or (C)FVa
FVRIamide	FVRIa	(C)FVRIa

The full name and abbreviation of neuropeptide precursors that contain the neuropeptides used for immunoEM. The FMRFa, RYa, MIP short and long, RGWa, FVa short and long, and FVRIa antibodies have been described previously (*Conzelmann and Jékely, 2012*; *Conzelmann et al., 2011*; *Conzelmann et al., 2013a*; *Jékely et al., 2008*). All 11 neuropeptides are amidated (a). A Cys (C) was added to the N-terminus of each peptide to allow coupling during immunization and affinity purification. All antibodies were generated in rabbits. For FVa long, a rat antibody was also generated.

DOI: 10.7554/eLife.11147.004

sections and traced these neurites across all sections. We also selected 50 control neurites along a coronal transect spanning the VNC and traced these across all sections (*Figure 3A*). We then counted all gold particles in each traced neurite and tabulated the results (*Figure 3—source data 1*). The gold particles were also summed for each antibody to show a concise summary of all gold labels (*Figure 3B and D*). Since not all ultra-small gold particles were enhanced during silver-enhancement (*Figure 2D–F*) and non-enhanced particles are not visible on the lower resolution images we used for scoring, the gold counts likely underestimate the intensity of gold labeling.

Our quantifications revealed a high neurite-specificity of immunogold labeling with all 11 neuropeptide antibodies (*Figure 3*). In sections where we omitted the primary antibody, we did not see any gold labeling in any of the traced neurites (*Figure 3B*). The VNC in our sample contained approximately 1600 neurite cross-sections and the majority of these showed no gold labeling. However, for each antibody we could identify a small number of neurites that consistently showed strong labeling across different sections (*Figure 3*, *Figure 3—source data 1*). The pattern of the labeled neurites in the VNC showed bilateral symmetry, supporting the labeling of specific peptidergic neuron populations on the left and right sides of the body. Most neurites that were labeled on one grid were also strongly labeled on their grid pair with the same antibody separated by approximately 50 sections. There were some exceptions, for example neurite n5 that was labeled strongly with the FVamide antibody in layers 18–23 but not in layers 69–74 (*Figure 3—source data 1*). To determine whether the lack of labeling was due to the lack of DCVs in these sections, we scored the number of DCVs across all sections for selected neurites (*Figure 3—figure supplement 1*). We found that DCVs were non-uniformly distributed in the neurites and some sections completely lacked DCVs. Importantly, we only detected gold labeling on sections that contained DCVs in the respective neurite (*Figure 3—source data 1*).

siGOLD also allowed us to detect the coexpression of some neuropeptides in the same neurons. For example, we found coexpression of FVa and PDF neuropeptides in a subset of the neurites labeled by these two antibodies (*Figure 3D*). Some antibodies showed extensive overlap in labeling, including the FMRFa, luqin and RYa antibodies.

To test whether the antibodies specifically recognize the neuropeptides used for immunization, we performed morpholino-mediated knockdown experiments of proneuropeptide expression. The specificity of the MIP antibody was demonstrated previously (*Williams et al., 2015*). We performed microinjections with 10 different translation-blocking morpholinos, one targeting each remaining
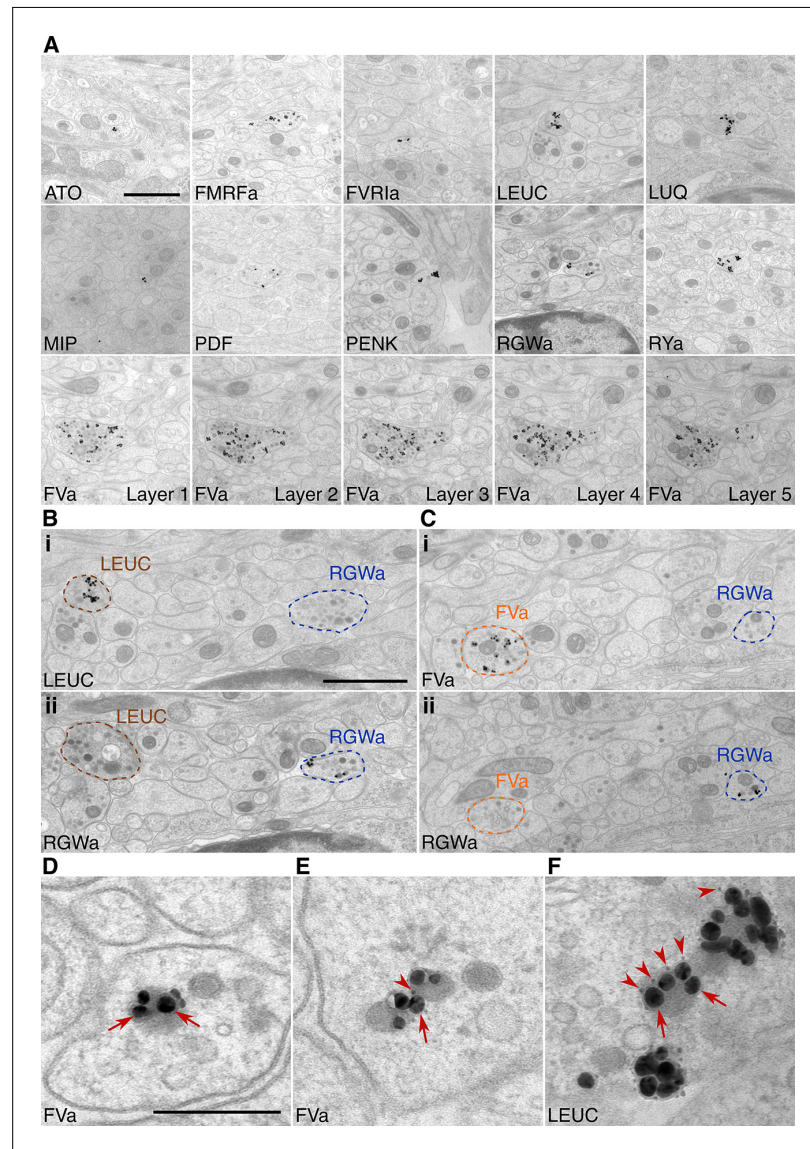
Figure 2. Immunolabeling with neuropeptide antibodes on Epon sections. (**A**) Representative micrographs with immunogold labeled axons for the neuropeptide antibodies indicated. For the FVa neuropeptide antibody, five adjacent sections are shown (FVa Layer 1–5). (**B, C**) Neurite-specific labeling in adjacent sections (seven sections apart) labeled with different antibodies. (**D–F**) High-resolution micrographs of immunogold labeled, silver-enhanced gold particles (arrows), and unenhanced ultra small gold particles (arrowheads) Scale bar: (**A-C**) 1 μm; (**D–F**) 200 nm. High-resolution images are available in (*Shahidi, et al., 2015*).

DOI: 10.7554/eLife.11147.005

proneuropeptide. We then performed triple IF in whole-mount 72 hpf larval samples using an acetylated tubulin antibody, a rat FVa antibody, and the respective rabbit neuropeptide antibodies. The acetylated tubulin antibody allowed us to exclude developmental abnormalities caused by morpholino injection. The rat FVa antibody provided a further control to exclude that morpholino injection affected proneuropeptide processing in general. For 8 out of 10 antibodies (FVa, FMRFa, ATO, FVRIa, PDF, RGWa, PENK, LEUC), morpholino injection strongly reduced IF signal with the respective antibody (*Figure 4—figure supplement 1*). For the FMRFa antibody, we did not detect staining
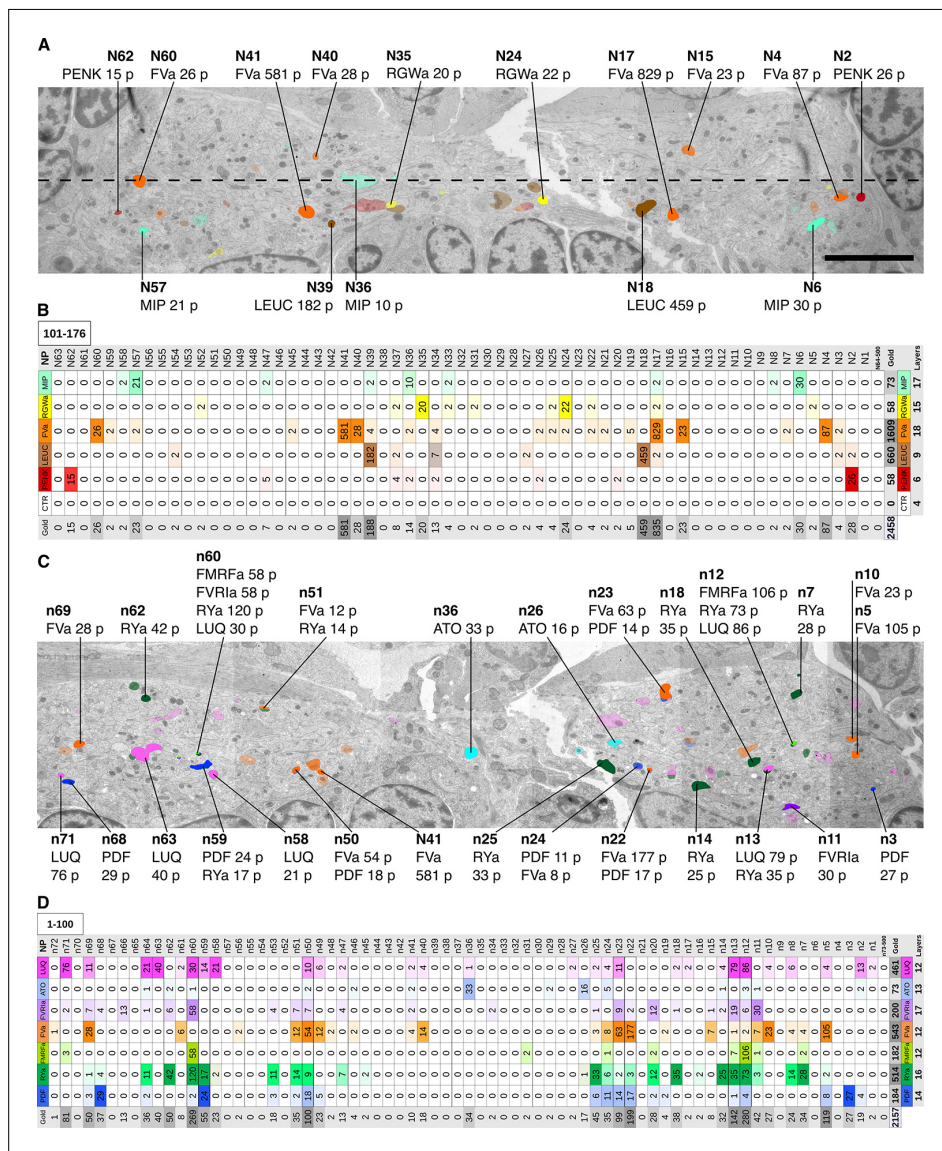
Figure 3. Identification of peptidergic neurites by siGOLD in a 72 hpf *Platynereis* specimen (HT9-5). (**A, C**) Anterior view of EM cross-section through the VNC near the first commissure. Dorsal side of larva is to the top. Strongly labeled neurites were analyzed across the whole VNC region. Control axon profiles were analyzed along a transect (dotted line), two axon profiles were sampled every 1 μm. Total of 72 and 63 axons were examined for the first and second series of sections respectively (an approximately 10-section gap occurs between the two series). Colored cell profiles indicate gold labeled neuropeptidergic axons. Different shades of a color represent an approximation of labeling intensity. Positive axons are tagged with neuron number, neuropeptide name, and total number of gold particles per total number of layers for that neuropeptide. (**B, D**) Tables show number of gold particles per axon for each neuropeptide. All strongly labeled axons across the VNC and control axons along the sampled transect are shown. Data were arranged according to the spatial distribution of the corresponding neurites in the VNC. Each sampled axon was traced across all layers and counted for its total number of gold particles. Columns indicate neurons and an ID with 'n' is given to each neuron in the first series of sections and 'N' for neurons in the second series of sections. Rows indicate neuropeptide immunogold labels. Different shades of the same color indicate intensity of gold labeling. Totals are shown for each row (neuropeptide) and each column (axon profile). In

Figure 3 continued on next page

in the VNC following morpholino injection but we could still detect staining in the head. The FMRFa antibody therefore likely recognizes other antigens, such as other RFa peptides in the head (*Conzelmann et al., 2013b*). For the RYa and LUQ antibodies, we did not see a reduction in staining intensity in the VNC following morpholino injection. These two antibodies may cross-react with other R[Y F]amide peptides as suggested by the labeling of an overlapping set of neurites with the FMRFa, LUQ, and RYa antibodies (*Figure 3*). Without knowing the exact antigen specificity for these antibodies, we can nevertheless use them as specific markers of R[Y|F]amidergic neurons.

Comparison of siGOLD labeling to whole-mount immunofluorescence

siGOLD labeling of consecutive sections with 11 antibodies revealed the arrangement of several peptidergic neurites in the VNC (*Figure 3*). To test if this spatial arrangement is consistent between siGOLD and IF labeling of whole specimens, we analyzed the labeling with all 11 antibodies in whole-mount *Platynereis* 72 hpf larval samples. All antibodies labeled subsets of longitudinal axons spanning the entire length of the VNC and occurring in different mediolateral positions (*Figure 4*).

To display the spatial relationships of 11 distinct IF labels, we employed image registration to a reference template of whole-body confocal scans. High-accuracy image registration of different specimens is possible in *Platynereis*, due to the stereotypic anatomy and neuronal connectivity of the larvae (*Asadulina et al., 2012*; *Randel et al., 2015*; *Tomer et al., 2010*). For optimal VNC registration, we generated an unbiased average whole-body reference template based on the non-rigid registration of the acetylated tubulin IF signal from 36 specimens. We aligned whole-body confocal scans of IF specimens to this reference using non-rigid image registration (*Figure 5A,B*; *Video 1*). We then took virtual cross sections from this registered dataset to analyze the spatial relationships of distinct peptidergic axons (*Figure 5C–E*). The arrangement of peptidergic axons in the VNC reconstructed by IF and image registration was similar to that of the VNC reconstructed by siGOLD (*Figure 5F–H*). To allow a more direct comparison of the spatial relationship of peptidergic axons, we performed double IF with each of the RGWa, PDF, and LEUC antibodies generated in rabbits in combination with a FVa antibody generated in rats. The spatial relationships of the neurites labeled with the RGWa, PDF, and LEUC antibodies relative to six prominent FVa neurites was very similar between IF and siGOLD (*Figure 5I,J*). We could also detect the coexpression of FVa and PDF in some axons, both by double-IF and siGOLD. The high specificity of immunoEM, the reproducibility of labeling across sections, and the spatial correspondence of the labels between siGOLD and whole-mount IF indicate that we could accurately identify different peptidergic neurites in a serial EM dataset.

Application of siGOLD to a whole-body connectome dataset

Next, we tested siGOLD on a whole-body EM series of 5056 sections encompassing an entire 72 hpf *Platynereis* larva (specimen HT9-4) (*Randel et al., 2015*). During sectioning of this larva, we set aside series of 1–6 sections for later immunoEM (*Figure 6—source data 1*).

In the full-body series, we used the 11 rabbit antibodies (*Table 1*) to label a total of 154 sections (3% of all sections) distributed along the length of the larva (*Figure 6A*). We used at least two grids for each antibody, separated by up to 1000 sections. Gold labeling in a whole-body context allowed us to identify several strongly labeled neurite profiles throughout the body. It is worth noting that sections were successfully gold labeled up to 3 years after sectioning the specimen, demonstrating the long-term stability of neuropeptide antigens in Epon sections.

We identified and traced 83 neurons (67 of them with a soma; *Figure 6B*; *Video 2*) with different peptidergic identities. We mapped the distribution of peptidergic axons crossing a section in the first trunk segment in a position comparable to that of HT9-5 and found similar patterns across both siGOLD-labeled larvae and the IF samples (*Figure 7A,B*; compare to *Figure 5*). For selected neurons, we quantified the number of gold particles in every immunolabeled section in HT9-4 (*Figure 8*, *Figure 9*). These counts again demonstrated that we could repeatedly label the same neurons in different sections, often spaced several hundred sections apart.

The reconstruction of several neurons in the whole-body serial EM dataset allowed us to further test the specificity of the immunogold labels by comparing the morphology and position of reconstructed neurons to neurons that were identified by whole-body IF. We found comparable cellular morphologies and positions for six FVa, several PDF (*Figure 8*), two RGWa, and four MIP neurons (*Figure 9*) between siGOLD and IF. This close anatomical correspondence further supports the specificity of siGOLD and demonstrates that the method can be used to unambiguously tag fully reconstructed neurons in serial EM.

Connectome reconstruction of a siGOLD-labeled peptidergic circuit

The whole-body serial EM dataset combined with siGOLD labeling allows the reconstruction of circuits of neurons with specific peptidergic identities. To demonstrate this, we focused on the nuchal organs in the *Platynereis* larval head as an example. The nuchal organ is a paired putative chemosensory organ in the annelid head with sensory neurons projecting a sensory dendrite into an olfactory pit. The olfactory pit is covered by cuticle and is associated with a patch of motile cilia (*Figure 10A–*
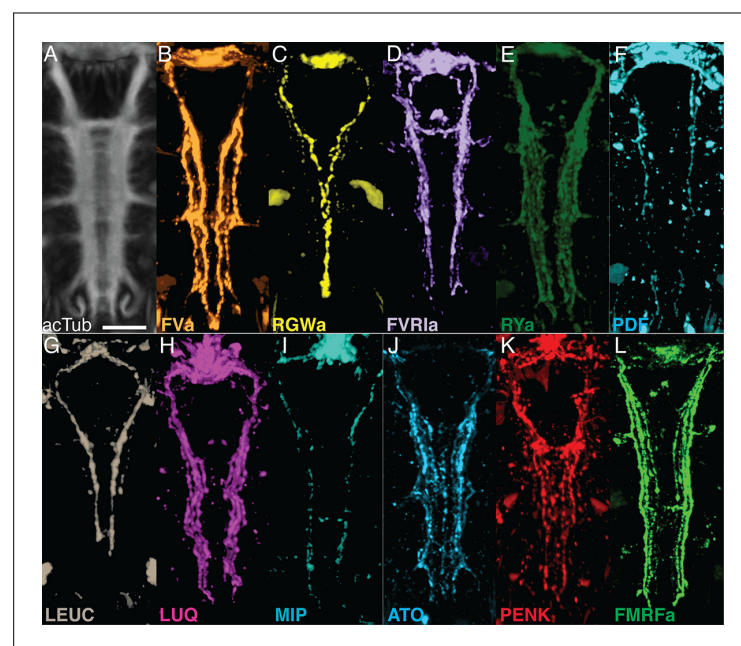
Figure 4. Whole-mount IF of *Platynereis* larvae with antibodies raised against neuropeptides labels distinct subsets of neuronal tracks in the VNC. (**A**) Ventral view of *Platynereis* VNC, stained with an anti-acetylated tubulin antibody. This is the registered average VNC generated from scans of 36 larvae. (**B–L**) Whole-mount IF of *Platynereis* larvae with an antibody raised against (**B**) FVa, (**C**) RGWa, (**D**) FVRIa, (**E**) RYa, (**F**) PDF, (**G**) LEUC, (**H**) LUQ, (**I**) MIP, (**J**) ATO, (**K**) PENK, (**L**) FMRFa. Whole-mount scans were cropped to show only the VNC region. Scale bar: 20 µm.

DOI: 10.7554/eLife.11147.009

The following figure supplement is available for figure 4:

Figure supplement 1. Morpholino-mediated knockdown of proneuropeptides followed by whole-mount IF indicates antibody specificities.
DOI: 10.7554/eLife.11147.010
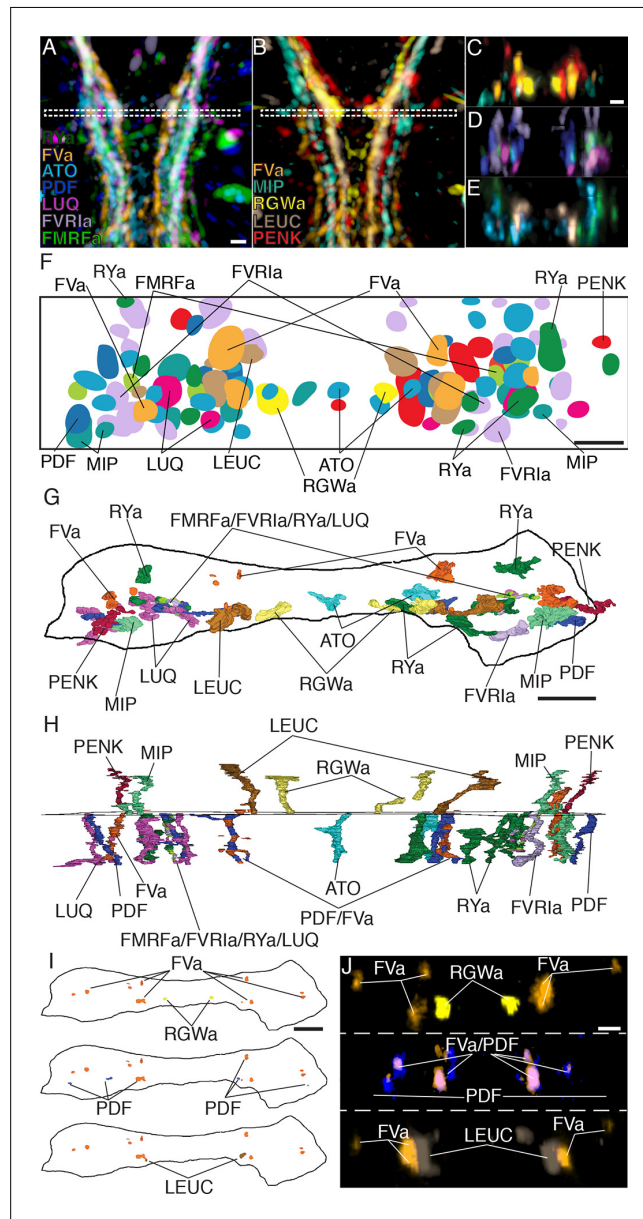
Figure 5. Axonal arrangements in the VNC detected by whole-body IF spatially match those detected by siGOLD. (A, B) Ventral overview of individual registered full-body IF with antibodies raised against 11 different neuropeptides (colors). Image is cropped to show only the VNC in the first segment. White dashed box indicates the region where a 5 μm virtual transverse section shown in (C–E) was taken. (C–E) 5 μm virtual transverse section of individual registered full-body IFs from (A, B) in anterior view to indicate their spatial position in the VNC relative to each other. (C) RGWa, FVa, PENK, MIP, (D) FVRIa, PDF, LUQ, FMRFa (E) RYa, LEUC, ATO. (F) Schematic overview of (C–E) indicating relative positioning of individual registered antibody stainings in the VNC, anterior view. (G, H) Reconstruction of neurites labeled by siGOLD in the VNC of specimen HT9-5 with antibodies raised against 11 different neuropeptides, (G) anterior view, (H) ventral view. For comparison with registered IF labeling in (A–F). (I) Position of neurites in specimen HT9-5 siGOLD-labeled with FVa and RGWa (top), FVa and PDF (middle), and FVa and LEUC antibodies (bottom). For comparison with double-IF in (J). (J) 2 μm virtual transverse sections of the VNC of 72 hpf *Platynereis* larvae double-stained with the FVa antibody (orange) and the RGWa (yellow, top), the PDF (blue, middle) or the LEUC (brown, bottom) antibodies. Scale bars: (A–E) 15 μm, (F–J) 5 μm.
Figure 5 continued on next page

C; *Video 3*) (*Purschke, 2005*). We found that several sensory neurons of the nuchal organs (SN^{nuch}) were strongly labeled by the PDF antibody in three different PDF-labeled sections in the head (*Figure 6A*; *Table 2*). Of the 35 SN^{nuch} cells we identified, 15 were labeled with the PDF antibody, with some of the neurons showing strong gold labeling in multiple sections (*Table 2*). This is consistent with the labeling of the nuchal organ with the PDF antibody in IF (*Figure 8G*). We traced all SN^{nuch} neurons and identified their direct postsynaptic targets. We found that the most strongly connected neurons, receiving up to 22 synapses from SN^{nuch} cells, were two pairs of interneurons (IN^{arc}) with a unique biramous morphology and contralaterally projecting axons (*Figure 10D–F*; *Figure 10—figure supplement 1*; *Video 4*). Two of the IN^{arc} neurons were previously shown to be postsynaptic to the photoreceptor cells of the larval eyespots and have connections to the ventral motorneurons (*Randel et al., 2015*). This represents a potential functional path linking the nuchal organs to the locomotor apparatus. We also identified several other neurons that received a few synapses from the SN^{nuch} cells, including two interneurons (IN$^{RGWa-dcr1}$, IN$^{RGWa-dcl1}$) that were identified by siGOLD labeling to express the RGWa neuropeptide (*Figure 9A,B*). Additionally, 87 neurons received only one synapse from one of the SN^{nuch} cells (*Figure 10—figure supplement 2*). The strong connectivity of the IN^{arc} cells to the nuchal organ relative to these other neurons suggests that the IN^{arc} cells represent the functionally relevant targets in the circuit.

Mapping the position of presynaptic sites of SN^{nuch} cells revealed that these cells form synapses bilaterally (*Figure 10 H, I*). This is in contrast to the adult eye photoreceptor cells that only form ipsilateral synapses (*Figure 10 H, I*) (*Randel et al., 2014*).

To characterize the synapses of the PDF-positive SN^{nuch} cells in more detail, we examined several synapses in high-resolution (2.22 nm/pixel) images (*Randel et al., 2015*). We found that SN^{nuch} presynaptic sites contained only DCVs (*Figure 10J,K*). These synapses could be clearly distinguished from classical neurotransmitter synapses (*Figure 10L*) (*Randel et al., 2014*) based on the larger size of the synaptic vesicles (mean diameter=63 nm, S.D. = 8.4, n=100 vesicles) and the electrondense core of the vesicles (*Figure 10J,K*). Furthermore, mapping classical neurotransmitter markers by in situ hybridization did not reveal the presence of any classical neurotransmitters in the nuchal organ region (*Randel et al., 2014*). Although we did not directly immunogold label any of the SN^{nuch} synapses, these observations suggest that the SN^{nuch} neurons signal to their target interneurons by PDF-containing vesicles concentrated at peptidergic synapses.


Video 1. Neuronal arrangements in the ventral nerve cord detected by whole-body IF and image registration. Ventral view of 72 hpf *Platynereis*. VNC (grey) of average whole-body reference template stained with acetylated tubulin, generated from scans of 36 individuals. Onto this reference scaffold, we project individual registered immunostaining patterns generated by the different neuropeptide antibodies. In order of appearance: FVa (orange), RGWa (yellow), LEUC (brown), FVRIa (lavender), RYa (forest green), LUQ (magenta), MIP (aqua), ATO (sky blue), FMRFa (lime green), PENK (red), PDF (royal blue).
DOI: 10.7554/eLife.11147.013

Discussion

In this paper, we introduced siGOLD, a method to molecularly identify specific neurons in large serial EM datasets based on the immunogold labeling of subsets of sections followed by serial reconstruction of the tagged neurons. Due to the sparse labeling of a few sections across many, siGOLD allows the use of several different antibody labels, each at different sections, within a single dataset. siGOLD relies on continuous series of sections of sufficient quality that allow the tracing of neurites in order to reconstruct the morphologies of labeled neurons.
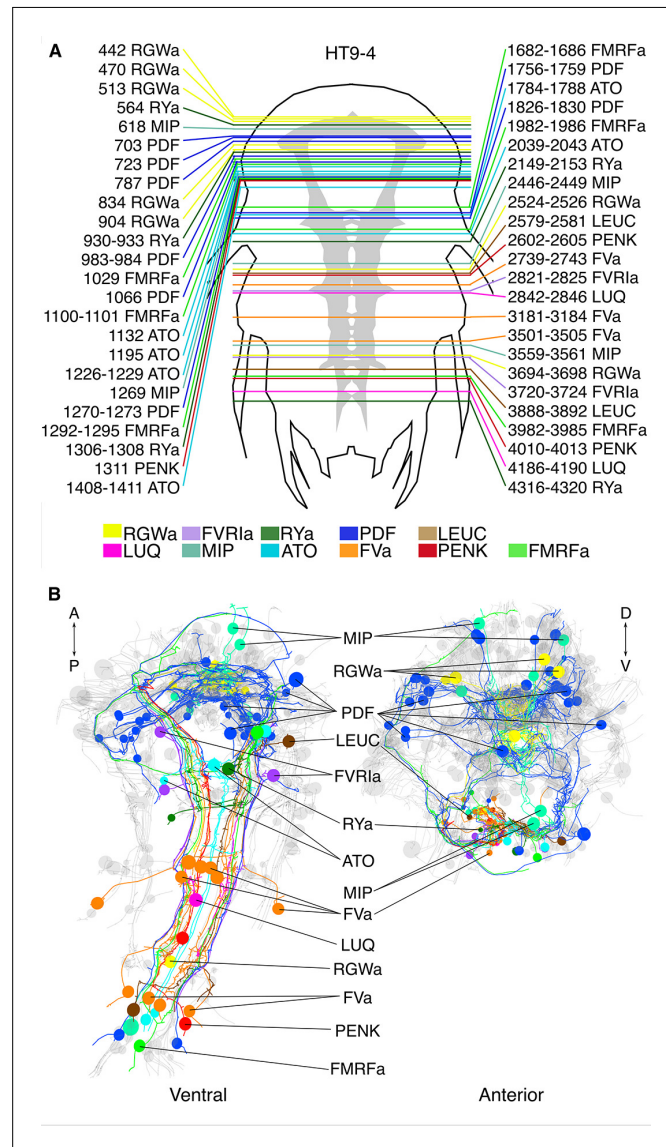
Figure 6. siGOLD labeling in a whole-body serial EM dataset (HT9-4). (**A**) Schematic of the HT9-4 specimen showing the position of the VNC (grey), ventral view. The entire larva was fully sectioned and imaged. Colored lines indicate the position of sections that were used for immunolabeling. For each line, layer number(s) followed by the name of the neuropeptide that was immunogold-labeled in those layers are indicated. (**B**) Ventral and anterior views of all fully traced immunogold-labeled peptidergic neurons. Detailed layer information is available in *Figure 6—source data 1*.

DOI: 10.7554/eLife.11147.014

The following source data is available for figure 6:

Source data 1. Complete layer statistics of the sections and images of HT9-4.
DOI: 10.7554/eLife.11147.015

Since siGOLD requires the sparse labeling of small subsets of sections, it is ideally used with markers that broadly label a neuron's morphology. We established siGOLD using neuropeptide antibodies for two reasons. First, neuropeptides are distributed along the entire length of axons, due to their active circulation throughout the axon (*Wong et al., 2012*). Second, neuropeptide antigens
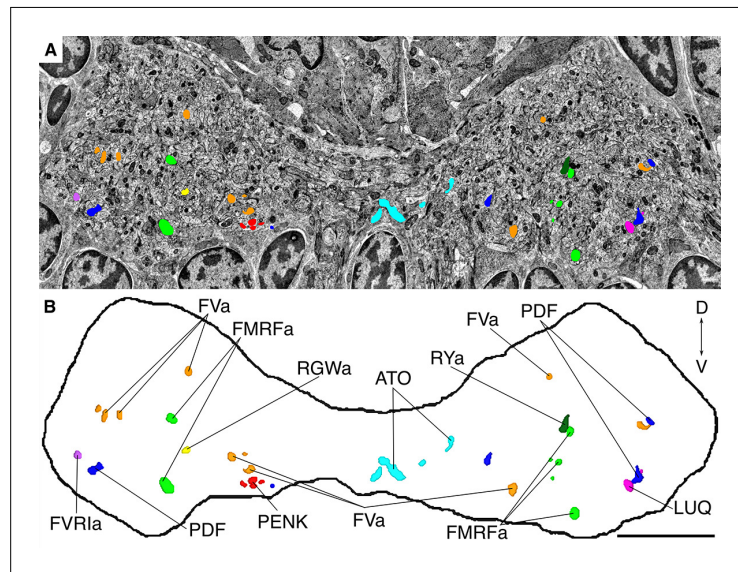
Figure 7. Position of siGOLD-labeled neurites in a cross-section of the VNC in HT9-4. (**A**) TEM image of a VNC cross-section with the segmented profiles of peptidergic neurites identified by siGOLD. Different colors represent different neuropeptide-antibody labeling. (**B**) Segmented profiles of peptidergic axons in a cross-section through the VNC near the base of the circumesophageal connectives at the first commissure. All traced neuropeptidergic axons crossing the VNC at that level in the HT9-4 specimen are shown. Scale bar: (**B**) 5 μm.
DOI: 10.7554/eLife.11147.016

have unique properties, including their small size, high abundance, concentration in DCVs, and frequent C-terminal amidation, a modification that confers increased stability and immunogenicity to mature neuropeptides (*Conzelmann and Jékely, 2012*; *Eipper et al., 1992*). In agreement with the extreme stability of neuropeptide immunoreactivity, we could perform immunoEM of 'set-aside' layers using neuropeptide antibodies years after sectioning and the acquisition of the complete image series had been completed.

We did not test other antibodies, but several generally used antibody markers, including antibodies against neurotransmitters, transporters, or enzymes (*Collman et al., 2015*), could in principle be suitable for neuron identification using siGOLD. We established siGOLD on Epon-embedded samples that allowed robust sectioning of thousands of sections and provided high ultrastructural detail. Since Epon-embedding is known to compromise the immunogenicity of some antigens (*Brorson, 1998*; *Brorson and Reinholt, 2008*; *De Paul et al., 2012*), labeling for such antigens may require the use of alternative embedding resins such as Lowicryl HM-20 that provides excellent ultrastructural contrast and is compatible with many antibodies (*Collman et al., 2015*).

siGOLD is compatible with conventional TEM using sections collected on slotted, plastic-coated nickel grids (*Skepper and Powell, 2008*). It is also compatible with sectioning methods that collect long ribbons of sections on a glass slide (*Blumer et al., 2002*) or the high-throughput automatic tape-collecting ultramicrotome (ATUM) method (*Hayworth et al., 2014*). However, siGOLD is not compatible with sectioning procedures that destroy the sections, such as focused ion beam (FIB) SEM (*Reyntjens and Puers, 2001*) or the serial block-face method (*Denk and Horstmann, 2004*).

The siGOLD method differs from conjugate light-electron array tomography (*Collman et al., 2015*) and CLEM in several aspects. Array tomography was developed to provide detailed molecular profiling of individual synapses, and uses repeated immunolabeling of every section. siGOLD does not rely on the staining of every section with multiple markers, but rather the staining of sparsely distributed sections with one marker each. The aim of siGOLD is to assign molecular tags to several different neurons and to trace them through many layers. Array tomography and CLEM involves the registration of separately acquired IF and EM images, and the relocation of the sample between the different imaging setups can be challenging and time consuming (*Timmermans and Otto, 2015*). In
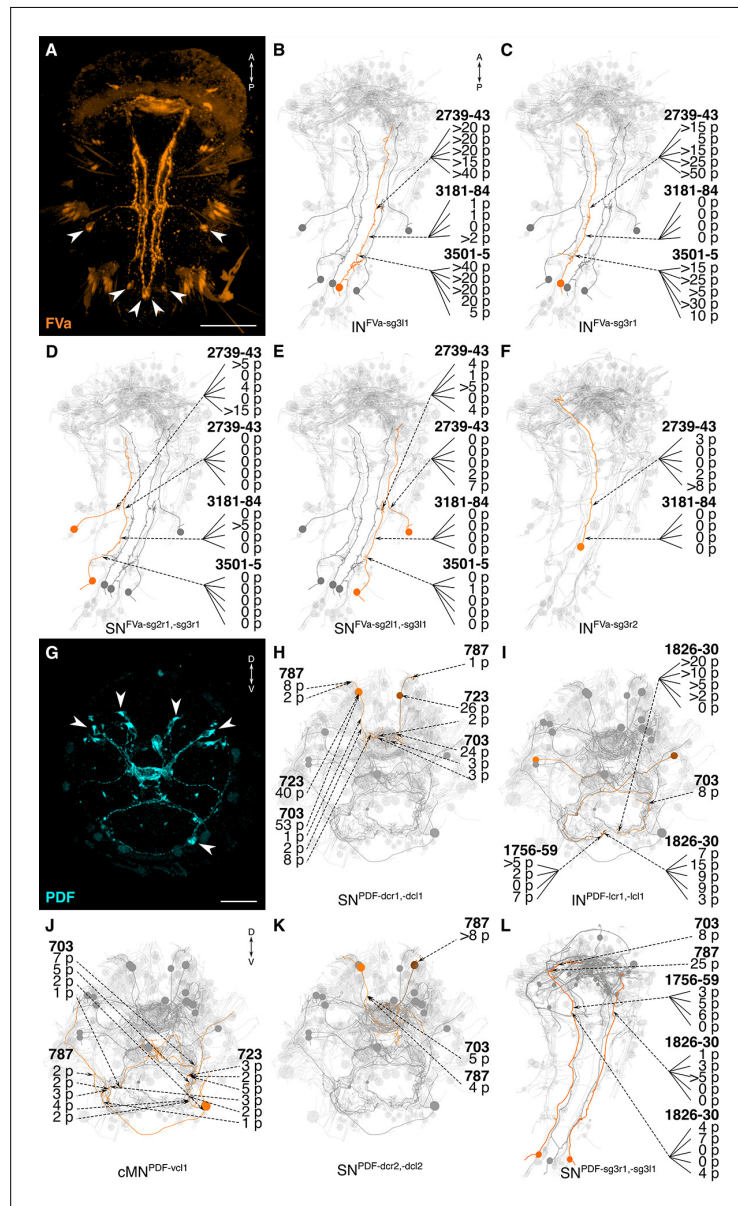
**Figure 8.** siGOLD labeling and whole-body neuron reconstructions in HT9-4. (A, G) Full body IF labeling of FVa and PDF-positive cells, ventral view and anterior view, respectively. Note that (A) is 72 hpf and (G) is 48 hpf. Arrowheads point to neuron cell-bodies that were traced in EM reconstructions. (B–F, H–L) Fully reconstructed neurons, identified using the siGOLD method in the full body HT9-4 dataset. Dashed arrows indicate immunogold labeled layers along the neurite, layer number(s) and number of gold particles per layer are shown. Reconstructed FVa (B–F) and PDF (H–L) positive cells. Scale bars: (A) 50 μm; (G) 30 μm.
DOI: 10.7554/eLife.11147.017

contrast, siGOLD relies on the direct immunoEM labeling of sections and no registration step is needed. With siGOLD, we enjoy the full resolving power of the electron microscope, and in this study we could also identify individual DCVs that carry strong immunogold signal in the neurite profile of specific peptidergic neurons.
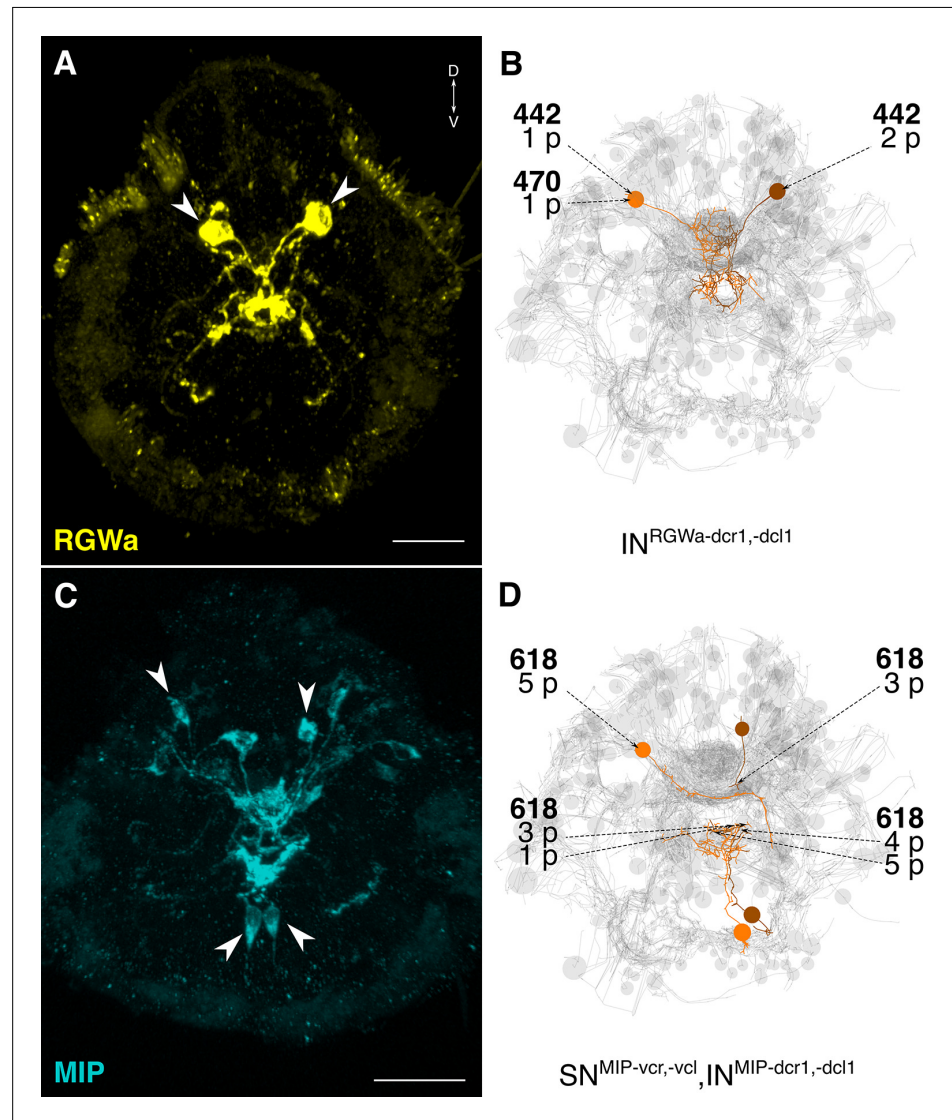
Figure 9. siGOLD labeling and whole-body neuron reconstructions in HT9-4. (**A, C**) Full body IF labeling of RGWa and MIP-positive cells in 72 hpf larvae, anterior views. Arrowheads point to neurons that were traced in EM reconstructions. (**B, D**) Traced neurons, identified using the siGOLD method in the full body HT9-4 dataset. Dashed arrows indicate immunogold-labeled layers along the neurite, layer number(s) and the number of gold particles per layer are shown. Reconstructed RGWa (**B**) and MIP (**D**) positive cells. Scale bars: (**A, C**) 30 μm.
DOI: 10.7554/eLife.11147.018

One shortcoming of the immunoEM approach is that sections cannot be relabeled after they have been contrasted and exposed to the electron beam. However, given that in siGOLD only a subset of the sections is processed for immunoEM, it is possible to use an arbitrarily large number of antibodies at different sections from a series that encompasses a large volume of tissue, allowing the multiplex identification of neuron types.

We demonstrated that siGOLD can be used to molecularly identify neurons in large serial EM datasets, in conjunction with the reconstruction of the synaptic connectivity of these neurons. We reconstructed the sensory neurons of the nuchal organs and their postsynaptic partners, representing a candidate chemotactic circuit in the *Platynereis* larval head. siGOLD labeling revealed that the
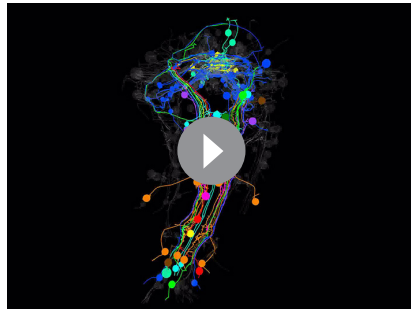
Video 2. 3D view of the 72 hpf HT9-4 larva showing fully-traced peptidergic neurons identified by siGOLD. Ventral view of the 72 hpf *Platynereis* siGOLD-tagged peptidergic neurons are shown in the following colors: FVa (orange), RGWa (yellow), LEUC (brown), FVRIa (lavender), RYa (forest green), LUQ (magenta), MIP (aqua), ATO (sky blue), FMRFa (lime green), PENK (red), PDF (royal blue). Other non-labeled traced neurons (grey) provide the outline of the larva.
DOI: 10.7554/eLife.11147.019

sensory neurons express the PDF neuropeptide. The presence of DCVs and lack of clusters of clear vesicles at presynaptic sites in these neurons suggest the presence of peptidergic transmission to the target interneurons.

The bilateral projection of the nuchal organ sensory neurons is similar to that seen for olfactory receptor neurons in *Drosophila*. These neurons form bilateral projections, and the lateralization of odor processing is achieved by an asymmetry in neurotransmitter release (*Gaudry et al., 2013*). The nuchal organ circuit may use a similar computational strategy, and this is likely different from the processing of visual information (*Randel et al., 2014*; *Randel et al., 2015*). The molecular information obtained by siGOLD provides a useful entry point to the genetic investigation of this putative chemotactic circuit in *Platynereis*.

The mapping of peptidergic neurons by siGOLD, together with the recent identification of several neuropeptide receptors in *Platynereis* (*Bauknecht and Jékely, 2015*), open up the possibility of a cellular-level analysis of peptidergic neurotransmission in diverse circuits in *Platynereis*. In total, we have identified 83 different peptidergic neurons out of approximately 2000 total in the *Platynereis* whole-body dataset. Further connectome tracing in these data will provide a rich source of information about specific peptidergic circuit motifs in this animal.

The siGOLD approach and the use of neuropeptide antibodies could also be adapted to enrich connectome data with molecular information in other organisms. In *Platynereis*, as well as vertebrates, *C. elegans*, and *Drosophila*, the majority of mature neuropeptides are amidated (*Jékely, 2013*; *Mirabeau and Joly, 2013*), and several antibodies are available (e.g. (*Johard et al., 2008*; *Nässel, 1993*)) or could readily be generated. Some neuropeptide antibodies have already been shown to work with immunoEM. For example, PDF neuropeptide-containing neurons were identified in the *Drosophila* brain by immunoEM and their local synaptic inputs were reconstructed from a series of sections (*Yasuyama and Meinertzhagen, 2010*). This and other antibodies could be used for siGOLD labeling in larger-scale connectome projects in *Drosophila*. Similar protocols and reagents could also be established for other organisms. siGOLD could also be adapted to organisms where transgenic tools to deliver EM-compatible markers are not available. In such organisms, the use of cross-species antibodies (*Conzelmann and Jékely, 2012*; *Nässel, 1993*) is a promising approach that would also allow the comparison of specific peptidergic neurons and their circuits across species.

The direct overlaying of chemical neuromodulatory maps onto synaptic connectomic maps by siGOLD opens up new possibilities for the study of nervous systems.

Materials and methods

Transmission electron microscopy

Fixation and embedding was carried out on 72 hpf *Platynereis* larvae (HT9-4 and HT9-5) as described previously (*Conzelmann et al., 2013a*). Forty nanometer serial sections were cut on a Reichert Jung Ultracut E microtome using a 45° DiATOME Diamond knife. The sections were collected on single-slotted copper grids (NOTCH-NUM 2_1 mm, Science Service, Munich) with Formvar support film. For the HT9-5 serial sections, the samples were collected on single-slotted nickel grids coated with Formvar support film. The ribbons of sections were picked up from underneath and on the underside (the notch side) of the grids. This method allowed the section ribbons to stay afloat and stretch while being dried in the oven, eliminating most wrinkles from the sections. The section statistics for
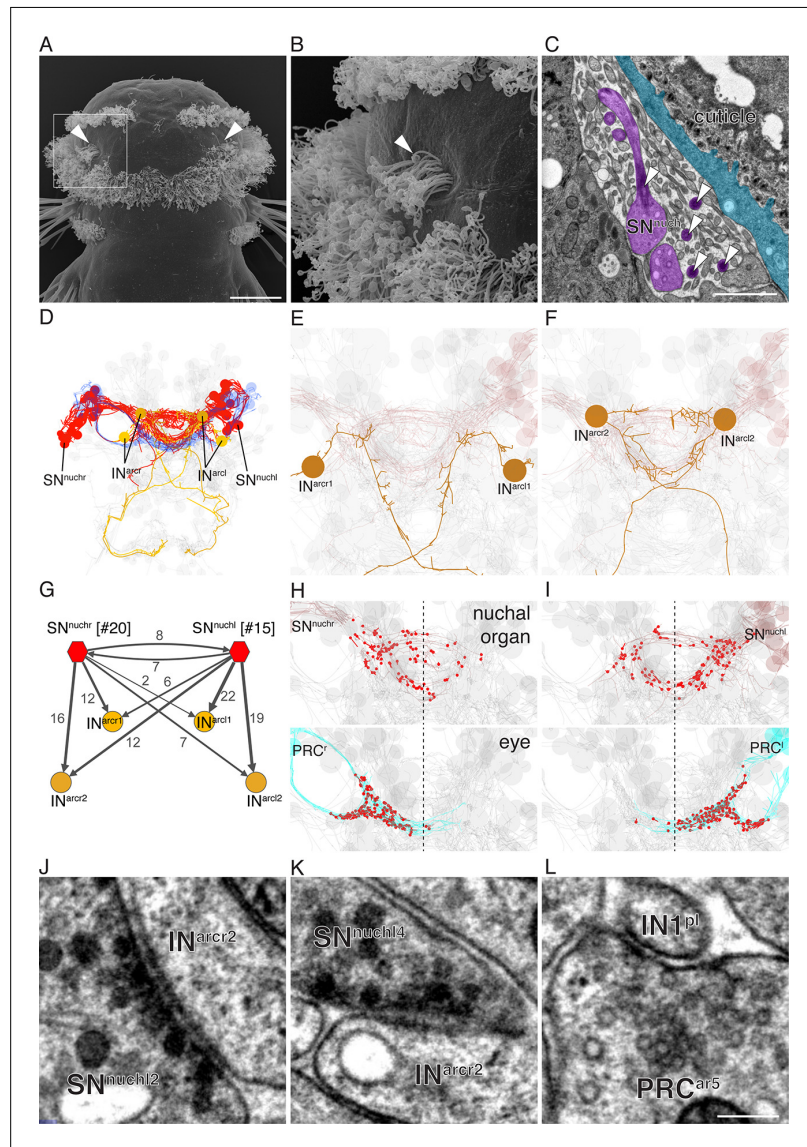
Figure 10. Reconstruction of a siGOLD-labeled peptidergic circuit. (A, B) SEM image of the nuchal organs (arrowhead) in the dorsal-posterior head of a 72 hpf *Platynereis* larva, dorsal view. Boxed area is shown enlarged in (B). Arrowheads point at motile cilia above the olfactory pit. (C) TEM image of a cross section of the nuchal organ showing the olfactory pit with sensory neurons and microvilli. Arrowheads point at sensory cilia. Sensory endings in the olfactory pit are highlighted in magenta, an epithelial cell underneath the cuticle is highlighted in blue. (D) 3D reconstruction of the nuchal organ circuit. SN^{nuch} neurons (red), and IN^{arc} (orange) interneurons are shown. The photoreceptor cells of the adult eyes are shown in blue as a reference. (E, F) 3D reconstruction of IN^{arc} (orange) interneurons. (G) Graph representation of SN^{nuch} connectivity. Nodes represent neurons or groups of neurons, edges represent synaptic connections. The number of synapses is indicated on each arrow. Edge thickness is proportional to the square root of the number of synapses. (H, I) Presynaptic sites (red dots) in SN^{nuch} neurons and adult-eye photoreceptor cells (PRC) with their soma on the right (H) or left (I) side of the body. (J, K) Peptidergic synapses in SN^{nuch} neurons. (L) A glutamatergic synapse in an adult eye photoreceptor cell. Scale bar: (A) 30 μm; (C) 1 μm; (L) 150 nm.

The following figure supplements are available for figure 10:

Figure 10 continued on next page

the HT9-4 specimen (or NAOMI) were previously described (*Randel et al., 2015*) and an updated table with the immunoEM information is shown in *Figure 6—source data 1*. For HT9-5, 200 sections were cut from the VNC (first segment) and imaged for tracing, segmentation and analysis.

Grid handling

To meet the demand for consistent section processing in large-scale serial reconstruction projects, we have developed an effective method of grid handling based on a method first described in *Rowley and Moran (1975)*. The following method has proven safe for contrast staining, immunolabeling, and carbon coating. It stabilizes the grids during the staining procedures and saves time by eliminating the need for one-by-one grid manipulation.

A 6 × 12 hole microwell mini tray plate (NUNC™ Brand MicroWell® Mini Trays) was cut into two 3 × 12 hole plate strips. Holes were drilled through each of the plate's micro-cups using a fine drill to later allow the plastic support film to dry evenly on both sides. Plates were rinsed with 75% ethanol, followed by distilled water, then sonicated to eliminate dust and burr particles. This procedure produced two lightweight plates similar to that described in *Rowley and Moran (1975)* with the additional benefit of 'raised', separated walls. This approach prevents cross-contamination by diffusion of solutions during the staining and labeling procedures. A strip of Formvar support film was used to coat the microwell mini plate on the topside of the plate. A small water droplet (10 µl) was placed on each hole of the plate on the support film using a filtered syringe. A grid containing previously cut sections was placed (sections facing up) on each droplet and dried in the 50°C oven until the grids and the plastic support film had fused. Grids were then ready for immunolabeling and contrast staining by inverting and matching to the micro-cups of a full mini tray with desired solutions (*Figure 1A* – Mini tray).

Table 2. Number of gold particles in SN[nuch] neurons in three layers labeled with the PDF antibody.

	Layer				Layer		
SN[nuch]	703	723	787	SN[nuch]	703	723	787
r1	0	2	0	l1	0	0	0
r2	0	0	0	l2	1	0	4
r3	0	0	0	l3	0	0	0
r4	0	0	7	l4	0	0	0
r5	0	0	0	l5	0	0	0
r6	2	0	0	l6	0	3	10
r7	0	0	0	l7	0	0	2
r8	0	1	2	l8	1	0	3
r9	0	0	0	l9	0	0	0
r10	0	0	0	l10	0	0	0
r11	0	0	0	l11	0	0	0
r12	0	3	0	l12	6	1	0
r13	1	3	2	l13	9	9	6
r14	0	0	0	l14	18	0	0
r15-r20	0	0	0	l15	0	0	0

Number of gold particles in SN[nuch] neurons identified in three different immunogold layers labeled with the PDF antibody in all SN[nuch] sensory neurons.
DOI: 10.7554/eLife.11147.023
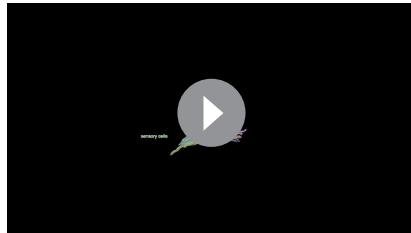
Video 3. Reconstruction of the nuchal organ. Reconstruction of the nuchal organ from the dorsal head of the 72 hpf *Platynereis* larva dataset HT9-4. The nuchal organ consists of three multiciliated cells and 16 sensory cells which project a sensory cilium and branching microvilli into an olfactory pit just below the cuticular layer.
DOI: 10.7554/eLife.11147.024

Contrasting

Dried sections were contrast stained with drops of 2% aqueous uranyl acetate for 6 min. Grids were washed by gently lowering the entire plate into a clean glass beaker of filtered distilled water. Excess water was wicked away with filter paper, and the grids were dried at 50°C for 1–2 min. Next, the grids were stained with drops of Sato's triple lead stain (*Hanaichi et al., 1986*) for 4 min. Grids were washed and dried as described above and dried at 50°C for 1 min. Grids were then carbon coated before being imaged with a FEI TECNAI Spirit electron microscope.

Immunogold silver-enhancement method

For immunoEM, we have eliminated the etching step prior to primary antibody incubation. We have observed that the treatment with the etching solution destroys ultrastructural integrity. In our technique, the use of sheep serum and bovine serum albumin mixed with Tween-20 at pH of 7.9 greatly enhanced the immunogold signal.

The following protocol was performed over a 1-day period and is an optimized version of a protocol by Stierhof (*Stierhof et al., 1991*) for Epon-embedded sections. All incubations up to the silver enhancement point were done in the TBST-BGN (Tris buffer saline with Tween-20, BSA, Fish Gelatin and Normal Sheep Serum, pH 7.9; see section below on preparing the buffer). First, sections were blocked with TBST-BGN for 10 min; blocked sections were then incubated with primary antibody (1:25 dilution) in TBST-BGN for 2 hr. Grids were washed twice with TBST-BGN for 5 min, and then incubated with secondary goat anti-rabbit IgG antibody with gold conjugates (AURION Ultra Small Immunogold Reagents; size 0.8 nm) at 1:50 dilution for 1 hr. Grids were then washed with TBST-BGN twice for 5 min, then washed twice with filtered distilled water for 5 min, followed by fixation with 1% glutaraldehyde in filtered distilled water for 5 min. Sections were washed in filtered distilled water twice for 5 min. Silver enhancement was applied with Aurion silver-enhancement kit for up to 47 min. The time interval of silver enhancement was dependent on temperature and concentration of the silver-enhancement solution. Gold size growth was approximately 15–20 nm within this time interval, a size appropriate for observation of gold particles in EM. Silver enhancement was stopped with three 3-min washes in filtered distilled water. Excess water was gently wicked from the back of the plate and individual holes with wedges of Whatman filter paper. Grids were dried in a 50°C oven and then contrasted (see above).

Preparation of blocking and wash buffer solution

Buffer concentration and consistency is very important in immunological reactions. We compared many protocols to achieve the best buffer for our experiments. We found that a saline buffer with Tris, Tween, bovine serum albumin (BSA), fish Gelatin, and normal serum (TBST-BGN), worked well. Our solutions were always freshly prepared on the day of the experiment.

Video 4. Reconstruction of the nuchal organ circuit. The nuchal organ sensory cells (SN[nuch], red) connect to two pairs of IN[arc] interneurons (orange). The adult eye photoreceptors (dark blue) are shown for reference. Several other neurons are shown in pale grey to highlight the shape of the larval nervous system.
DOI: 10.7554/eLife.11147.025

To prepare the buffer for immunoEM, three separate solutions were made: (1) 0.61 g Trizma, 0.90 g NaCl, and 70 ml of distilled water, (2) 1.0 g of BSA, 1.5 ml normal sheep serum, 500 µl Tween-20, and 20 ml distilled water, and (3) 0.01 of fish Gelatin and 10 ml of distilled water. Solution 3 was heated to dissolve and then cooled before being added to solutions 1 and 2. Finally, solutions 1–3 were combined and gently mixed. The buffer solution was then adjusted to pH of 7.9 using 1 M HCl and syringe filtered with a 0.45 µm filter.

Imaging and post-processing

Image acquisition of TEM serial sections was performed on a FEI TECNAI Spirit transmission electron microscope equipped with an UltraScan 4000 4X4k digital camera using the image acquisition software Digital Micrograph (Gatan Software Team Inc., Pleasanton) and SerialEM (*Mastronarde, 2005*). The images for the HT9-4 and HT9-5 samples were scanned at a pixel resolution of 5.71 nm/pixel and 2.22 nm/pixel, respectively. Image stitching and alignment were accomplished using TrakEM2 (*Cardona et al., 2010*; *Cardona et al., 2012*). All structures were segmented manually as area-lists, and exported into 3Dviewer and Blender as previously described (*Asadulina et al., 2015*). Tracing and annotation of the connectome were performed with CATMAID, a collaborative annotation toolkit for large-scale image data (*Saalfeld et al., 2009*; *Schneider-Mizell et al., 2015*).

IF and image registration

Antibodies were generated by immunizing rats or rabbits with synthetic, amidated peptides. Some of the antibodies were used in previous studies (*Conzelmann and Jékely, 2012*; *Conzelmann et al., 2011*; *Conzelmann et al., 2013a*; *Jékely et al., 2008*). All peptides contained an N-term Cys that was used for coupling. Antibodies were affinity purified from sera as previously described (*Conzelmann and Jékely, 2012*). Immunostainings were carried out as previously described (*Conzelmann and Jékely, 2012*). For triple IF, we used secondary antibodies coupled to three different fluorophores (FVa rat, AF488 secondary antibody rat; other neuropeptide rabbit, AF647 secondary antibody rabbit; acetylated-tubulin mouse, high-fidelity AF555 secondary antibody mouse).

For image registration, an average full-body acetylated tubulin reference template was generated for 72 hpf *Platynereis* using a modification of a previously described method (*Figure 5—source data 1*) (*Asadulina et al., 2012*). We used full-body scans of 36 larvae generated on a Zeiss LSM 780 confocal microscope with ZenBlue software. All stacks were oriented and their centers of mass were aligned. Stacks were averaged, and all stacks were aligned to this first average template using affine transformation. The 24 registered stacks most similar to the first average (as determined by an iteration metric) were then used to create an affine-transformed average. All original oriented stacks were then aligned to the affine-transformed average using affine and deformable transformation. The 24 registered stacks most similar to the affine-transformed average were then used to create an affine/deformable-transformed average. All original oriented stacks were then aligned to the affine/deformable-transformed average using affine and deformable transformation. The 24 registered stacks most similar to the affine/deformable-transformed average were then used to generate the final average acetylated tubulin reference template. The final average stack was unbiased and was used for image registration.

Imaris was used for image processing (adjusting brightness and contrast uniformly) and to take virtual cross-sections of the VNC for comparison with siGOLD samples.

Morpholino injection

Morpholino injections were performed as previously described (*Conzelmann et al., 2013a*). We used the following morpholinos to target the various neuropeptide precursor genes (GeneTools, LLC): Pdu-FMRFa-start MO CCACTGGTCCCTCATGGCAGGGTTT, Pdu-PDF-start MO CTGAACTGTCTTGCTT-GATCCCATC, Pdu-ATO-start MO CACAGGACTACCTTCATTTTTCTGA, Pdu-LUQ-start MO GTATT-TGCACAACATAGTGATAGTC, Pdu-PENK-start MO GAGGAGGACCACCAATATCTTCATC, Pdu-RYa-start MO TATAGACATGACACCTTGTTGGAGT, Pdu-LEUC-start2 MO TCTTGGCTGAACTCATT-GCGGCC, Pdu-FVa-start MO CCATCCGCCCACGCTCATATGCATC, Pdu-FVRIa-start MO CCCCCTT-CATACTGTCACAACGGAC, Pdu-RGWa-start MO CGACGACCCCCTGTAGCTTCATGTC.

Acknowledgements

Additional information

Funding

Author contributions

RS, Immunogold microscopy, Conception and design, Acquisition of data, Analysis and interpretation of data, Drafting or revising the article; EAW, Morpholino injections, IF, image registration, Conception and design, Acquisition of data, Analysis and interpretation of data, Drafting or revising the article; MC, Antibody generation, Acquisition of data, Analysis and interpretation of data; AA, Development of image registration protocol, Conception and design, Analysis and interpretation of data; CV, SJ, LABC, EM tracing, Analysis and interpretation of data; GJ, Conception and design, Analysis and interpretation of data, Drafting or revising the article

Author ORCIDs

Gáspár Jékely, http://orcid.org/0000-0001-8496-9836

Additional files

Major datasets

The following datasets were generated:

Author(s)	Year	Dataset title	Dataset URL	Database, license, and accessibility information
Shahidi R, Williams EA, Conzelmann M, Asadulina A, Verasztó C, Jasek S, Bezares-Calderón LA, Jékely G	2015	Data from: A serial multiplex immunogold labeling method for identifying peptidergic neurons in connectomes	http://dx.doi.org/10.5061/dryad.c7366	Available at Dryad Digital Repository under a CC0 Public Domain Dedication.

References

Asadulina A, Conzelmann M, Williams EA, Panzera A, Jékely G. 2015. Object-based representation and analysis of light and electron microscopic volume data using blender. *BMC Bioinformatics* **16**. doi: 10.1186/s12859-015-0652-7

Asadulina A, Panzera A, Verasztó C, Liebig C, Jékely G. 2012. Whole-body gene expression pattern registration in platynereis larvae. *EvoDevo* **3**. doi: 10.1186/2041-9139-3-27

Backfisch B, Veedin Rajan VB, Fischer RM, Lohs C, Arboleda E, Tessmar-Raible K, Raible F. 2013. Stable transgenesis in the marine annelid platynereis dumerilii sheds new light on photoreceptor evolution. *Proceedings of the National Academy of Sciences of the United States of America* **110**:193–198. doi: 10.1073/pnas.1209657109

Bannister S, Antonova O, Polo A, Lohs C, Hallay N, Valinciute A, Raible F, Tessmar-Raible K. 2014. TALENs mediate efficient and heritable mutation of endogenous genes in the marine annelid platynereis dumerilii. *Genetics* **197**:77–89. doi: 10.1534/genetics.113.161091

Bargmann CI, Marder E. 2013. From the connectome to brain function. *Nature Methods* **10**:483–490. doi: 10.1038/nmeth.2451

Bargmann CI. 2012. Beyond the connectome: how neuromodulators shape neural circuits. *BioEssays* **34**:458–465. doi: 10.1002/bies.201100185

Bauknecht P, Jékely G. 2015. Large-scale combinatorial deorphanization of platynereis neuropeptide GPCRs. *Cell Reports* **12**. doi: 10.1016/j.celrep.2015.06.052

Blumer MJ, Gahleitner P, Narzt T, Handl C, Ruthensteiner B. 2002. Ribbons of semithin sections: an advanced method with a new type of diamond knife. *Journal of Neuroscience Methods* **120**:11–16.

Bock DD, Lee WC, Kerlin AM, Andermann ML, Hood G, Wetzel AW, Yurgenson S, Soucy ER, Kim HS, Reid RC. 2011. Network anatomy and in vivo physiology of visual cortical neurons. *Nature* **471**:177–182. doi: 10.1038/nature09802

Briggman KL, Helmstaedter M, Denk W. 2011. Wiring specificity in the direction-selectivity circuit of the retina. *Nature* **471**:183–188. doi: 10.1038/nature09818

Brorson SH, Reinholt FP. 2008. The intensity of immunogold labeling of deplasticized acrylic sections compared to deplasticized epoxy sections-theoretical deductions and experimental data. *Micron* **39**:144–150. doi: 10.1016/j.micron.2006.11.006

Brorson SH. 1998. Comparison of the immunogold labeling of single light chains and whole immunoglobulins with anti-kappa on LR-white and epoxy sections. *Micron* **29**:439–443.

Bucher D, Marder E. 2013. SnapShot: neuromodulation. *Cell* **155**:482–482.e1.

Bumbarger DJ, Riebesell M, Rödelsperger C, Sommer RJ. 2013. System-wide rewiring underlies behavioral differences in predatory and bacterial-feeding nematodes. *Cell* **152**:109–119. doi: 10.1016/j.cell.2012.12.013

Cardona A, Saalfeld S, Preibisch S, Schmid B, Cheng A, Pulokas J, Tomancak P, Hartenstein V. 2010. An integrated micro- and macroarchitectural analysis of the drosophila brain by computer-assisted serial section electron microscopy. *PLoS Biology* **8**:e1000502. doi: 10.1371/journal.pbio.1000502

Cardona A, Saalfeld S, Schindelin J, Arganda-Carreras I, Preibisch S, Longair M, Tomancak P, Hartenstein V, Douglas RJ. 2012. TrakEM2 software for neural circuit reconstruction. *PLoS One* **7**:e38011. doi: 10.1371/journal.pone.0038011

Collman F, Buchanan J, Phend KD, Micheva KD, Weinberg RJ, Smith SJ. 2015. Mapping synapses by conjugate light-electron array tomography. *The Journal of Neuroscience* **35**:5792–5807. doi: 10.1523/JNEUROSCI.4274-14.2015

Colombelli J, Tängemo C, Haselman U, Antony C, Stelzer EHK, Pepperkok R, Reynaud EG. 2008. A correlative light and electron microscopy method based on laser micropatterning and etching. *Methods in Molecular Biology* **457**:203–213. doi: 10.1007/978-1-59745-261-8_15

Conzelmann M, Jékely G. 2012. Antibodies against conserved amidated neuropeptide epitopes enrich the comparative neurobiology toolbox. *EvoDevo* **3**. doi: 10.1186/2041-9139-3-23

Conzelmann M, Offenburger S-L, Asadulina A, Keller T, Munch TA, Jekely G. 2011. Neuropeptides regulate swimming depth of platynereis larvae. *Proceedings of the National Academy of Sciences of the United States of America* **108**:E1174–E1183. doi: 10.1073/pnas.1109085108

Conzelmann M, Williams EA, Krug K, Franz-Wachtel M, Macek B, Jékely G. 2013b. The neuropeptide complement of the marine annelid platynereis dumerilii. *BMC Genomics* **14**.

Conzelmann M, Williams EA, Tunaru S, Randel N, Shahidi R, Asadulina A, Berger J, Offermanns S, Jekely G. 2013a. Conserved MIP receptor-ligand pair regulates platynereis larval settlement. *Proceedings of the National Academy of Sciences of the United States of America* **110**:8224–8229. doi: 10.1073/pnas.1220285110

De Paul A, Mukdsi JH, Petiti JP, Gutierrez S, Quintar AA, Maldonado CA, Torres AI. 2012. Applications of Immunocytochemistry. In:Dehghani H eds *Immunoelectron Microscopy: A Reliable Tool for the Analysis of Cellular Processes.*

Denk W, Horstmann H. 2004. Serial block-face scanning electron microscopy to reconstruct three-dimensional tissue nanostructure. *PLoS Biology* **2**:e329. doi: 10.1371/journal.pbio.0020329

Eipper BA, Stoffers DA, Mains RE. 1992. The biosynthesis of neuropeptides: peptide alpha-amidation. *Annual Review of Neuroscience* **15**:57–85. doi: 10.1146/annurev.ne.15.030192.000421

Gaudry Q, Hong EJ, Kain J, de Bivort BL, Wilson RI. 2013. Asymmetric neurotransmitter release enables rapid odour lateralization in drosophila. *Nature* **493**:424–428. doi: 10.1038/nature11747

Gühmann M, Jia H, Randel N, Verasztó C, Bezares-Calderón LA, Michiels NK, Yokoyama S, Jékely G. 2015. Spectral tuning of phototaxis by a go-opsin in the rhabdomeric eyes of platynereis. *Current Biology* **25**:2265–2271. doi: 10.1016/j.cub.2015.07.017

Hamanaka Y, Park D, Yin P, Annangudi SP, Edwards TN, Sweedler J, Meinertzhagen IA, Taghert PH. 2010. Transcriptional orchestration of the regulated secretory pathway in neurons by the bHLH protein DIMM. *Current Biology* **20**:9–18. doi: 10.1016/j.cub.2009.11.065

Hanaichi T, Sato T, Iwamoto T, Malavasi-Yamashiro J, Hoshino M, Mizuno N. 1986. A stable lead by modification of sato's method. *Journal of Electron Microscopy* **35**:304–306.

Hayworth KJ, Morgan JL, Schalek R, Berger DR, Hildebrand DG, Lichtman JW. 2014. Imaging ATUM ultrathin section libraries with WaferMapper: a multi-scale approach to EM reconstruction of neural circuits. *Frontiers in Neural Circuits* **8**. doi: 10.3389/fncir.2014.00068

Johard HA, Enell LE, Gustafsson E, Trifilieff P, Veenstra JA, Nässel DR. 2008. Intrinsic neurons of drosophila mushroom bodies express short neuropeptide f: relations to extrinsic neurons expressing different neurotransmitters. *The Journal of Comparative Neurology* **507**:1479–1496. doi: 10.1002/cne.21636

Jékely G, Colombelli J, Hausen H, Guy K, Stelzer E, Nédélec F, Arendt D. 2008. Mechanism of phototaxis in marine zooplankton. *Nature* **456**:395–399. doi: 10.1038/nature07590

Jékely G. 2013. Global view of the evolution and diversity of metazoan neuropeptide signaling. *Proceedings of the National Academy of Sciences of the United States of America* **110**:8702–8707. doi: 10.1073/pnas.1221833110

Koizumi O, Wilson JD, Grimmelikhuijzen CJ, Westfall JA. 1989. Ultrastructural localization of RFamide-like peptides in neuronal dense-cored vesicles in the peduncle of hydra. *The Journal of Experimental Zoology* **249**:17–22. doi: 10.1002/jez.1402490105

Lin T-Y, Luo J, Shinomiya K, Ting C-Y, Lu Z, Meinertzhagen IA, Lee C-H, Lee CH. 2015. Mapping chromatic pathways in the *drosophila* visual system. *Journal of Comparative Neurology*:n/a. doi: 10.1002/cne.23857

Maco B, Cantoni M, Holtmaat A, Kreshuk A, Hamprecht FA, Knott GW. 2014. Semiautomated correlative 3D electron microscopy of in vivo-imaged axons and dendrites. *Nature Protocols* **9**:1354–1366. doi: 10.1038/nprot.2014.101

Maco B, Holtmaat A, Cantoni M, Kreshuk A, Straehle CN, Hamprecht FA, Knott GW. 2013. Correlative in vivo 2 photon and focused ion beam scanning electron microscopy of cortical neurons. *PloS One* **8**:e57405. doi: 10.1371/journal.pone.0057405

Marder E. 2012. Neuromodulation of neuronal circuits: back to the future. *Neuron* **76**:1–11. doi: 10.1016/j.neuron.2012.09.010

Martell JD, Deerinck TJ, Sancak Y, Poulos TL, Mootha VK, Sosinsky GE, Ellisman MH, Ting AY. 2012. Engineered ascorbate peroxidase as a genetically encoded reporter for electron microscopy. *Nature Biotechnology* **30**:1143–1148. doi: 10.1038/nbt.2375

Mastronarde DN. 2005. Automated electron microscope tomography using robust prediction of specimen movements. *Journal of Structural Biology* **152**:36–51. doi: 10.1016/j.jsb.2005.07.007

Merighi A, Cruz F, Coimbra A. 1992. Immunocytochemical staining of neuropeptides in terminal arborization of primary afferent fibers anterogradely labeled and identified at light and electron microscopic levels. *Journal of Neuroscience Methods* **42**:105–113.

Micheva KD, Smith SJ. 2007. Array tomography: a new tool for imaging the molecular architecture and ultrastructure of neural circuits. *Neuron* **55**:25–36. doi: 10.1016/j.neuron.2007.06.014

Mirabeau O, Joly JS. 2013. Molecular evolution of peptidergic signaling systems in bilaterians. *Proceedings of the National Academy of Sciences of the United States of America* **110**:E2028–E2037. doi: 10.1073/pnas.1219956110

Morgan JL, Lichtman JW. 2013. Why not connectomics? *Nature Methods* **10**:494–500. doi: 10.1038/nmeth.2480

Nässel DR. 1993. Insect myotropic peptides: differential distribution of locustatachykinin- and leucokinin-like immunoreactive neurons in the locust brain. *Cell and Tissue Research* **274**:27–40.

Ohyama T, Schneider-Mizell CM, Fetter RD, Aleman JV, Franconville R, Rivera-Alba M, Mensh BD, Branson KM, Simpson JH, Truman JW, Cardona A, Zlatic M. 2015. A multilevel multimodal circuit enhances action selection in drosophila. *Nature* **520**:633–639. doi: 10.1038/nature14297

Purschke G, Wolfrath F, Westheide W. 1997. Ultrastructure of the nuchal organ and cerebral organ in onchnesoma squamatum (sipuncula, phascolionidae). *Zoomorphology* **117**:23–31.

Purschke G. 1997. Ultrastructure of nuchal organs in polychaetes (annelida) - new results and review. *Acta Zoologica* **78**:123–143.

Purschke G. 2005. Sense organs in polychaetes (annelida). *Hydrobiologia* **535**:53–78.

Randel N, Asadulina A, Bezares-Calderón LA, Verasztó C, Williams EA, Conzelmann M, Shahidi R, Jékely G. 2014. Neuronal connectome of a sensory-motor circuit for visual navigation. *eLife* **3**. doi: 10.7554/eLife.02730

Randel N, Shahidi R, Verasztó C, Bezares-Calderón LA, Schmidt S, Jékely G. 2015. Inter-individual stereotypy of the platynereis larval visual connectome. *eLife* **4**. doi: 10.7554/eLife.08069

Reyntjens S, Puers R. 2001. A review of focused ion beam applications in microsystem technology. *J. Micromech. Microeng* **11**:287–300.

Rowley JC, Moran DT. 1975. A simple procedure for mounting wrinkle-free sections on formvar-coated slot grids. *Ultramicroscopy* **1**:151–155.

Saalfeld S, Cardona A, Hartenstein V, Tomancak P. 2009. CATMAID: collaborative annotation toolkit for massive amounts of image data. *Bioinformatics (Oxford, England)* **25**:1984–1986. doi: 10.1093/bioinformatics/btp266

Schlötzer-Schrehardt U. 1987. Ultrastructural investigation of the nuchal organs of pygospio elegans (polychaeta). *Zoomorphology*.

Schneider-Mizell CM, Gerhard S, Longair M, Kazimiers T, Li F, Zwart MF, Champion A, Midgley F, Fetter R, Saalfeld S. 2015. Quantitative neuroanatomy for connectomics in drosophila. *bioRxiv* . doi: 10.1101/026617

Shahidi R, Williams EA, Conzelmann M, Asadulina A, Verasztó C, Jasek S, Bezares-Calderón LA, Jékely G. 2015. Data from: A serial multiplex immunogold labeling method for identifying peptidergic neurons in connectomes. *Dryad Digital Repository*. doi: 10.5061/dryad.c7366

Shu X, Lev-Ram V, Deerinck TJ, Qi Y, Ramko EB, Davidson MW, Jin Y, Ellisman MH, Tsien RY. 2011. A genetically encoded tag for correlated light and electron microscopy of intact cells, tissues, and organisms. *PLoS Biology* **9**:e1001041. doi: 10.1371/journal.pbio.1001041

Skepper JN, Powell JM. 2008. Immunogold staining of epoxy resin sections for transmission electron microscopy (tEM). *CSH Protocols* **2008**:pdb.prot5015. doi: 10.1101/pdb.prot5015

Stierhof YD, Humbel BM, Schwarz H. 1991. Suitability of different silver enhancement methods applied to 1 nm colloidal gold particles: an immunoelectron microscopic study. *Journal of Electron Microscopy Technique* **17**: 336–343. doi: 10.1002/jemt.1060170307

Timmermans FJ, Otto C. 2015. Contributed review: review of integrated correlative light and electron microscopy. *The Review of Scientific Instruments* **86**:011501. doi: 10.1063/1.4905434

Tomer R, Denes AS, Tessmar-Raible K, Arendt D. 2010. Profiling by image registration reveals common origin of annelid mushroom bodies and vertebrate pallium. *Cell* **142**:800–809. doi: 10.1016/j.cell.2010.07.043

Tosches MA, Bucher D, Vopalensky P, Arendt D. 2014. Melatonin signaling controls circadian swimming behavior in marine zooplankton. *Cell* **159**:46–57. doi: 10.1016/j.cell.2014.07.042

Urwyler O, Izadifar A, Dascenco D, Petrovic M, He H, Ayaz D, Kremer A, Lippens S, Baatsen P, Guérin CJ, Schmucker D. 2015. Investigating CNS synaptogenesis at single-synapse resolution by combining reverse genetics with correlative light and electron microscopy. *Development* **142**:394–405. doi: 10.1242/dev.115071

Veedin-Rajan VB, Fischer RM, Raible F, Tessmar-Raible K. 2013. Conditional and specific cell ablation in the marine annelid platynereis dumerilii. *PloS One* **8**:e75811. doi: 10.1371/journal.pone.0075811

Viswanathan S, Williams ME, Bloss EB, Stasevich TJ, Speer CM, Nern A, Pfeiffer BD, Hooks BM, Li WP, English BP, Tian T, Henry GL, Macklin JJ, Patel R, Gerfen CR, Zhuang X, Wang Y, Rubin GM, Looger LL. 2015. High-performance probes for light and electron microscopy. *Nature Methods* **12**:568–576. doi: 10.1038/nmeth.3365

White JG, Southgate E, Thomson JN, Brenner S. 1986. The structure of the nervous system of the nematode caenorhabditis elegans. *Philosophical Transactions of the Royal Society B* **314**:1–340. doi: 10.1098/rstb.1986.0056

Williams EA, Conzelmann M, Jékely G. 2015. Myoinhibitory peptide regulates feeding in the marine annelid platynereis. *Frontiers in Zoology* **12**. doi: 10.1186/s12983-014-0093-6

Wong MY, Zhou C, Shakiryanova D, Lloyd TE, Deitcher DL, Levitan ES. 2012. Neuropeptide delivery to synapses by long-range vesicle circulation and sporadic capture. *Cell* **148**:1029–1038. doi: 10.1016/j.cell.2011.12.036

Yasuyama K, Meinertzhagen IA. 2010. Synaptic connections of PDF-immunoreactive lateral neurons projecting to the dorsal protocerebrum of drosophila melanogaster. *The Journal of Comparative Neurology* **518**:292–304. doi: 10.1002/cne.22210

Zantke J, Bannister S, Rajan VB, Raible F, Tessmar-Raible K. 2014. Genetic and genomic tools for the marine annelid platynereis dumerilii. *Genetics* **197**:19–31. doi: 10.1534/genetics.112.148254

Zupanc GK. 1996. Peptidergic transmission: from morphological correlates to functional implications. *Micron* **27**: 35–91. doi: 10.1016/0968-4328(95)00028-3

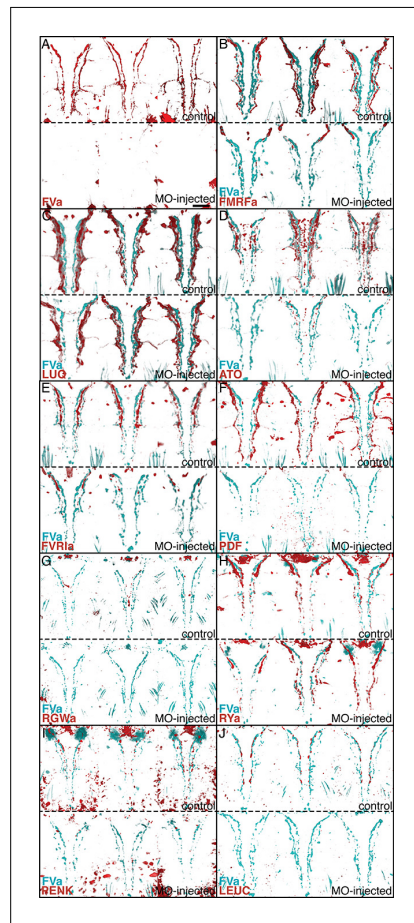# figure supplements

A serial multiplex immunogold labeling method for identifying peptidergic neurons in connectomes
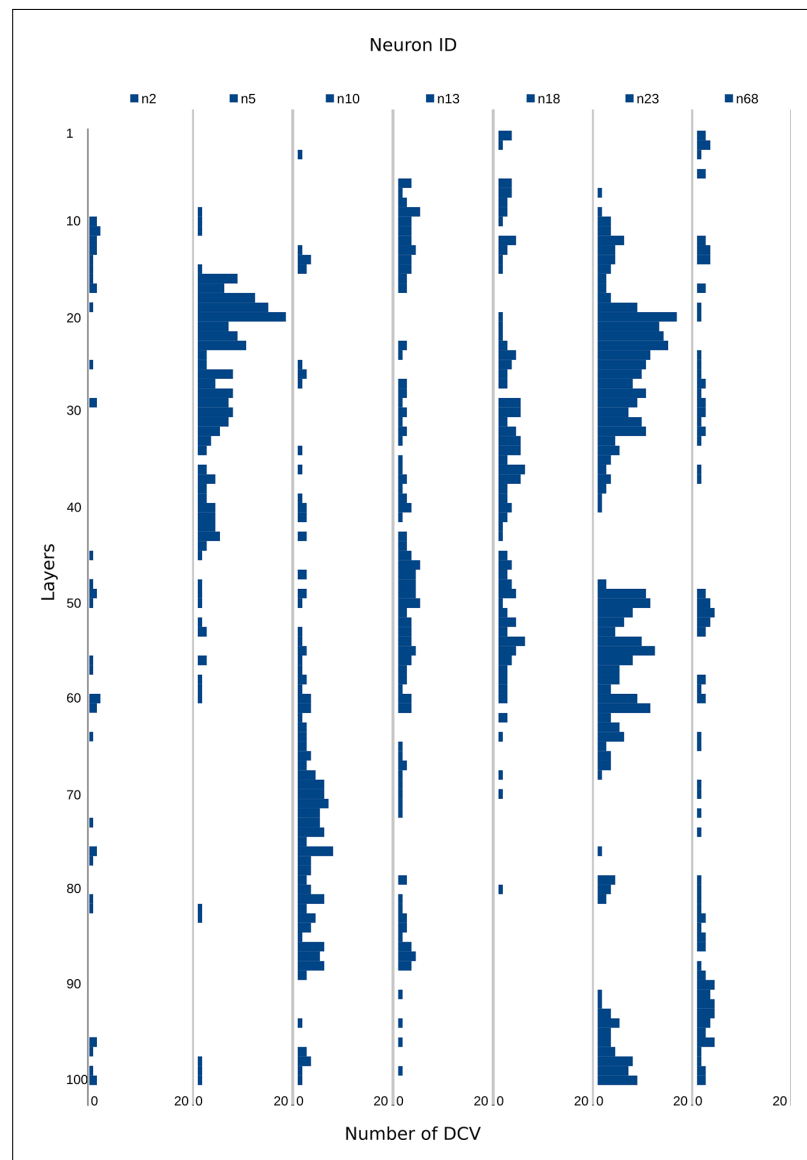
Figure 3—figure supplement 1. Number of DCVs in selected neurite profiles along 100 layers. Number of DCVs scored along 100 layers in selected neurites in the HT9-5 dataset. The gold counts for the corresponding profiles are shown in *Figure 3—source data 1*.
DOI: http://dx.doi.org/10.7554/eLife.11147.008

Figure 4—figure supplement 1. Morpholino-mediated knockdown of proneuropeptides followed by whole-mount IF indicates antibody specificities. Whole-mount IF of 72 hpf uninjected control *Platynereis* larvae and larvae micro-injected with translation-blocking morpholinos (MOs) targeting different neuropeptide precursor genes. FVa-knockdown and control larvae were stained with an antibody raised against FVa and counterstained with acetylated tubulin. All other control and knockdown larvae were co-stained with an antibody raised against FVa and an antibody raised against the MO target peptide indicated and counterstained with acetylated tubulin. All larvae are shown in ventral view. For each neuropeptide, three control larvae (top) and three MO-knockdown larvae (bottom) are shown. (**A**) FVa knockdown and control larvae with antibody raised against FVa. (**B**) FMRFa knockdown and control larvae with antibody raised against FMRFa. (**C**) LUQ knockdown and control larvae with antibody raised against LUQ. (**D**) ATO knockdown and control larvae with antibody raised against ATO. (**E**) FVRIa knockdown and control larvae with antibody raised against FVRIa. (**F**) PDF knockdown and control larvae with antibody raised against PDF. (**G**) RGWa
*Figure 4—figure supplement 1 continued on next page*

Figure 4—figure supplement 1 continued

knockdown and control larvae with antibody raised against RGWa. Note that the staining in the head is eliminated following knockdown. The staining in the VNC was too weak in these samples. (**H**) RYa knockdown and control larvae with antibody raised against RYa. (**I**) PENK knockdown and control larvae with antibody raised against PENK. (**J**) LEUC knockdown and control larvae with antibody raised against LEUC. Scale bar: 30 µm.
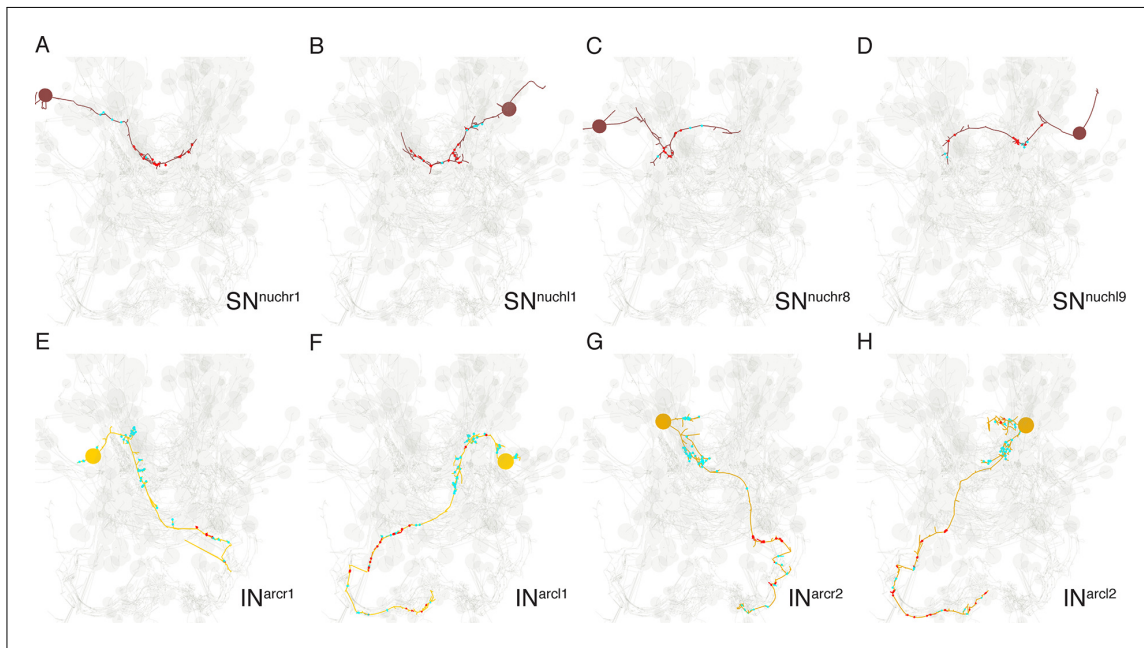
Figure 10—figure supplement 1. Morphology of SN^{nuch} and IN^{arc} neurons. (A, D) Four examples of SN^{nuch} sensory neurons with the presynaptic (red) and postsynaptic sites shown. (E, H) Morphology of the four IN^{arc} interneurons with the presynaptic (red) and postsynaptic sites shown.
DOI: http://dx.doi.org/10.7554/eLife.11147.021
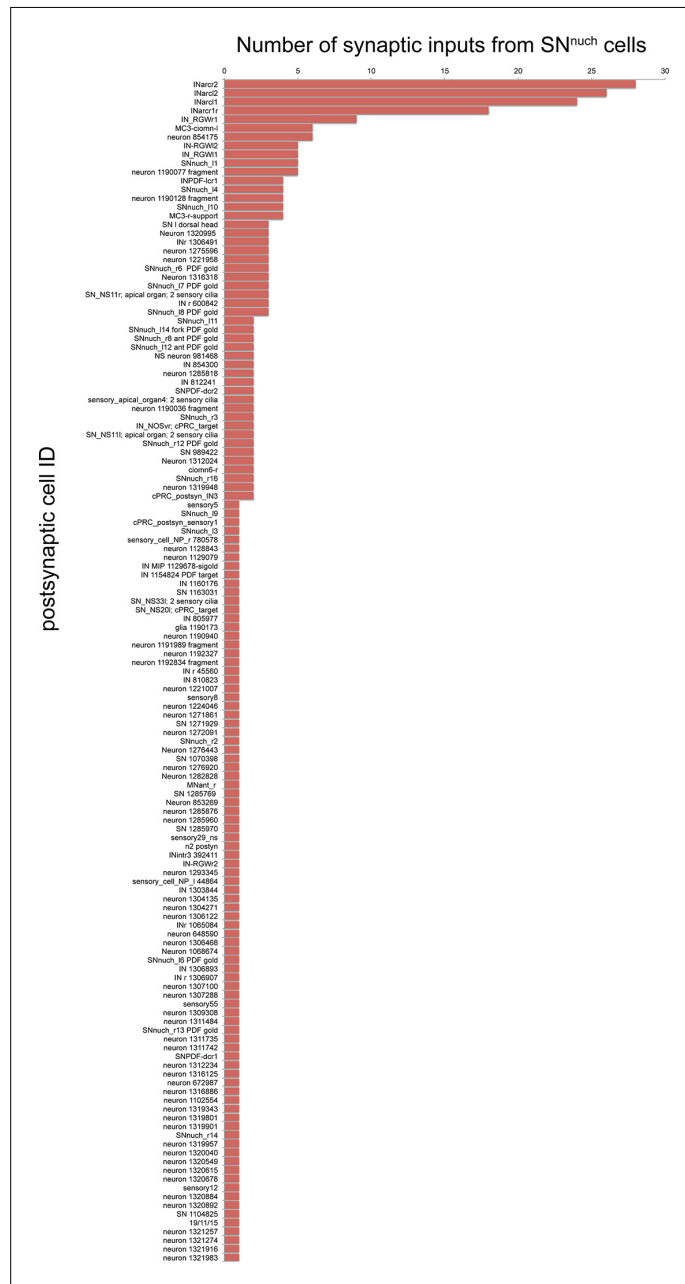
Figure 10—figure supplement 2. Number of synaptic inputs from SN[nuch] cells to all postsynaptic targets. All postsynaptic targets of the SN[nuch] neurons are listed.
DOI: http://dx.doi.org/10.7554/eLife.11147.022